The Institute of Paper Science and Technology

Atlanta, Georgia

Doctoral Dissertation Reprint

THE DEFORMATION OF PAPER IN THE z-DIRECTION

A thesis submitted by

Gary P. Van Liew

B.A. 1968, Western Washington State College

M.S. 1970, Lawrence University

in partial fulfillment of the requirements
of The Institute of Paper Chemistry
for the degree of Doctor of Philosophy
from Lawrence University
Appleton, Wisconsin

June, 1973

TABLE OF CONTENTS

SUMMARY

The in-plane (x- and y-direction) mechanical properties of paper have been studied in detail, and methods for their evaluation have received considerable attention and development. In comparison, relatively little is known about the mechanical properties, other than failure stress, perpendicular to the plane (z-direction).

The purpose of this study was to measure and interpret load-deformation behavior in the z-direction to improve understanding of the relationship between structure and strength when paper is subjected to tensile stresses perpendicular to the plane. Handsheet specimens were adhesive bonded between two 1-inch diameter metal cylinders, and an experimental apparatus was constructed to measure the deformation behavior as a function of load and time under load. Stress-strain and creep and creep-recovery curves were obtained and analyzed to establish the basic mechanical behavior of paper during z-directional loading.

The experimental evidence for handsheet specimens prepared from a mildly beaten and classified western hemlock sulfite pulp has shown that tensile strain in the z-direction was typically nonuniform, as indicated by the nonparallel separation of the cylinder surfaces when a tensile load was applied. Despite wide variations in the extent of nonuniformity, the average force versus average deformation curves for 1-inch diameter specimens were reasonably reproducible and satisfactory for the study of z-direction mechanical behavior.

The following description is typical of the z-direction mechanical behavior for the paper specimens used in this work. Upon application of a z-direction tensile load, the specimens responded almost immediately in a nonlinear manner to the applied force. In tests at loading rates of 0.3 kg./cm.^{2}/sec., the slope of the load-elongation curve at the zero stress-zero strain intercept was low, leading to an estimated elastic modulus in the z-direction of only 20 to 60

kg./mm.^{2} (about one tenth the apparent in-plane elastic modulus of paper). The strain at failure fell within a range of 0.25 to 0.7%, and the z-direction failure stresses were within a range of about 5 to 9 kg./cm.^{2}, or approximately one hundred times lower than the failure stress normally observed in the in-plane direction. The z-direction deformation was quite elastic to failure, with a large amount of time-dependent recovery observed during unloading.

Specimens could withstand creep loads of 73% of the failure load for 10,000 seconds without rupture. For loads about 81% of the failure load, total failure occurred between 2,000 and 4,000 seconds. In tests at higher loads, the creep rate increased with time as the specimen approached the point of complete fracture. This was contrary to the reported behavior for in-plane creep. The nonrecoverable z-direction deformation could be correlated with the nonuniformity of strain.

In load-elongation tests, the specimens could be subjected to 85% of their normal breaking load without exhibiting a measurable change in the scattering coefficient. A change in scattering coefficient of about 14 cm.^{2}/g. resulted in a reduction in failure stress to about one fifth the normal value. If it was assumed that the change in scattering coefficient was linearly related to the work involved in rupturing fiber-to-fiber bonds, then a Nordman bonding strength value calculated in the z-direction was estimated to be from 200 to 2,000 times lower than that calculated in the in-plane direction.

It was concluded that intrafiber deformation as a result of z-direction tensile loading was severely limited because of the ease with which fiber-to-fiber bonds fail due to a peeling action. This peeling action requires less force for bond rupture than the shearing action involved in in-plane tensile loading. The concentration of stress at the periphery of interfiber bonds leads to progressive debonding of the structure, which soon is localized at narrow planes. The early

onset of fracture at a concentrated plane determines the strength of the specimen and makes it difficult to determine an average mechanical property for a hypothetically uniform fibrous structure.

INTRODUCTION AND OBJECTIVES

The strength of paper is related in part to its structure. A key to the better understanding of how strength is related to structure is a careful analysis of the mechanical behavior of paper. The failure stress, failure strain, work to rupture, how the paper stretches as a function of load or time under load, etc., collectively, are the principal mechanical properties which can be obtained experimentally. They represent a complex series of events involving stress, deformation, and time.

To study mechanical properties in relation to structure, it is desirable to have some knowledge of the mechanisms by which paper deforms under load. An association of the mechanical behavior with intrafiber (within fiber) and interfiber (between fibers) mechanisms of deformation is of particular interest in paper. One attempts, for example, to relate the strength of the structure to the strength of the fibers and the strength of the bonds between the fibers. Knowledge of the structural changes which occur when paper deforms under load is most helpful in assessing the relative importance of the different structural parameters to the strength and mechanical behavior of paper.

Knowledge of how paper deforms under z-direction tensile loading is meager. Studies of the z-direction properties of paper to the present time have been confined largely to measurements of the failure load. These data are often used to characterize the bonding potential of a pulp, or to measure the extent and strength of bonding in a sheet of paper. No data have been developed illustrating z-direction deformation as a function of load or time under load. Such knowledge is of practical importance in processes such as printing, where emphasis is placed on resistance to failure in the z-direction.

The essential objective of this research was to measure and interpret the load-deformation behavior of paper in the z-direction. Qualitative descriptions of the deformation mechanisms were desired.

BACKGROUND REVIEW

Paper consists of a three-dimensional arrangement of fibers bonded together at their points of contact. When the paper is subjected to a load, forces are applied to the fibers by way of the bonded areas. Therefore, the manner in which the fibrous structure deforms is dependent on the structure of the individual fibers, and the area and structure of the fiber-to-fiber bonds. To understand this relationship between structure and mechanical properties, it is necessary to have some understanding of the structure of paper at both the macroscopic and microscopic levels, in addition to detailed knowledge of the way it deforms when subjected to a load.

This review is intended to provide an understanding of the existing relationships between structure and mechanical behavior. It includes the structure of fibers, interfiber bonds, and paper as a whole, and a description of the various mechanisms of response to loading.

PAPER STRUCTURE

Paper consists of a three-dimensional array of fibers bonded together at their points of contact. The fibers are oriented in different ways within the sheet, but are primarily parallel to the plane. Although considered to be heterogeneous in its entirety, paper can be described at various levels in terms of the structure of the individual fibers and the bonds between them. The following review is general in its scope and should be viewed accordingly.

INDIVIDUAL FIBERS

The wood pulp fiber consists of an outer primary wall plus a secondary wall made up of three layers: S_1, S_2, and S_3, all concentric about the lumen of the

fiber (1). Each layer consists of one or more lamellae, or aggregates of fibrils, distinguished from one another by their angle of orientation to the axis of the fiber. The S_2 layer occupies the major part of the cell wall (80% for springwood and 90% for summerwood) and may vary considerably in its angle of orientation with the fiber axis.

The fibrils are further subdivided into elementary fibrils and microfibrils. Their minimum dimensions are difficult to determine because surface tension forces draw them into larger bundles during the process of drying from water used in preparing them for the electron microscope.

Further subdivision of these microfibrils would eventually lead to aggregates of cellulose molecules in either amorphous or crystalline phases within the structure. The fine structure of the microfibril is still a topic of much research interest and has not been conclusively established (2). The fibrillar structure of the fiber wall is embedded within an amorphous matrix of lignin and hemicelluloses.

This description applies to fibers as they occur in the tree. The structure and chemical composition of fibers used in papermaking will vary according to the treatment they receive in the pulping and bleaching processes.

INTERFIBER BONDS

The area and strength of the fiber-to-fiber bond is dependent upon the surface tension forces drawing the fibers together, the conformability of the fibers, and the intrinsic strength of the bond. Since a load applied to a paper specimen is transmitted through the network structure via the bonding sites, the structure of these interfiber bonds is of considerable importance.

Van den Akker (3), in a critical review of the structural aspects of bonding, has described two extreme cases of interfiber bonding. These are bonds between unfibrillated fiber surfaces and bonds between fibrillated surfaces. The tendency toward one or the other extremes would depend on the previous pulping and refining treatments.

In the first class of bonds, the surface fibrillar structure is essentially intact, whereas in the second class a substantial percentage of the macro- and microfibrils has been partially torn away from the fiber surface by refining and other mechanical action. This latter surface would be fuzzy in appearance with pieces of the lamella structure and fibrils protruding from the walls. The bonds between the intact surfaces might differ in interfiber molecular contact, compared to bonds between well-fibrillated fiber surfaces, because of the potentially better intermeshing of the macro- and microfibrils.

The fact that the structure of interfiber bonds does differ has been confirmed by observation with the electron microscope. Asunmaa and Steenberg (4) found that the contact areas of fiber-to-fiber bonds ranged from almost point contacts to areas of 100 $\mu m.^2$ They concluded that optical contact could exist between all distinguishable structural layers and components of the fiber wall. Optical contact was confirmed for the following fiber wall combinations: S_1-S_1, S_1-S_2, and S_2-S_2.

Buchanan and Lindsay (5) showed, with the aid of the electron microscope, that a high-yield, unbeaten kraft pulp had fibers that were relatively stiff and did not conform well to one another. They also exhibited very little evidence of fibrillation. An unbeaten, low-yield kraft pulp, on the other hand, had more collapsed fibers, and these conformed better to one another. There was evidence of some fibrillar attachment between fibers. A beaten, low-yield kraft pulp

showed that the fibers conformed very well to one another and had collapsed even further. These fibers exhibited considerable fibrillar attachment in paper. Further evidence of the differences in bonding was obtained from an examination of the tension fracture areas. Paper fracture for the high-yield pulp was characterized by few broken fibers and very little disturbance of the surface at the debonded areas. Debonding, by stressing the low-yield, unbeaten paper in the z-direction, revealed fibrils protruding from the fiber surfaces. This occurred where a single fiber, which had previously been bonded on the upper surface of the sheet, was pulled off.

In the case of tension fracture of sheets prepared from beaten pulp, electron micrographs showed that in the debonded area there were not only fibrils but also larger fragments (bundles of fibrils) protruding from the surface (5). It was concluded that lowering the yield and beating increased the conformability of the fibers to one another, and therefore the amount of close contact between them. This conformability (or flexibility) was closely related to the degree of collapse of the fiber. The amount of fibrillar connecting material between the fibers was also increased by lowering the yield and beating. From the examination of debonded areas produced by tensile fracture in the paper sheets, it was observed that the amount of material transferred at a debonded junction increased with beating and lower yields.

Page and Tydeman (6) proposed that the transverse shrinkage of fibers (and fibril shrinkage, if present) gave rise to kinks in the free fiber segments, and microcompressions in the bonded areas throughout the structure to a degree controlled by drying restraints. They demonstrated that bonding at a fiber crossing within a sheet free to shrink would produce a longitudinal contraction of one fiber, because of the strong transverse shrinkage of the other. This effect,

and others that arise in the consolidation process are involved in determining the architecture of fiber-to-fiber bonds. A good discussion of the structural aspects of bonding has been given by Van den Akker (3).

At the molecular level, bonding is a result of the attractive forces between the various chemical constituents of the fibers. Swanson (7), in a study of the experimental evidence related to the molecular forces involved in bonding, has indicated that classical frictional forces between fibers and fibrils are not responsible for the strength of typical paper. Secondary valence forces (hydrogen bonding, general orientation or Keesom forces, induction or Debye forces, and dispersion or London forces) are responsible for molecular bonding. Many workers in the field tend to attribute the principal interfiber bonding to hydrogen bonds. However, the evidence is mainly indirect, and there is no reason to believe that other secondary valence forces are unimportant. It is expected that the same type of molecular forces responsible for bonding between fibers would also be responsible for bonding between fibrils within the fibers.

Ebeling (2) pointed out that an interfiber bond in a typical sheet of paper should not be visualized as a glued lap joint, but rather, it was essential to note the three-dimensional character of the bond. This followed from the earlier conclusions that the surface of the wet fibers is not a well-defined macroboundary, but a gradual transition region with molecular, elementary micro- and macrofibrillation, and with some partial detached surface lamellae of the cell wall. Hence, when such fiber surfaces are brought into contact by drainage, surface tension forces, and wet pressing, partial entanglement must occur at all levels, but especially on the molecular and elementary fibrillation level. In addition, this bonded matrix would be expected to contain various colloidally dispersed or soluble materials (cellulose, hemicellulose, etc.).

The bonded area between fibers is a three-dimensional matrix consisting of microfibrillar substance together with colloidal chemical constituents. The areas of the bonds will vary from point contact between intact fiber surfaces (with a small degree of surface fibrillation) to an intimate contact of all sizes of fibrils from the walls of both fibers.

LOAD-ELONGATION BEHAVIOR OF PAPER

MECHANISMS OF RESPONSE OF PAPER TO LOADING

A viscoelastic material exhibits both instantaneous elastic deformation and delayed, time-dependent deformation when subjected to a load. This deformation in paper depends on the molecular structure of the fibers as well as on how the fibers are bonded together. Brezinski (8) gave an excellent discussion of the manner in which paper responds to a load in terms of stress, strain, and time. The total deformation at any time following the application of a load can be divided into three general types of response: the immediate elastic deformation, the delayed elastic deformation, and the nonrecoverable deformation.

Immediate elastic deformation is considered to occur instantaneously with the application of load. It is not time dependent and is considered to be recovered instantly upon removal of the load. It is the result of the deformation of primary valence bonds, the changes in primary valence bond angles, and the extensions of the various secondary bonds. The ratio of the applied stress to the immediate elastic strain is defined as the elastic modulus. In paper, which is not a perfectly elastic substance, the initial slope of the stress-strain curve is used as a measure of the elastic modulus, even though the strain may not be totally elastic.

The delayed elastic deformation is that deformation that occurs with time after the application of a load, and is recoverable (also distributed in time) after removal of the load. It is due primarily to molecular configurational changes and possibly some reversible phase changes.

Configurational elastic response involves the relative movement of molecular segments. When there is no applied stress, at equilibrium, the segment movements do not result in a shape change. When a stress is applied, the segment movements are biased in a direction tending to relieve the stress. Upon removal of the stress, the molecules tend to return to their original orientation in a time-dependent manner.

Nonrecoverable or plastic deformation is defined as that portion of the total deformation that is not recoverable within reasonable periods of time at the test conditions following removal of the load. For many materials, it is associated with viscous flow, and possible irreversible crystallization. Deformation that is attributable to the transfer of entire molecules is true viscous flow and is not recoverable. Brezinski (8) stated that it was generally agreed that deformation of this type was not possible for the typical crystalline polymer because molecules were so firmly bonded in the crystalline regions that relative movement of entire molecules was restricted at these juncture points.

It is possible that nonrecoverable deformation, attributable to crystallization, might occur as a result of increased alignment of the molecular chains in amorphous areas of the polymer during loading (8). However, Ebeling (2) concluded that there appeared to be no significant changes in crystallinity involved in the apparent plastic straining of dry paper. This was based on the result that the deduced linear thermal expansion coefficient of dry papers was not affected by the previous dry straining history.

In summary, there are two basic types of deformation: the elastic (both immediate and time dependent) and plastic (not recoverable within a reasonably long time under the conditions used in testing). Elastic deformation is primarily associated with the individual fibers, whereas plastic deformation can be associated with both individual fibers and fiber-to-fiber bonds. By studying this association, it is hoped to ascertain the relative importance of intra- and interfiber mechanisms to the response of paper to stress.

METHODS OF ANALYZING THE RELATIONSHIP BETWEEN THE STRUCTURE AND THE MECHANICAL PROPERTIES OF PAPER

The three most popular mechanical tests include the stress-relaxation test, the creep test, and the load-deformation test. The first two allow the study of time-dependent behavior at constant strain and constant stress, respectively.

In the tensile load-elongation test, it is preferable that either the load or deformation be increased at a constant rate. The test can be continued until the specimen ruptures, or it may be terminated at any point prior to rupture, thereby permitting the response to be studied during cycles of loading or unloading.

In the creep test, the external tensile load is applied rapidly and then held constant, and the deformation is measured as a function of time. The specimen continues to elongate with time as macro- and microscopic changes occur within the structure in an effort to relieve stress concentrations. This test and its interpretation have been discussed in considerable detail by Brezinski (8).

In the stress-relaxation test, the load is applied rapidly and the deformation of the specimen is held constant, and the reduction of tensile load required to keep the specimen at a constant elongation is measured. The tensile load is reduced with time as macro- and microscopic structural changes occur within the structure.

THEORIES RELATING STRUCTURAL AND MECHANICAL BEHAVIOR

There have been many theories proposed to relate the mechanical properties of paper to its structure. Although these theories deal primarily with properties in the x-y plane of the sheet, the fundamental principles are also applicable to the z-direction. Excellent comprehensive summaries of these theories have been presented by Algar (9) and Ebeling (2). Reference should be made to these works for a detailed discussion and criticism of the different theories.

Generally, the theories can be divided into two groups, according to whether they are qualitative or quantitative in nature. The description of paper in terms of mechanical analogues (systems of dashpots and springs) is not strictly a theory in the sense that it does not explain phenomena.

QUALITATIVE THEORY

A qualitative theory attempts to explain the mechanical behavior of paper through a conceptual picture of the structural changes occurring when the paper is subjected to a stress. They relate the behavior of the paper to its structure by altering the structure in various ways, such as changing fiber-to-fiber bonding, strength of fibers, etc., and observing the effect on the mechanical properties.

One theory of this kind is that of Rance (10). He proposed a comprehensive theory of the mechanical behavior of paper that centers around the strength of the interfiber bonds and the distribution of stress within the sheet. He suggested that the plastic region of the typical load-elongation curve was due to interfiber bond rupturing processes, which lead to a progressive decrease in the fraction of the sheet substance which carries the load. This resulted in an increase in the stress concentration on those units that are still firmly bonded in the network. The process was considered to be one of "progressive stress

concentration in a disintegrating medium," with final fracture occurring at a specific state of disintegration.

Some supporting evidence for the theory of interfiber bond failure was presented by Nordman and his coworkers (11-15). They studied the changes in the light-scattering properties of paper in conjunction with the load-elongation characteristics of paper. Their results showed that the increase in scattering power of paper during straining was linearly related to the energy lost in a load-unload cycle. The scattering coefficient increased only after the paper had been strained to a point corresponding roughly to the end of the elastic portion of the stress-strain curve. The increase in scattering coefficient was largely nonrecoverable and appeared to be connected with permanent strain. In analyzing the data, Nordman assumed that the energy and the change in scattering coefficient were due entirely to interfiber bond breakage. From the slopes of scattering coefficient-energy loss curves, a "bond strength value" was calculated. This method has been criticized because it ignores the separating of areas that are optically bonded only, changes in intrafiber scattering, and energy losses due to fiber deformation during straining (2, 16).

The fact that interfiber bonds do break during straining has been shown by Page, et al. (17, 18) by direct microscopic observation. It was observed that some bonds broke totally, while others showed only partial rupture during deformation. Also, it was found that the bonded area never increased when the stress was removed.

Brezinski (8) studied the viscoelasticity of paper utilizing creep tests at different relative humidities and temperatures and related these data to the tensile stress-strain relationships. He emphasized the importance of intrafiber molecular processes in determining the mechanical behavior.

Sanborn (19) expressed the relationship between inter- and intrafiber properties in his following hypothesis: "The rate of response shown by a sheet at any instant is controlled by molecular mechanisms, but this rate is altered by interfiber macroscopic effects in two ways. First, the fracture of fiber-to-fiber bonds decreases the load-bearing area, and second, it causes a stress redistribution to take place within a sheet. Neither of these phenomena can affect the fundamental mechanism by which deformation takes place, but they can alter both the rate and amount of deformation by changing the driving force (stress) to which the fiber elements within a sheet are subjected."

QUANTITATIVE THEORY

In quantitative theory, the sheet is considered as a model network structure. An attempt is made to relate the mechanical properties of the sheet to the mechanical properties of the individual fibers and the interfiber bonds. A principal difficulty lies in not being able to describe the structure of the sheet in a precise way. As a result, none of the theories are adequate for a satisfactory interpretation of all of the mechanical behavior of paper. Most deal with rather specific aspects and simplified models. These theories (some of which are quite complex) have been categorized and judiciously criticized by Algar (9), Van den Akker (20), and Ebeling (2).

THE z-DIRECTION PROPERTIES OF PAPER

The various methods employed to measure the bond strength of paper include film-splitting tests[1], z-direction tear tests, shear tests, and z-tensile strength

[1]This method is a dynamic, indirect z-direction tensile test in which the tensile force is provided by the splitting of a viscous film between the paper surface and the surface of the coating roll.

tests. These tests have been reviewed by Ebeling (2). In addition to the above tests on composite structures, attempts have been made to determine the shear strength of the fiber bond (21-24), either by measuring the shear strengths of the bonds between individual fibers or by measuring the shear strengths of the bond between fibers and cellulosic substrates. One feature of all the tests used to measure bond strength (including the z-tensile strength tests), is that they only provide an index of bond strength for the mechanism of bond failure involved in the test. For example, an index of bond strength determined by a z-tensile strength test may be proportional to the shear strength of a bond as determined by a shear test, but it might not be a good measure of shear bond strength because the bonds would be expected to fail differently under z-tension.

z-DIRECTION COMPRESSION

It is of interest to examine the z-direction compression behavior of fibrous structures because the same structural parameters are expected to affect the z-direction tensile behavior, at least for small strains. It is generally concluded that the primary mechanisms involved in the z-direction compression of fiber mats whether wet or dry are fiber bending, fiber compression at the points of contact, and fiber repositioning (slippage). The latter, however, would not be an important mechanism for dry paper, which is well bonded at its points of contact. Han (25) reviewed and discussed the various mechanisms of deformation of fibers in a fiber mat subjected to lateral compacting loads. The free spans, between points of contact below or above the fiber, are subjected to bending. As the deformation increases, further contacts may develop between the fibers resulting in a more dense and rigid structure.

Fiber bending has been illustrated pictorially by Spalding (26) in Fig. 1. When loading the structure under lateral compression, its response can be visualized more easily by considering the deformation of a single fiber. The fiber will deform in bending, as shown by the dotted line in the figure, and will be subjected to tensile, compressive, and shear forces.

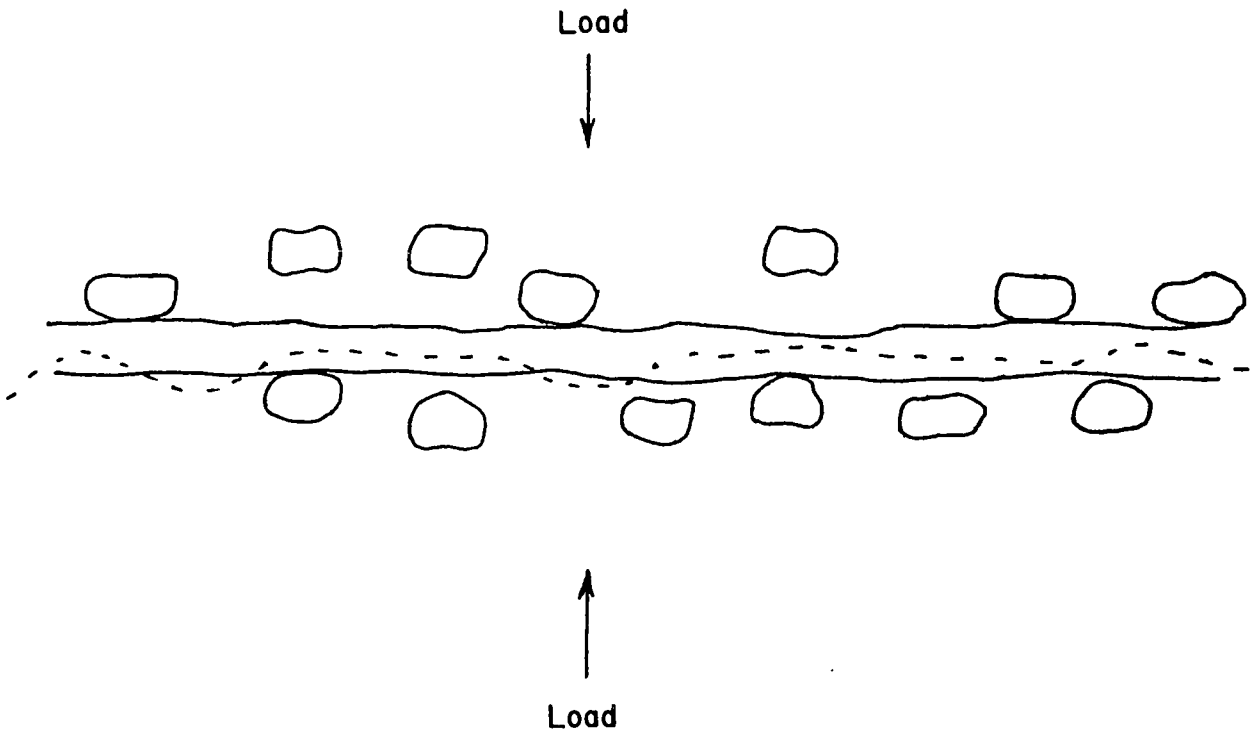

Figure 1. Simple Fiber Model Illustrating Bending Response to Compression Loading

The deformation of the fiber involves the various mechanisms of response discussed earlier (p. 11). With increased loading, there will continually be new contact points formed all along the fiber, and the stresses will be constantly changing and redistributed. As loading is continued, the character of the deformation will begin to change. This change will occur because now the fiber should begin to be compressed more along its diameter at various points

along its length. The change in character of the response will depend on the fiber properties, in addition to the initial apparent density of the fibrous structure.

This discussion has pointed out that the important fiber structural parameters affecting the compression deformation are fiber bending and resistance to transverse deformation. The important sheet structural parameter is contact area, which is proportional to the density. These should also be important parameters affecting the extension during loading in the z-direction.

z-DIRECTION EXTENSION

It is reasonable to predict that for very small strains, whether due to compression or extension, the mechanisms controlling the deformation should be similar. The true elastic modulus would be the same, whether determined by compressive loading or by loading in tension. However, for larger deformations in compressive loading, the contact area between fibers is increased, causing the load to be distributed over a larger area of contact. In tensile loading, the contact area would decrease when interfiber bond failure occurs. This would cause the load to be distributed over a smaller area of bonding. For this reason, with increasing compressive deformation, an increase in the slope of a load-deformation curve would be expected, whereas in tension, a decrease in slope might be expected. In z-direction tension, the important structural parameters expected to affect deformation and strength are the bending and transverse modulus of the fibers and the strength and area of the fiber-to-fiber bonds.

IMPORTANCE OF INTERFIBER BOND STRENGTH TO z-DIRECTION DEFORMATION

Trice (27) discussed some of the important parameters that would be expected to affect z-direction tensile strength. He pointed out that earlier

investigations have shown that the transverse tensile strength is linearly related to the scattering coefficient. Thus, the z-direction failure stress increased linearly with increasing bonded area. It has also been shown that removal of fines decreases the z-direction tensile strength to a larger extent than the in-plane tensile strength (28).

Ingmanson (29) proposed that a basic difference in stress distribution existed in the fibers during the in-plane tensile and z-tensile tests. This difference in stress distribution was used to explain the differences between z-direction tensile strength and in-plane tensile strength as functions of bonded area (Fig. 2).[2]

Ingmanson pointed out that the deviation from direct proportionality of in-plane tensile strength versus bonded area had three possible explanations, any one of which, or a combination of all three, would account for the deviation. First, at the break point in the curve, the bonding strength is approaching fiber strength, and sheet failure is caused as much by fiber failure as by bond failure. Second, as fiber bonding increases, there are increased stress concentrations at weaker spots in the sheet. The third explanation was that there might be differences in the specific strength of the fiber bonds that might account for the "saturation" effect.[3] However, based on Ingmanson's proposal that bonding strength is a linear function of bonded area, this explanation would be improbable since

[2]In this case, the film-splitting method was used as an index of bonding strength. A similar effect would be expected using the normal z-tensile test. The curves in Fig. 2 (29) are schematic and should be viewed as an indication that the bonding strength continues to increase with increasing bonded area, whereas the in-plane tensile strength does not.

[3]The author interprets this to mean that after a certain amount of increase in bonded area, the specific strength of bonds created beyond this point is less. Therefore, when the specimen is loaded in the in-plane direction, the bonds of lower specific strength are broken and the structure of the specimen is changed to one of lower bonded area.

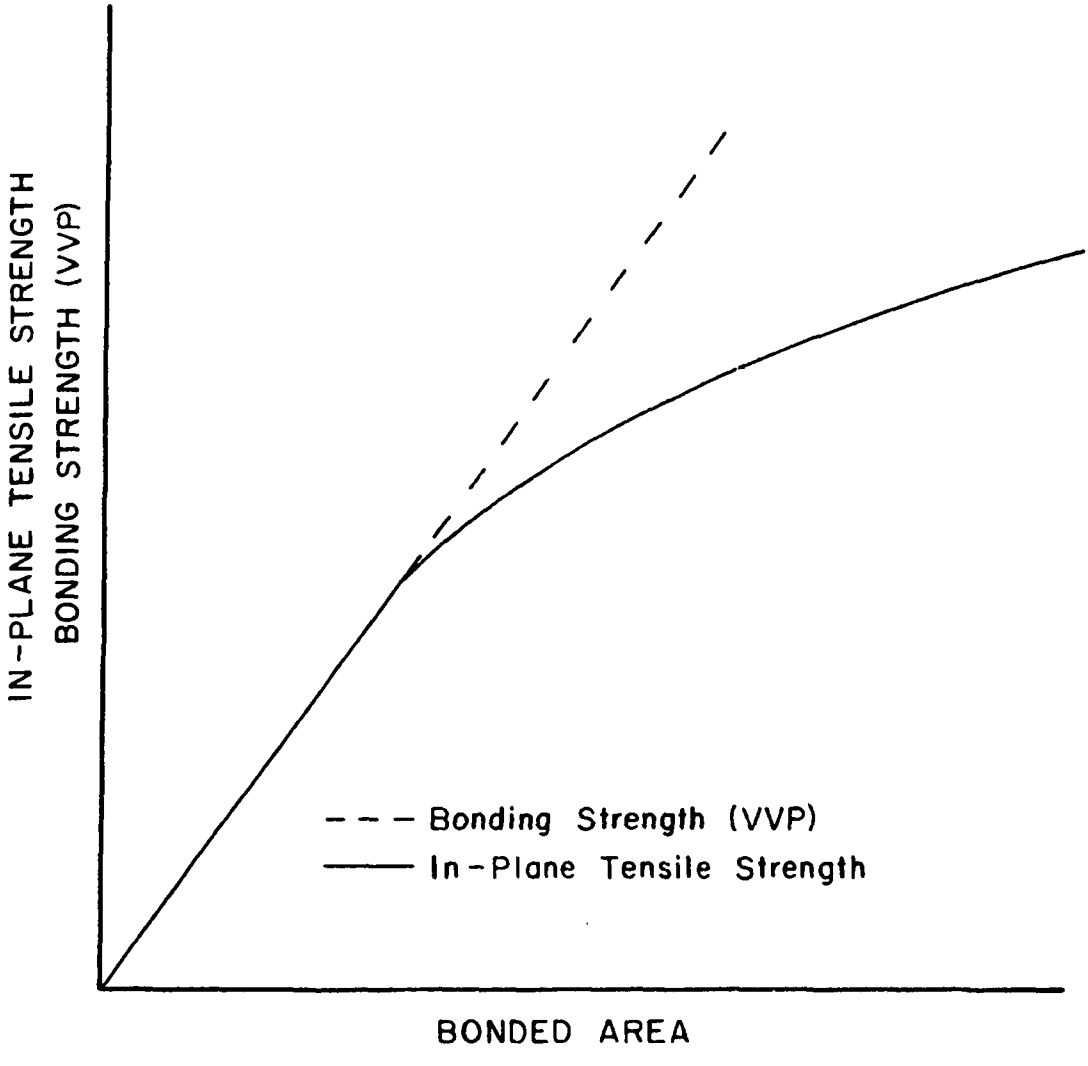

Figure 2. Comparison of In-Plane Tensile Strength and Bonding Strength Versus Bonded Area; Arbitrary Units (29)

the "saturation" effect would also be expected to influence bonding strength in the z-direction as well as bonding strength in the in-plane direction.

The question that arises is: Why does bonding strength increase in direct proportion to bonded area (Fig. 2), whereas the in-plane tensile strength does not? Ingmanson answered this question by considering the differences in stress distribution in the in-plane tensile strength and bonding strength tests. He concluded that, with increased loading, the stress concentration in the in-plane tensile test would favor fiber failure, whereas in the bonding strength test, the stress concentration would be greater in the fiber-to-fiber bond, and failure should occur there. Even though the lateral strength of individual fibers was thought to be less than the strength measured parallel to the fiber axis (30), fiber fracture should not take place in the bonding strength test because of the nature of the stress distribution. Therefore, the in-plane tensile strength-bonded area relationship was thought to deviate from a direct proportionality either because of fiber failure occurring or because of an increased stress concentration and intensification at weak areas[4], the true explanation probably being a combination of both. These two effects do not influence bonding strength, and hence there was no departure from linearity in the bonding strength-bonded area curve.

IMPORTANCE OF EXPERIMENTAL PARAMETERS TO z-DIRECTION DEFORMATION

Other important factors that might affect the measured z-direction deformation and strength values are the method of analysis and nonuniformity of structure.

[4]Although Ingmanson doesn't include the possibility of a decrease in specific bond strength with increasing bond area as a probable cause of the deviation from direct proportionality of in-plane tensile strength versus bonded area, the author feels that this concept should be included.

These problems are related to adhesive penetration[5], misalignment of pulling force, and structural nonuniformities involving basis weight and density (related to nonideal sheet-forming procedures). The experimental techniques have been steadily improved through the work of Eames (31), Kaustinen and Jappe (32), and Wink and Van Eperen (33) in working with the z-tensile test.

SUMMARY OF BACKGROUND REVIEW

The primary parameters affecting the deformation and strength of paper are the individual fiber structure, the structure of the interfiber bonds, and the manner in which the stress is distributed throughout the structure during loading. The structure of the individual fiber is important as its wet conformability and flexibility will influence its bonding potential within a sheet. The flexibility of the dry fiber is expected to affect the distribution of load and deformation within the structure. In spite of the importance of the individual fiber structure, the area and structure of the interfiber bond is expected to be the most important factor in determining z-direction tensile strength. The area, intrinsic strength and stress distribution within the bond will determine its failure resistance. Finally, the overall structure of the sheet in terms of the distribution of both fibers and bonds will affect the deformation and strength of the structure. Nonuniformity in the structure will result in a poor distribution of the load on the fibrous elements that will weaken the specimen.

The use of mechanical tests, such as load elongation, creep and creep recovery, and stress relaxation, provide the methods whereby the total response can be separated into the elastic and plastic components. This aids in determining the relative importance between intra- and interfiber properties. It is expected

[5]The specimens are adhesive bonded to two loading members for testing.

that although the response to loading of a sheet of paper at any instant is controlled by molecular mechanisms, the rate and amount of deformation will be significantly altered by interfiber bond failure.

By drawing a comparison between z-direction compression and tension response, it was speculated that the important fiber structural parameters affecting tension response were its flexibility (bending) and its resistance to bending and transverse deformation. The important sheet structural parameter was contact area, which is proportional to the density.

The z-direction is subject to the same fundamental mechanisms governing deformation and strength as the in-plane direction. However, because of the manner in which the force is applied to the structure, the relative importance of intra- and interfiber properties is expected to be considerably different.

EXPERIMENTAL

PROCEDURES

PREPARATION OF PULP

The pulp used was a Weyerhaeuser western hemlock bleached sulfite obtained in dry lap form. The pulp was refined in a 5-pound Valley beater at a consistency of 2.3% for 30 minutes with a bedplate load of 36 pounds. The S.-R. freeness was about 650.

The pulp was classified in 10-gram batches at 15 minutes per batch, using the Bauer-McNett classifier according to Institute Method 415 (34). The fractions retained on the 25- and 35-mesh screens were combined and all batches blended together. The pulp sample was dewatered in a centrifuge, placed in a polyethylene bag, and stored in a cold room for future use.

The objective was to obtain a pulp that was free of fines and composed primarily of coarse, long fibers. Handsheets were desired having sufficient strength and a relatively simple interfiber bond structure.

HANDSHEET FORMATION

Considerable effort was spent in trying to form handsheets that were uniform in structure. The problem was more difficult than usual because higher-than-normal-basis-weight handsheets were needed. This required special techniques to minimize flocculation, which might adversely affect the uniformity. It was necessary to use dilute fiber suspensions with rapid and constant forming times.

After considerable preliminary work, the technique finally considered the most satisfactory was the TAPPI Standard Method, but with a British sheet mold that had been extended in height to permit a more dilute suspension to be used. A Lucite cylinder fixed to the top of the standard sheet mold increased the volume of the sheet mold from 7 to 18 liters.

The following procedure was found to be satisfactory for couching the wet handsheet from the wire of the sheet mold:

1. The wet handsheet plus wire-covered septum was removed from the British sheet mold and placed (handsheet face down) on a single sheet of damp Whatman No. 1 filter paper that was backed by a damp blotter.
2. The couch roll was placed on the back of the mold and couched 5 times to transfer the handsheet to the damp filter paper and blotter.
3. The handsheet was covered with another damp filter paper and damp blotter.

The sandwich (damp blotter, damp filter paper, wet handsheet, damp filter paper, damp blotter) was then ready to be pressure dried.

PRESSURE DRYING HANDSHEETS

The handsheets were dried under pressure to obtain a smoother surface and greater interfiber bonding. The procedure was similar to that used by Sanborn (19):

1. The wet sandwich was placed between 8 dry blotters (4 on each side) and pressed for 5 minutes at the desired pressure.

2. The filter paper-handsheet-filter paper sandwich from Step 1 was then removed and pressed again between 8 new blotters for 10 minutes. This procedure was repeated for 15- and 30-minute pressing times, using new blotters at each pressing. A final pressing of 5 minutes between the Whatman No. 1 filter papers only was conducted to improve surface smoothness. When several handsheets were pressed at the same time, a stainless steel plate was placed between each group of 8 blotters.
3. The handsheets were conditioned between rings in a constant-temperature and -humidity room (73°F. and 50% R.H.) at least overnight prior to preparation for testing. A 36-kilogram load was placed on the rings to insure uniform restraint around the circumference of the sheet during conditioning.

CHARACTERIZATION OF TEST SPECIMENS

Individual (1-¼ inch) diameter specimens were cut with a die from the handsheets. Each specimen was weighed at 50% R.H. after cutting to determine individual basis weight. Specimen caliper was determined by measurement of the thickness of each specimen at five positions and reported as averages. The Federal gage was used at a pressure of 50 p.s.i. on a 3/16-inch diameter anvil. The density was calculated from the basis weight and thickness.

The pertinent data relating to the specimens are given in Table I. Two general classes of handsheets were prepared: those dried under a compacting stress of 3.5 kg./cm.^{2} (I), and those dried under a compacting stress of 7.0 kg./cm.^{2} (II). The letter following the Roman numeral identifies the individual specimen with respect to the handsheet from which it was cut. The Arabic numerals identify the individual specimen within the same handsheet. For

TABLE I

PHYSICAL PROPERTIES OF TEST SPECIMENS

Specimen	Thickness, cm.[a]	Basis Weight, g./m.^{2}	Apparent Density, g./cc.
IA 1	0.0384	330	0.862
IA 2	0.0373	322	0.863
IA 3	0.0384	332	0.866
IA 4	0.0358	310	0.866
IA 5	0.0381	330	0.865
IA 6	0.0373	320	0.857
IA 9	0.0384	336	0.877
IA11	0.0366	319	0.871
IA13	0.0374	320	0.856
IA14	0.0366	314	0.858
IB 4	0.0389	333	0.857
IB 5	0.0376	330	0.878
IB 6	0.0376	324	0.863
IB 7	0.0376	327	0.869
IB 8	0.0378	331	0.874
IB 9	0.0381	328	0.862
IB10	0.0381	338	0.886
IC 1	0.0300	251	0.837
IC 3	0.0287	242	0.842
IC 4	0.0279	242	0.866
IC 8	0.0305	264	0.865
IC 9	0.0282	240	0.853
ID 1	0.0368	311	0.845
ID 3	0.0373	319	0.854
ID 6	0.0378	318	0.841
ID 7	0.0368	315	0.856
IE 2	0.0536	445	0.831
IE 3	0.0531	449	0.845
IE 5	0.0523	430	0.821
IE 9	0.0551	463	0.840
IF 2	0.0622	523	0.841
IF 6	0.0621	510	0.816
IF 7	0.0615	500	0.813
IF 9	0.0617	516	0.836

[a] Measured with Federal gage.

TABLE I (Continued)

PHYSICAL PROPERTIES OF TEST SPECIMENS

Specimen	Thickness, cm.	Basis Weight, g./m.^{2}	Apparent Density, g./cc.
IG 1	0.0361	308	0.853
IG 2	0.0358	304	0.850
IG 3	0.0376	321	0.854
IG 4	0.0366	302	0.827
IG 5	0.0376	325	0.865
IG 6	0.0383	327	0.853
IG 7	0.0381	328	0.861
IG 8	0.0376	325	0.865
IG 9	0.0371	315	0.850
IIA 1	0.0351	328	0.935
IIA 2	0.0361	338	0.937
IIA 3	0.0345	327	0.947
IIA 4	0.0356	331	0.931
IIA 5	0.0348	327	0.941
IIA 7	0.0338	310	0.918
IIA 9	0.0358	330	0.921
IIA11	0.0350	330	0.944
IIA12	0.0348	324	0.932
IIA13	0.0340	318	0.937
IIB 1	0.0366	332	0.909
IIB 2	0.0348	321	0.923
IIB 3	0.0361	334	0.925
IIB 4	0.0361	333	0.925
IIB 5	0.0340	315	0.925
IIB 6	0.0363	327	0.901
IIB 7	0.0353	323	0.915
IIB 8	0.0363	332	0.913
IIB 9	0.0361	328	0.909
IIB10	0.0348	318	0.913
IIC 1	0.0342	321	0.939
IIC 2	0.0350	314	0.897
IIC 3	0.0348	316	0.908
IIC 4	0.0350	319	0.912
IIC 5	0.0340	310	0.912
IIC 6	0.0343	310	0.904
IIC 7	0.0350	321	0.917
IIC 8	0.0353	321	0.908
IIC 9	0.0361	325	0.899
RDD 1[b]	0.0269	289	1.07
RDD 2	0.0274	293	1.07
RDD 3	0.0272	292	1.07
RDD 4	0.0274	292	1.07

[b] Rubber dental dam.

example, Specimen IIA 3 would mean Specimen No. 3 from Handsheet A that had been dried under a compacting stress of 7.0 kg./cm.^{2} Electron micrographs of the surface and light micrographs of the cross sections of typical specimens are shown in Appendix I.

SPECIMEN PREPARATION FOR z-TENSILE TESTING

The procedure followed in preparing and adhesive-bonding specimens, except for some slight modifications appropriate for the specimens used in this work, was the same as that used by Wink and Van Eperen (33). The equipment used is shown in Fig. 3 and 4. Equal parts of the adhesive components (Shell Chemical Company's Epon 907)[6] were mixed and applied to the cylinder surface at a film thickness of 5 mils, using a special jig and doctoring tool (Fig. 3). The cylinders were set aside and the adhesive allowed to precure for 45 minutes, starting from the time of mixing. This controlled penetration of the adhesive and yet provided sufficient anchorage of the specimen to the cylinder surfaces. The specimens were placed in contact with the adhesive and one cylinder in the V-groove alignment fixture (Fig. 4). Another cylinder was placed in contact with the other side of the specimen, and the entire system was subjected to a compressive stress of 0.4 kg./cm.^{2} for from 1.5 to 2 hours[7], after which time the adhesive was hard enough to permit handling. The test units were then removed and set aside for a further curing period of at least 24 hours prior to testing.

[6]This two-part epoxy resin adhesive was found by Wink and Van Eperen to be the most satisfactory, based on its ease of handling, amenability to the forming of thin films of good uniformity, adequate pot life, relatively short curing time, and relatively high viscosity.

[7]This resulted in the extrusion of an adhesive bead that protruded just slightly beyond the periphery of the cylinders.

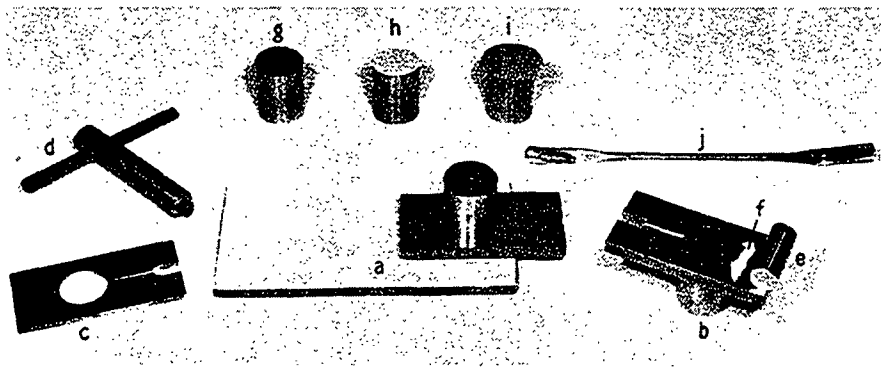

Figure 3. Equipment Used for Applying the Adhesive Film to the Cylinder Surfaces (33): (a) Jig and Cylinder Assembled on Glass Plate, (b) Cylinder Aligned in Jig with Doctoring Tool and Adhesive Bead Ready, for Spreading, (c) Jig (One Required), (d) Key, (e) Doctoring Tool, (f) Adhesive Bead, (g) Clean Cylinder, (h) Cylinder with Adhesive Film on Surface, (i) Cylinder with Adhesive Film and Specimen on Surface, and (j) Spatula

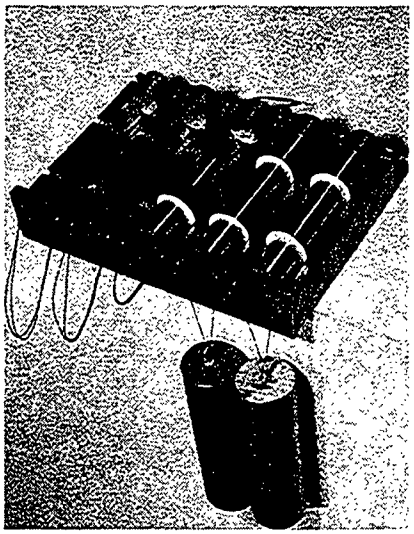

Figure 4. V-Grooved Alignment Fixture in Which the Specimen and Cylinders are Assembled and Subjected to Compressive Dead-Weight Load (33)

APPARATUS

An overall view of the experimental apparatus with the associated electronic equipment, and a close-up view of the specimen area of the z-Tensile Apparatus are shown in Fig. 5 and 6, respectively. This equipment was used for both constant rate of loading and creep testing. The working principle of the system is that of a lever-arm balance. The mechanical advantage that can be obtained with this particular equipment is about 10:1. The maximum load capability was about 250 kg.

The rate of loading was regulated by a Minarik Motor Speed Control, SH-54[8] (A), in conjunction with a Bodine motor, NSH-54[9] (B). This system raises or lowers the chain (C) at the end of the lever arm at various speeds to produce the desired rate of loading on the specimen (D). Three chains in parallel can be used if necessary.

The load on the specimen was measured continuously with a Model 911 load cell (E) in conjunction with a DG-600D series Dynagage[10]. This load cell is equipped with a load-sensitive stud, and contains a capacitance plate coupled to a specially designed line-matching transformer to provide good linearity. The output of the Dynagage was recorded on the y-axis of the Model 2D3 Autograf x-y recorder[11] (F).

[8]Minarik Electric Co., Los Angeles, Calif.

[9]Bodine Electric Co., Chicago, Ill.

[10]Dynasciences Corporation, Chatsworth, Calif.

[11]F. L. Mosely Co., Pasadena, Calif.

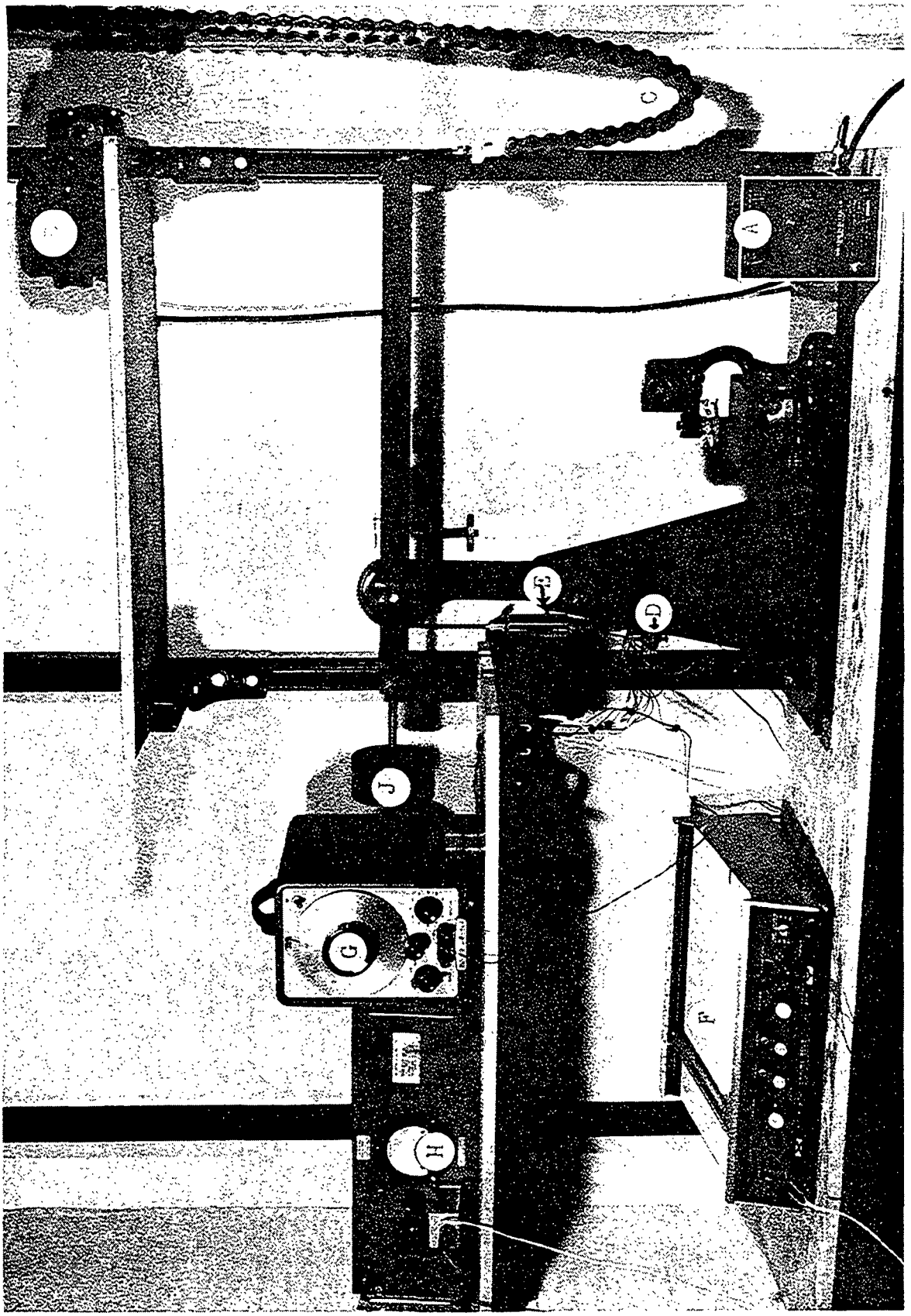

Figure 5. z-Tensile Apparatus (ZTA) for Measuring Mechanical Properties in the z-Direction

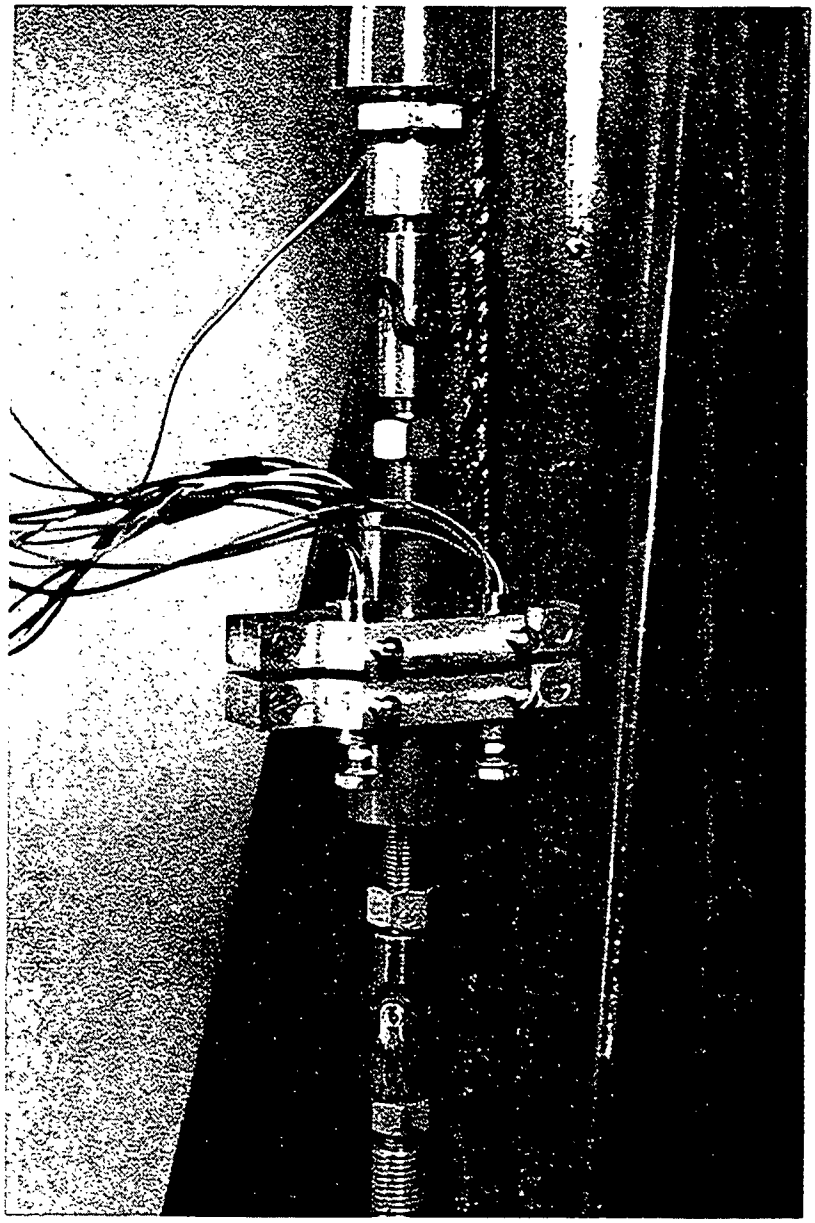

Figure 6. Close-up View of the Clamping and Displacement Sensing Equipment of the z-Tensile Apparatus (ZTA)

z-Direction deformation was measured with linear variable differential transformers[12] (LVDT's) attached to the loading cylinders at 120° angles around its periphery (Fig. 6). The LVDT is an electromagnetic device that will sense the position of a magnetic armature within a core (composed of primary and secondary coils). The primary coil was energized by the AC source (G), and the voltages were induced in the two secondary coils. The output voltage of the LVDT, which is a linear function of the magnetic armature displacement within a limited range, was amplified and converted into a d.c. signal at (H). This signal was then recorded on the x-axis of the x-y recorder (F).

CALIBRATION OF APPARATUS

Load Cell

The load cell was calibrated directly on the apparatus by substituting a rod, on which weights could be hung, in place of the adjustable screw. The rod passed through a hole drilled in the base plate and connected directly to the load cell. The output at the load recorder was proportional to the dead weight on the load cell. Depending on the desired sensitivity, the output could be varied according to the full-scale setting on the recorder.

A characteristic load-calibration curve is shown in Fig. 7. Three different calibrations gave results of 0.612, 0.618, and 0.627 kg./chart division when the recorder was set at 1 volt full scale. The calibration was checked several times during the experimental period.

Calibration of the chain-loading mechanism indicated that the rate of loading was linear except at the minimum and maximum extension of the chain.

[12]Columbia Research Laboratories, Woodlyn, Pa.

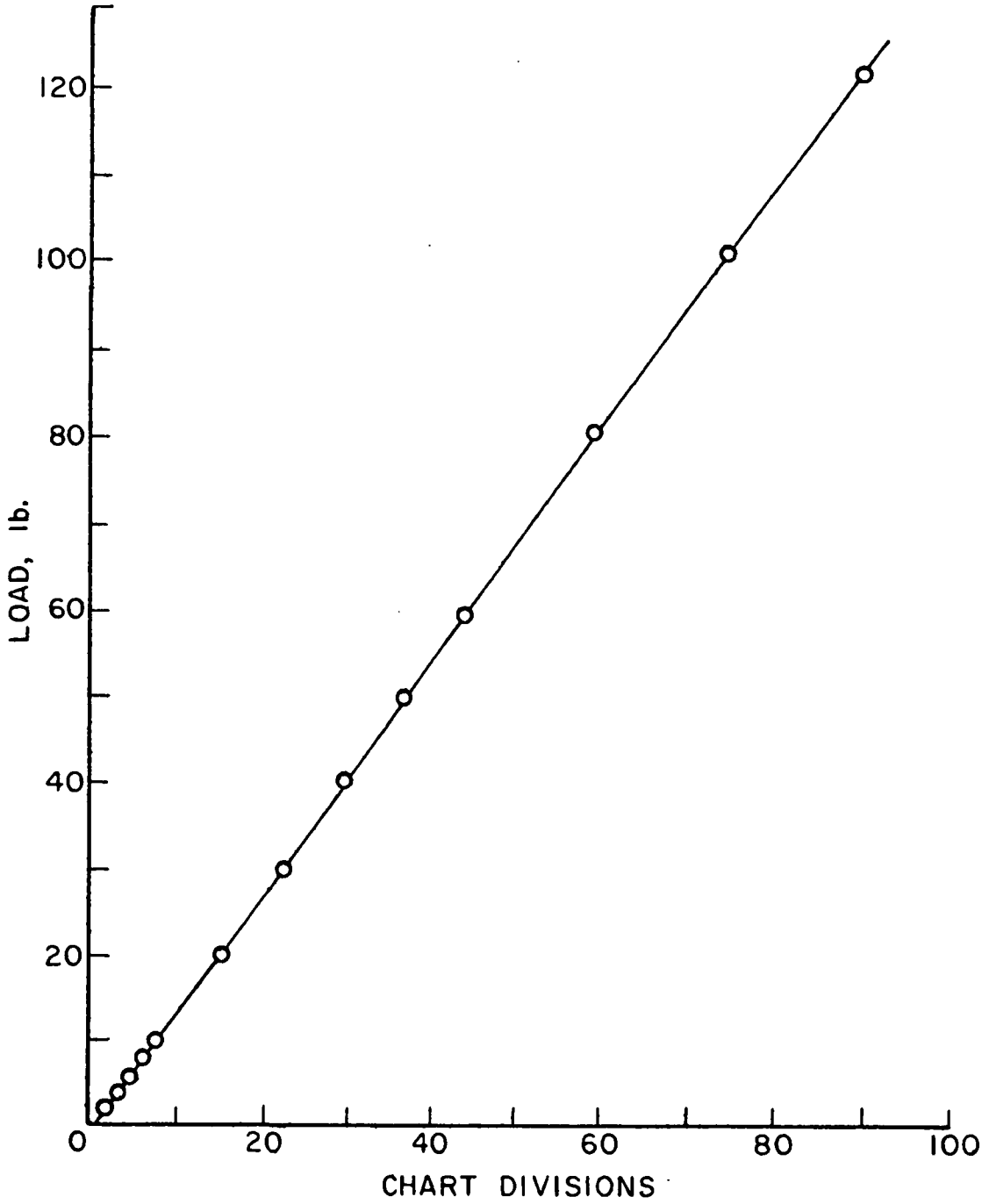

Figure 7. Load-Cell Calibration Curve Settings: Tuning Indicator, 37; Attenuater, G; Full-Scale Load Recorder, 1 Volt

Using the counterbalance (Fig. 5, J), it was possible to adjust the system so that it would be linear over various ranges of load.

LVDT's

The LVDT's used to measure deformation were calibrated with the apparatus shown in Fig. 8, which utilized the calibrated vertical movement of a microscope to displace the probes within the transformer cores. This simulates the actual testing conditions.

The probes (or magnetic armatures) of the LVDT's were fixed to the steel cylinder placed on the stage of the microscope at (A). The respective cores were fixed to the movable part (B), which is normally used to raise and lower the objective lenses in microscopic work. Vertical movement, and hence the displacement of the probe within the core (probes shown out of the cores) could be determined by the vernier scale (C), which is graduated in divisions corresponding to 2.5 μm.[13] The technique provided a means of correlating the output on the elongation axis of the recorder with known displacements of the probes in the transformer cores.[14]

Calibration curves for the three LVDT's are shown in Fig. 9-11. The average curves for each of the three LVDT's gave results of 0.131, 0.132, and 0.132 μm./chart division for LVDT's 1, 2, and 3, respectively. It is estimated that the displacement can be accurately measured within about ±3% of these values. The combined average of the three LVDT's (0.132 μm.) was satisfactory for the purposes of this work.

[13]This was calibrated with a Federal gage and shown to be accurate.

[14]Repeated tests showed that the position of the probes with respect to the inner core wall had no significant effect on the calibrations.

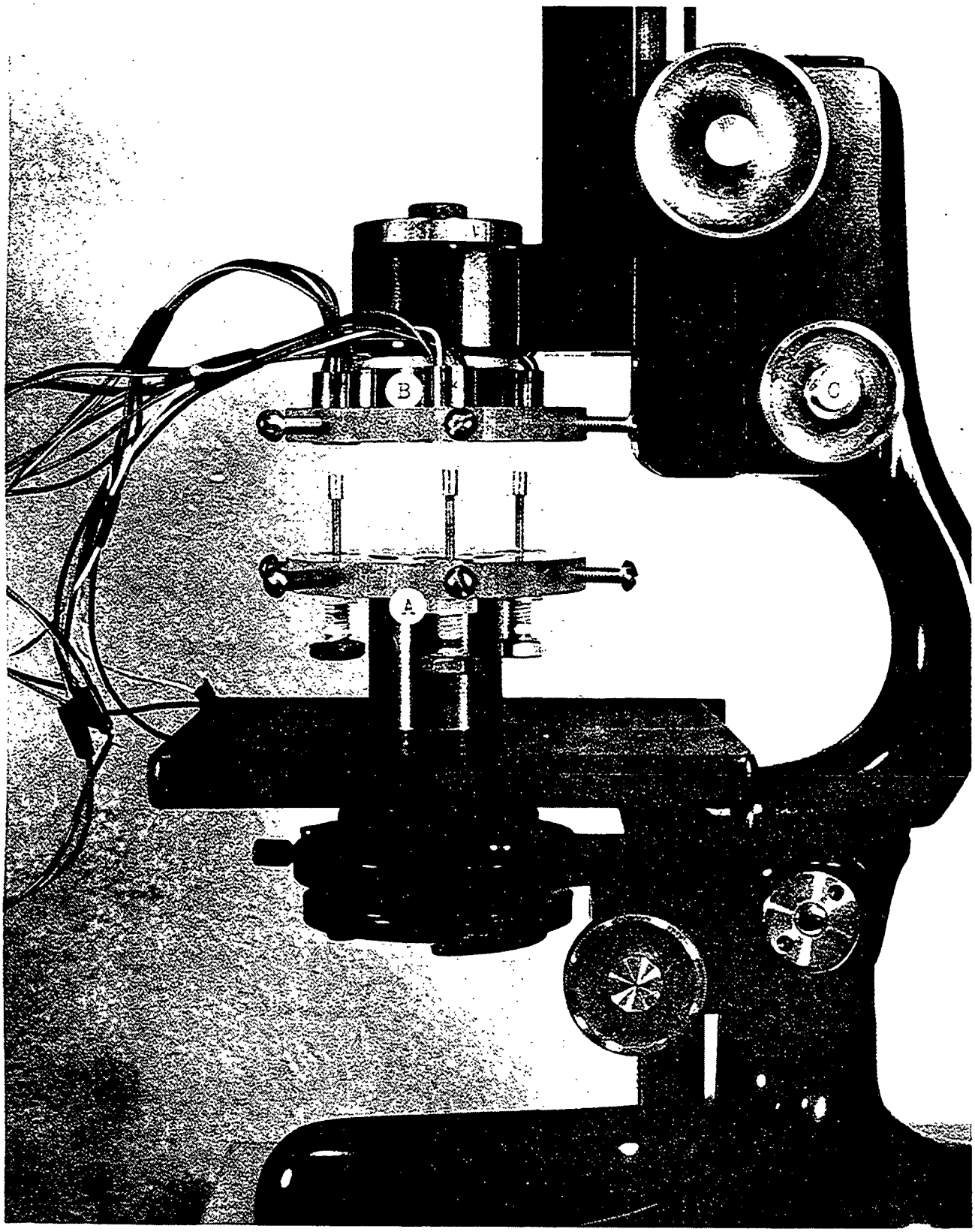

Figure 8. Apparatus for Calibrating LVDT's

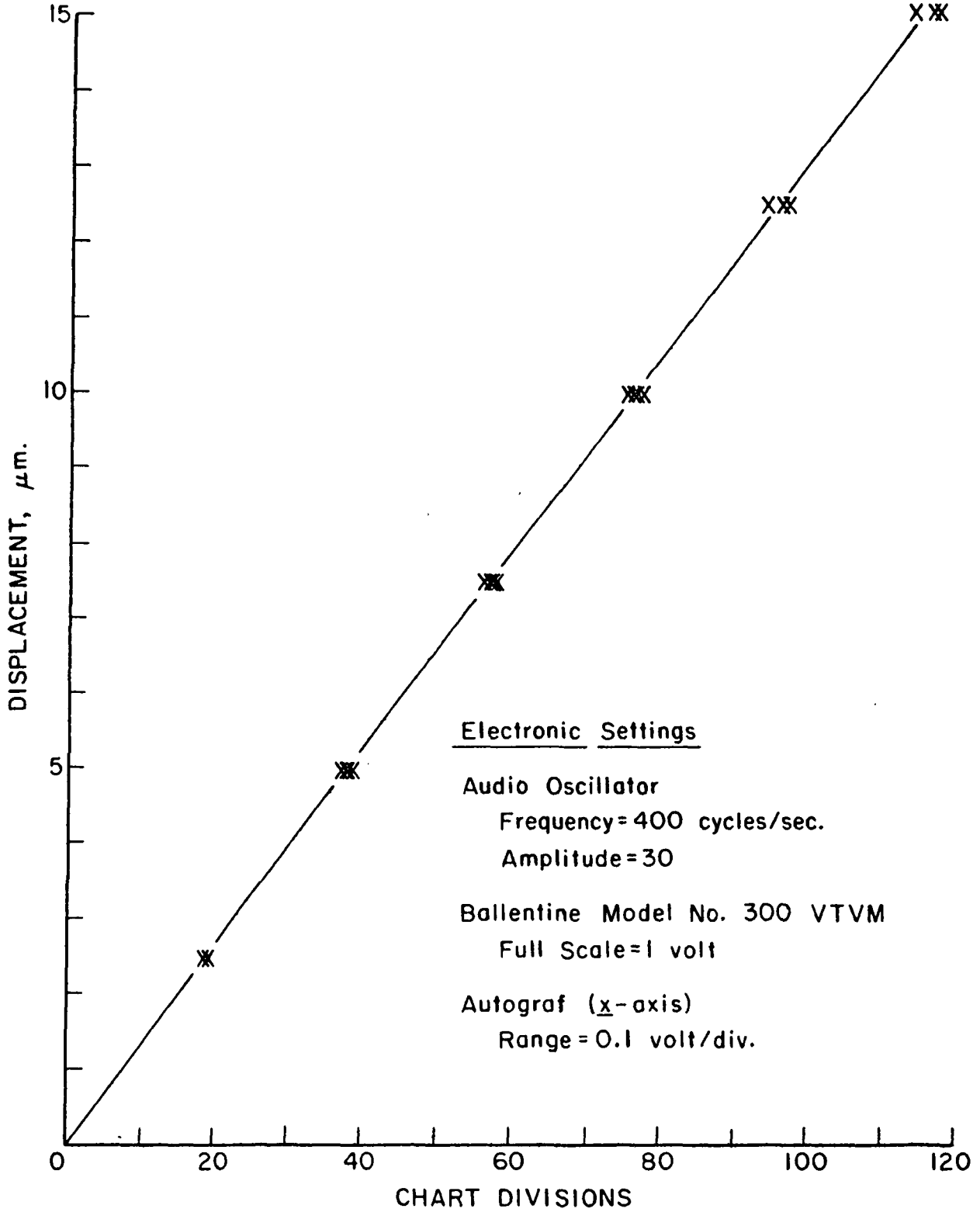

Figure 9. Calibration Curve for LVDT No. 1. At Least 3 Points at Each Displacement

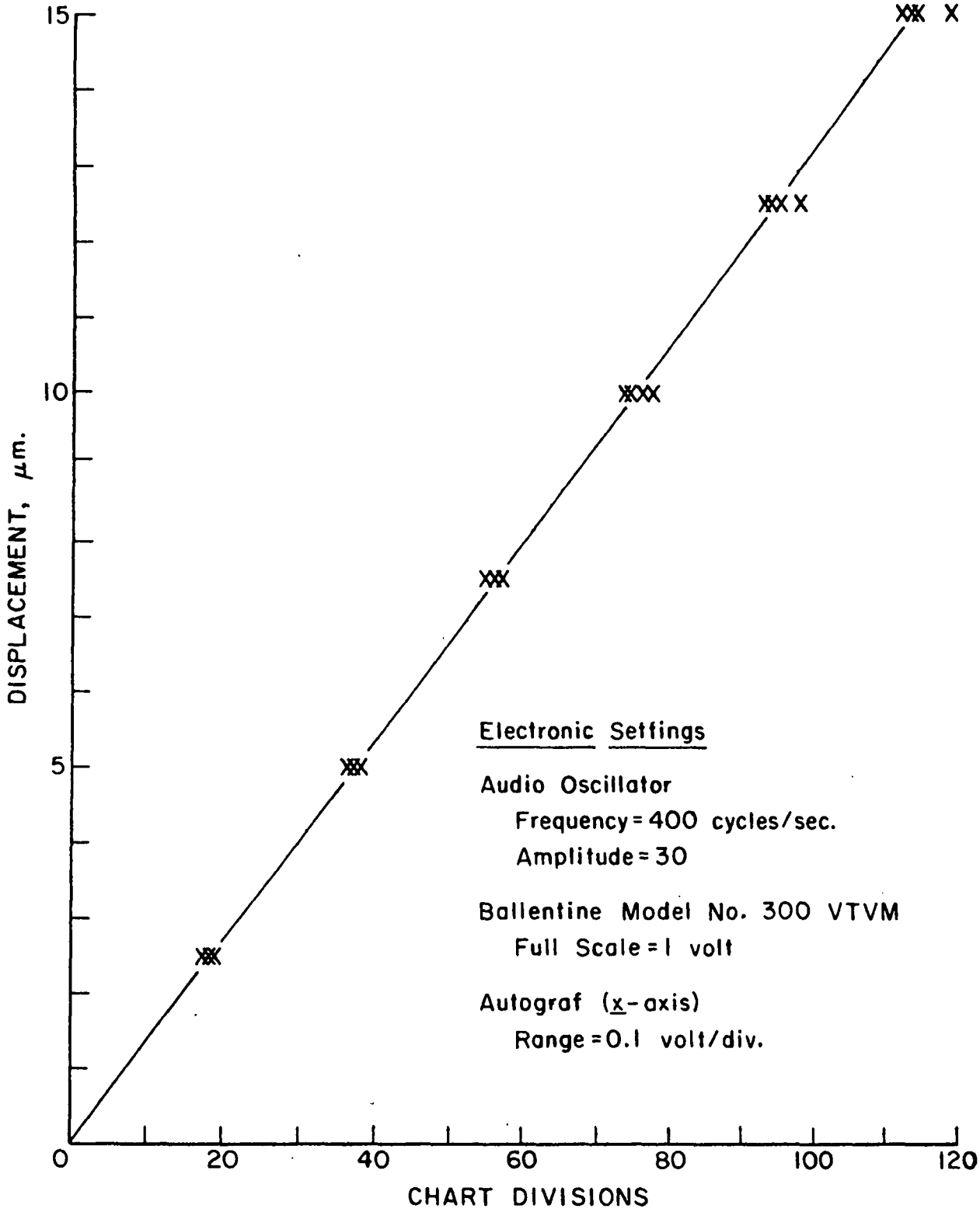

Figure 10. Calibration Curve for LVDT No. 2. At Least 3 Points at Each Displacement

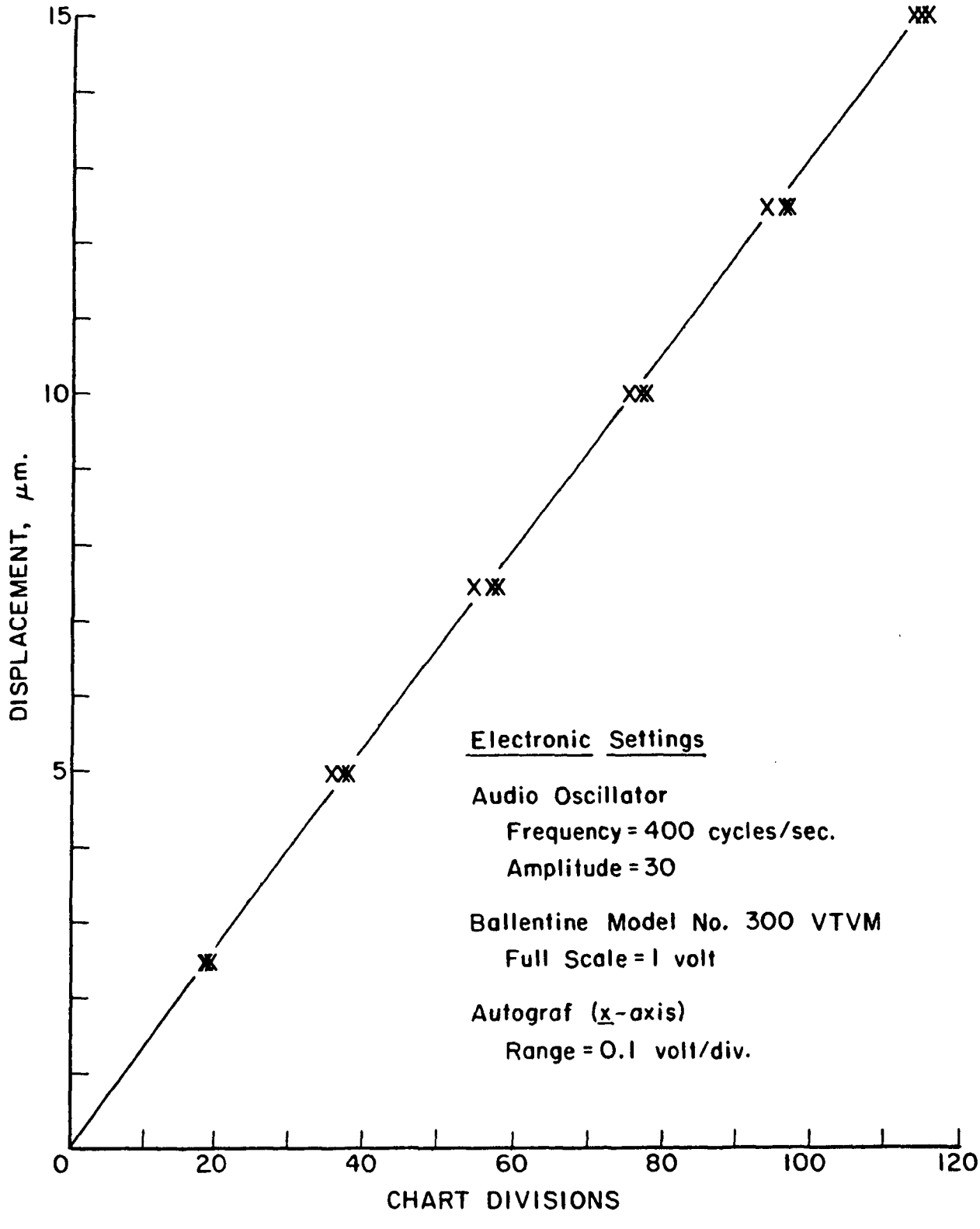

Figure 11. Calibration Curve for LVDT No. 3. At Least 3 Points at Each Displacement

TESTING PROCEDURE

The displacement jig holding the probe and core components of the LVDT's was fixed to the loading cylinders on either side of the adhesive-bonded specimen (Fig. 6). Because of a slight nonlinearity close to the null point, the positions of the probes were adjusted with the screws [Fig. 8, at approximately one microscope division away from the null point (located at the core center)].[15] A three-way switch, located on the control panel (not shown), allowed the circuitry to be transferred from one LVDT to another. The typical output on the x-y recorder was therefore three intermittently plotted load-elongation curves with alternating gaps (Fig. 12).[16]

STRESS-INDUCED CHANGES IN LIGHT SCATTERING

In addition to the methods used to prepare the specimens for normal z-tensile testing, special techniques were also employed to measure stress-induced changes in light scattering. The procedure was to obtain transmittance and reflectance data before and after subjecting a specimen to particular stress levels in order to determine how z-direction loading affected the light-scattering properties of the paper. This technique was expected to provide evidence of interfiber bond failure that might be occurring during the deformation process. (See Appendix II for theory.)

[15] Adjusting the starting point so that the probes were approximately one microscope division (2.5 μm.) from the null point insured that the probes were in the best linear portion of the calibration curve.

[16] When creep data were being gathered, the load was held constant and the deformation output was recorded as a function of time on a Model ELLOIS Esterline-Angus recorder. Displacement was calibrated using the same techniques described for the Autograf recorder. The average calibration for the three LVDT's was 0.120 μm./division at 50 mv. full scale.

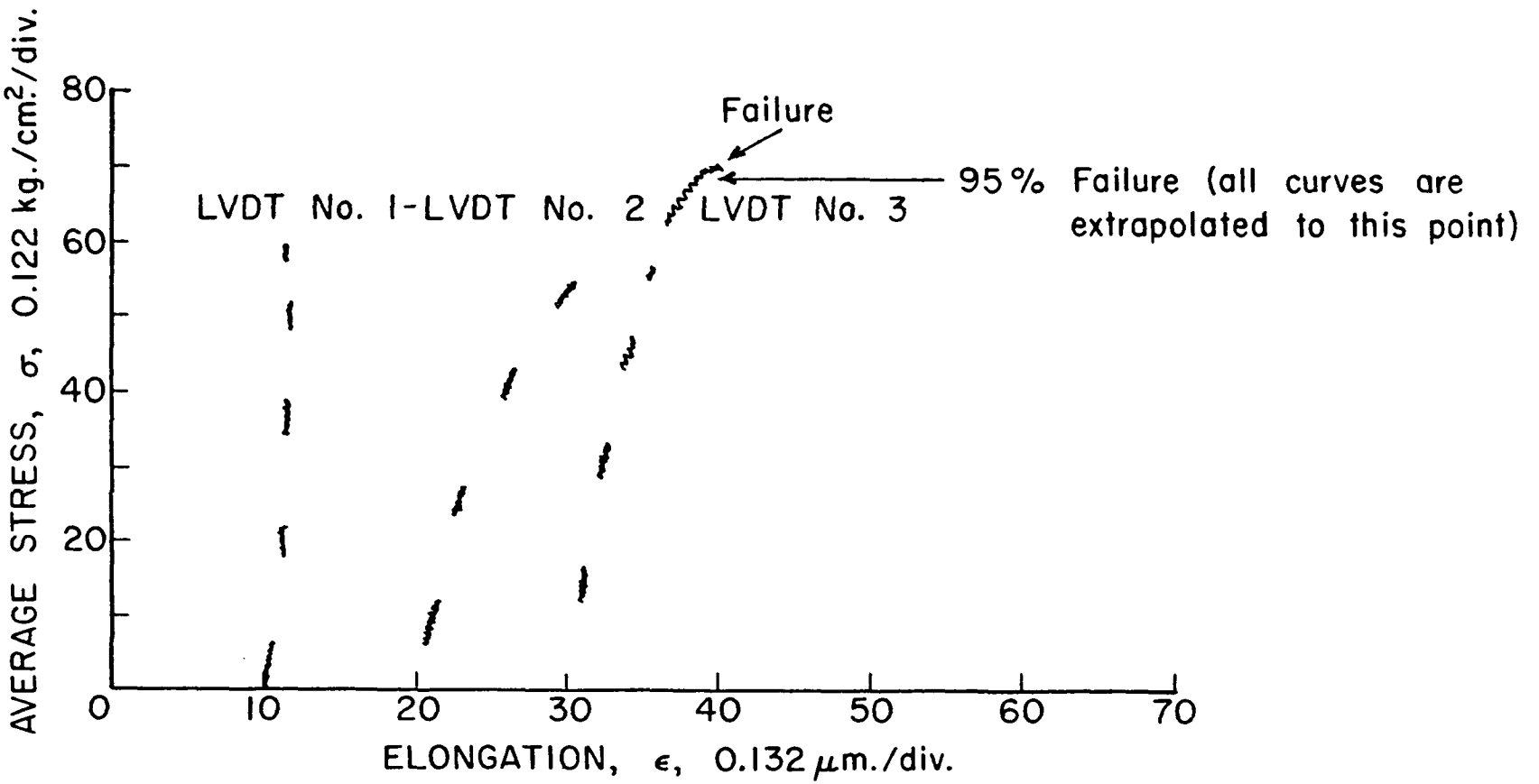

Figure 12. Typical Recorder Output for the Individual LVDT's During a Normal Test Run; Specimen IIA1. The Intersection of the Curves with the Horizontal Axis Represents the Position of the Probes in Their Respective Cores at Zero Stress and Strain

In order to measure stress-induced changes in light-scattering properties, there had to be modifications of the normal specimen preparation and testing procedures. A clear adhesive (Ecobond 45-clear)[17] was used, and the specimens were sandwiched between Lucite disks, which could then be fixed to the loading cylinders with two-sided tape.[18] The objective was to obtain a specimen that could be loaded between the steel cylinders in the ZTA and then removed to measure light-scattering properties with the General Electric Recording Spectrophotometer (GERS). This system and the special jigs for adapting to the GERS are shown in Fig. 13 and 14.

The procedure for obtaining the light-scattering data was as follows:

1. The transmittance ($\underline{T}$) and reflectance ($\underline{R}_o$) of 1.5-inch square specimens were measured on the GERS according to standard procedures.[19]
2. The specimens for testing on the ZTA were die-cut from the squares, the weight and thickness measured, and the basis weight determined.
3. The specimens were adhesive bonded between Lucite disks with Ecobond 45-clear and $\underline{T}$ and $\underline{R}_o$ of this Lucite-specimen-Lucite sandwich[20] were measured (Fig. 14).

[17] Emerson and Cuming, Inc. Dielectric Materials Division, Canton, Mass. There was no significant change in mechanical behavior when this adhesive was used instead of the usual Epon 907. Mixing conditions were the same except that Ecobond 45 was allowed to precure for 3 hours and remained under the compressive stress for 5 hours because of its longer curing time.

[18] Scotch Double Coated Tape No. 401.

[19] Wavelength of light = 650 nm. Reflectance of MgO standard = 0.991. Area of specimen illuminated = $\underline{T}$ = 0.2 in.^{2}; $\underline{R}_o$ = 0.6 in.^{2}

[20] $\underline{T}$ and $\underline{R}_o$ in this system, because of modifications, should not be considered the same as the values required for the Kubelka-Munk theory. However, the change in scattering coefficient determined from the measured $\underline{T}$ and $\underline{R}_o$ should be a satisfactory index of changes of bond area.

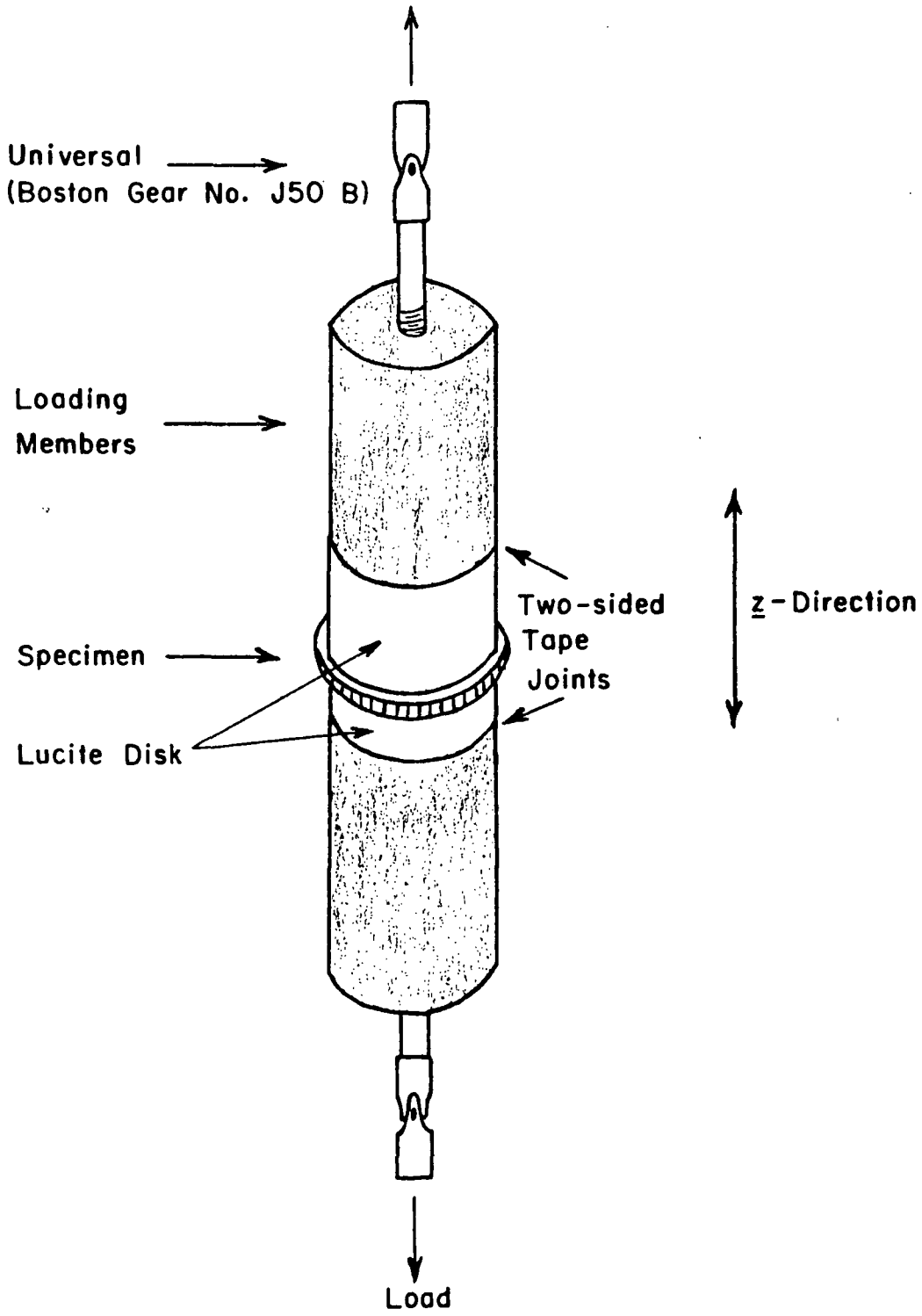

Figure 13. Loading System for Determining Stress-Induced Changes in Light-Scattering Properties

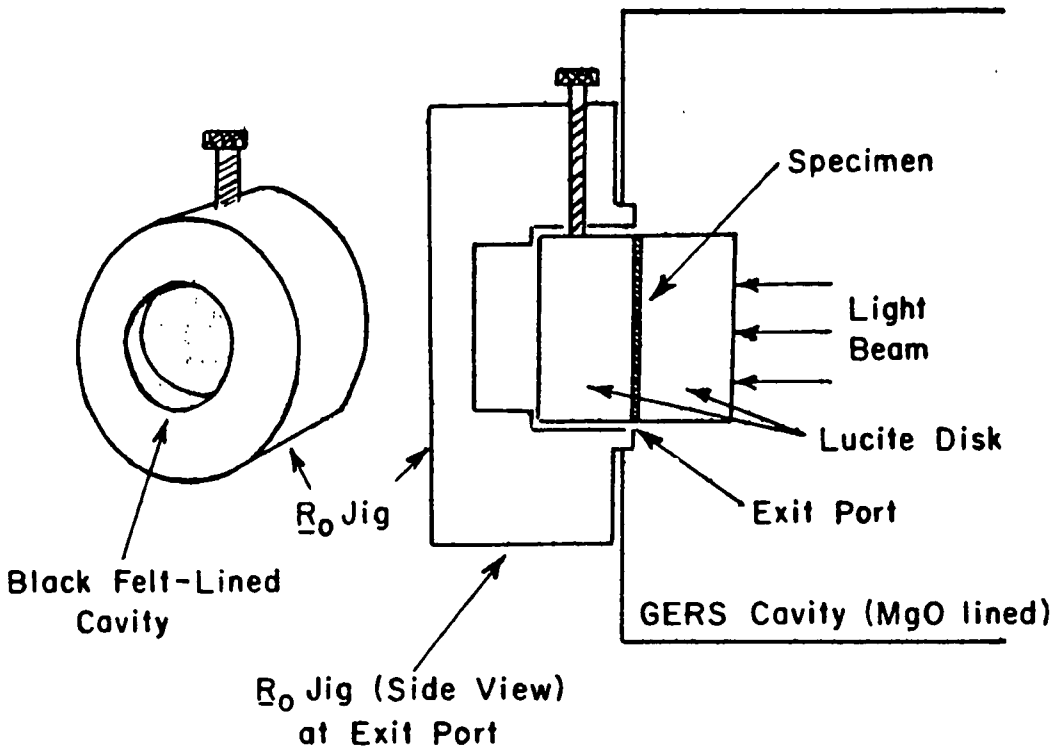

A. Jig for Holding Specimen (Between Lucite Cylinders) at Exit Port of GERS to Measure R_o

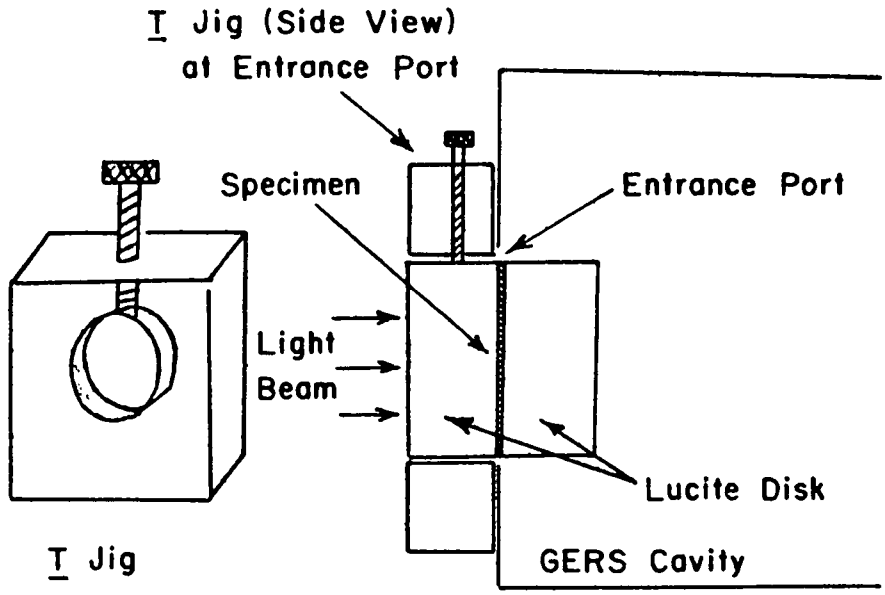

B. Jig for Measuring T of Specimen (Between Lucite Cylinders) at Entrance Port of GERS

Figure 14. Equipment for Determining Stress-Induced Changes in Light-Scattering Properties

4. The sandwich was mounted between the steel loading cylinders with two-sided tape, and the desired load applied.
5. A razor blade was used (as a wedge) to carefully remove the Lucite sandwich from between the steel cylinders, and $\underline{T}$ and $\underline{R}_o$ were again measured.
6. From the $\underline{T}$ and $\underline{R}_o$ values, the change in scattering coefficient due to loading was calculated.

PRESENTATION OF DATA AND DISCUSSION OF RESULTS

ADHESIVE PENETRATION AND INITIAL SPAN

In the acquisition of z-tensile data on paper specimens, the specimen is adhesive bonded to metal cylinders. There are two principal problems which result in the securing of specimens for testing in this way: the extent to which adhesive penetrates the porous structure and the roughness of the specimens. Both factors affect the amount and the distribution of the substance between the stressing cylinders that must deform to match the separation of the cylinder. An uncertainty exists, therefore, in amount of fibrous substance involved in strain. The extension which is measured is the separation of the metal cylinders. It will be essentially the separation of the surfaces of the epoxy. Variations in the apparent initial span from point to point will lead to different strains and therefore to different forces over local areas.

The extent of adhesive penetration into the sheet can be viewed by microtome sectioning of specimens as prepared and tested with adhesive in place at the two surfaces. Debonding at the cylinder-adhesive interfaces is possible by soaking in methyl alcohol for a period of 30 minutes. A typical section is illustrated by the example of Fig. 15 for a handsheet of 315 g./m.^{2} basis weight and a caliper of 350 μm.[21] The penetration of the adhesive (dark colored) is seen to be limited to the easily penetrated surface structure. No penetration is noted in the more compact portions of the structure. Nonetheless, because of surface pits and normal roughness, there are local areas where the effective span between the two adhesive layers is only about 80% of the average span. An estimate of

[21] Determined with Federal gage at a pressure of 50 p.s.i. The caliper is approximately the same whether determined with the Federal gage or measured directly from the micrographs.

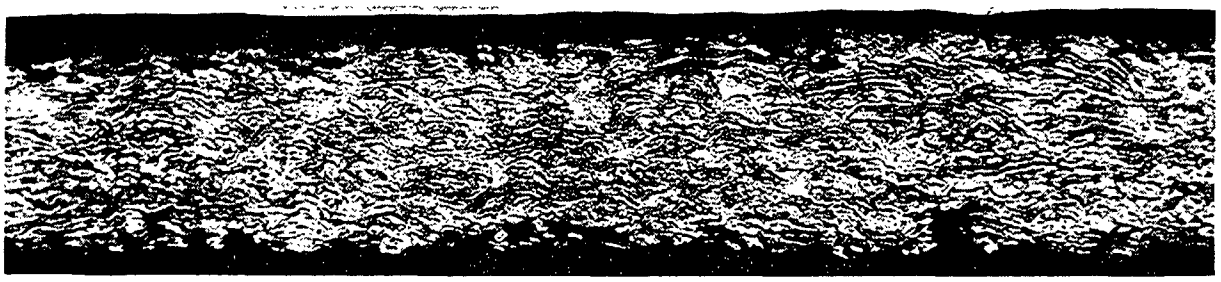

Magnification = 75X

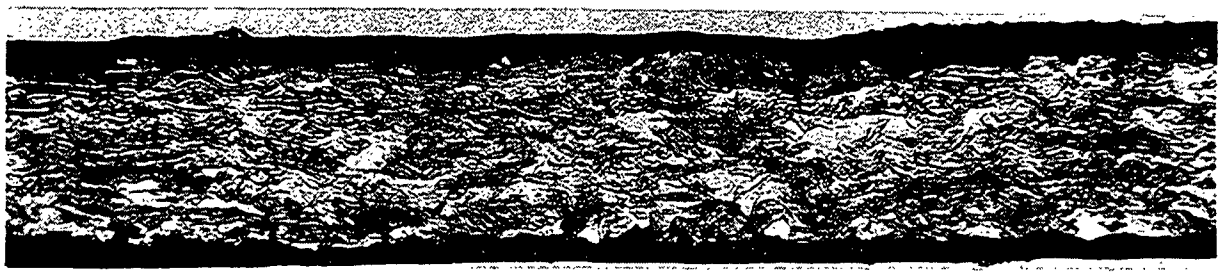

Magnification = 75X

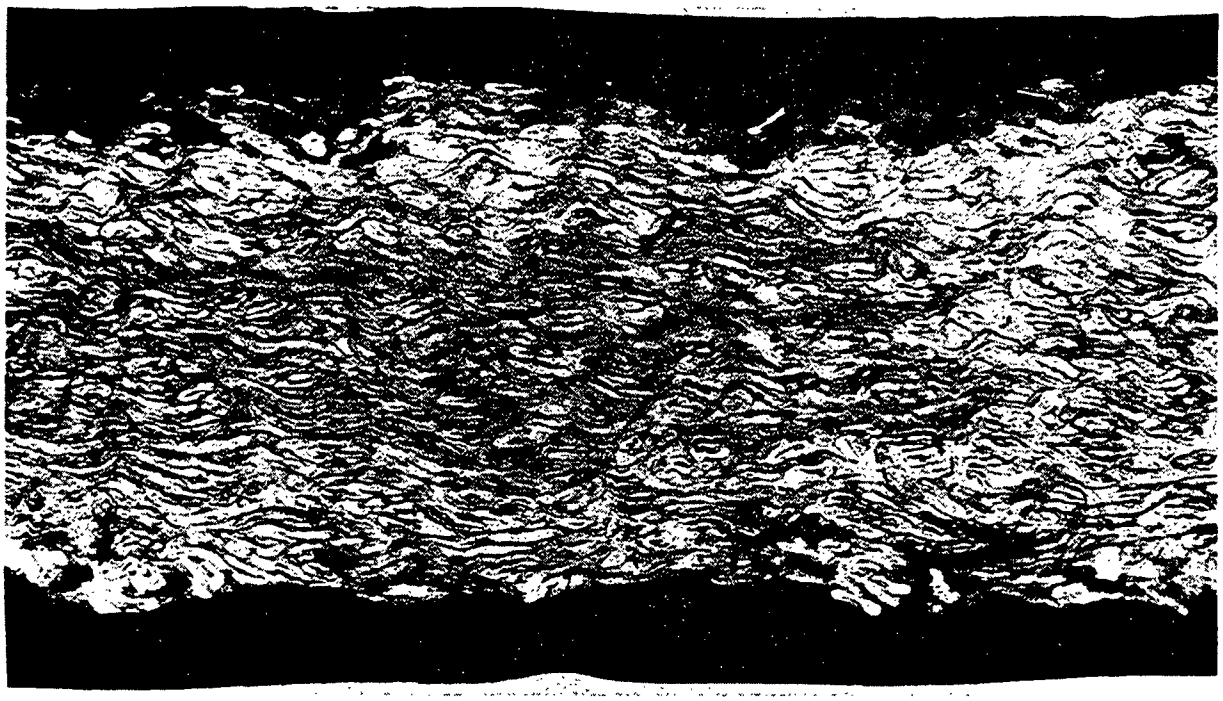

Magnification = 185X

Figure 15. Light Micrographs of the Typical Cross Section of an Adhesive-Bonded Specimen Illustrating Adhesive Penetration. These Specimens were Pressure Dried at 3.5 kg./cm.^{2}, and Have Already Been Loaded to Failure in the z-Direction

the average amount of fiber at each surface which is immobilized by the adhesive and unavailable as part of the test specimen is difficult to obtain from such photographs. The differences between the outermost parallel planes, which just bracket the fibrous structure (touching only the highest spots of the two paper surfaces), and the parallel planes, which just exclude all visible adhesive, is appreciable for this specimen with a ratio of dimension of 8 to 5. Thus, hypothetically, the test spans can vary over this range. If the fibrous substance were of similar structure and properties, strains and stresses would vary over the same range.

NONUNIFORM DEFORMATION

It became apparent, after some preliminary work with a single LVDT, that the deformation might be nonuniform over the specimen surface. This was confirmed when three LVDT's were positioned around the periphery of the specimen. An example of nonuniform deformation was shown in Fig. 12. All specimens exhibited behavior of this kind to some degree.

Nonuniform deformation posed the question of whether the nonuniformity was caused by a misalignment of the pulling force or whether it was the result of nonuniform specimen properties or dimensions. Experimental work with specimens of rubber dental dam (0.0270 cm. thickness) in which the position of the specimen had been marked relative to the three LVDT's and the orientation of the displacement jig noted with respect to the specimen, supported nonuniform deformation as a characteristic property of the specimen. The pattern of deformation did not change when the specimen was rotated in the ZTA. Although it was impossible to obtain a perfect central and perpendicular alignment of the pulling force, even with universals positioned above and below the specimen, it was concluded that

any nonuniform deformation caused by misalignment was negligible and that the nonuniform deformation was caused by nonuniform structural parameters.

MATHEMATICAL TREATMENT OF THE DATA

It was concluded that nonuniform mechanical behavior was a problem that would not easily be eliminated. Data of this kind must be analyzed, therefore, as the implications this has on an interpretation of the z-direction mechanical properties is of concern. It is necessary to answer such questions as: How meaningful is the average load-deformation curve for one-inch diameter specimens determined with the experimental equipment?[22] What might the force distribution be over the specimen surface, and how might it change with load? What types of specimens are the most likely to have nonuniform behavior? In general, it is desirable to estimate the variation in stress-strain behavior within a single specimen. The following approach was adopted to reduce the data to a form suitable for describing the nonuniform elongation behavior.

To simplify the discussion, the nonuniform deformation will be referred to as a "wedge effect." The specimen is being extended in the z-direction, so as to cause the specimen to open in a wedge shape. Several simplifying assumptions had to be made that detract somewhat from the generality of the model. The technique describes the variation in strain which occurs in terms of a variation in modulus over the area of the specimen. It is assumed, then, that only modulus differences are responsible for the "wedge effect."

[22]The procedure used during the preliminary experimental work had been to simply average the displacement of the three LVDT's at given loads and use the measured average force for determining the average mechanical behavior of the one-inch diameter specimens.

The variation in strain and modulus is to be defined only along the projected axis of a line connecting the point of minimum strain to the point of maximum strain. Thus, the probable variations in modulus over the area are considered only in terms of variations along a line to conform to the one-dimensional distribution of strain along the same line (the $\bar{y}$ axis) from the minimum to the maximum points of strain, or from the closed portion of the wedge to the open portion. (See Fig. 16.)

The data of the experiment do not permit any conclusions regarding the linear variation in modulus perpendicular to this line, and hence the modulus is assumed to be constant in the $\bar{x}$ direction. This latter assumption would be valid only when the minimum and maximum points of strain remain in the same orientation during loading. (It will be shown later that this was not always the case.) Therefore, the modulus is considered to be a function of strain (the ratio of stress to strain) and a function of distance along the $\bar{y}$ axis, but constant in the $\bar{x}$ axis direction.

Before it was possible to mathematically describe the variation in modulus from the point of minimum strain to the point of maximum strain, it was necessary to establish the frame of reference as illustrated in Fig. 16 so that these points could be determined. This was accomplished by specifying the location of the LVDT's at the periphery of the specimen with reference to an arbitrary $\underline{xy}$ coordinate system. This original coordinate system was rotated through an angle, α, to form a new coordinate system, $\bar{\underline{xy}}$, in which the projection of the line running from the point of minimum strain to the point of maximum strain was along $\bar{y}$. The variation in stress and modulus can then be described as a function of $\underline{z}$ and $\bar{y}$ in the two-dimensional system. The procedure for performing this rotation is described in Appendix III.

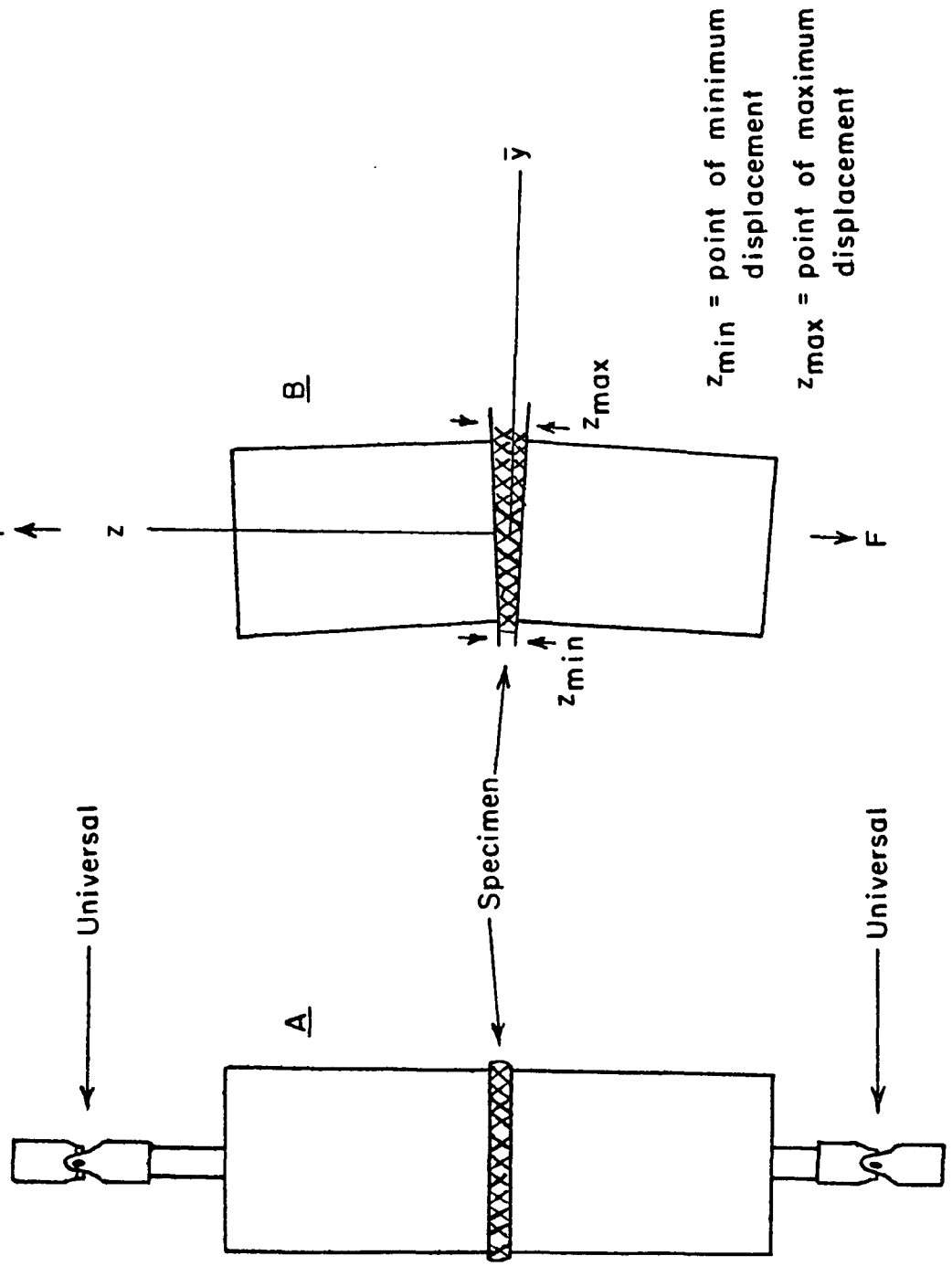

Figure 16. System Used to Describe Variation in Strain and Modulus During z-Direction Loading. Illustration Represents a Cross-Sectional View with the Plane of this Sheet Running Down Through the Center of the Cylinders. A Is the Unload System. B Illustrates the Wedge Effect During Loading, with the Closed Portion of the Wedge (z_{min}) and the Open Portion of the Wedge (z_{max}) Lying in the Same Plane

Once the system was in the proper two-dimensional frame of reference it was possible to estimate a distribution of modulus along the $\bar{y}$ axis, which could lead to the particular wedge deformation. In defining the stress, σ, as a function of strain, z, for some area, dA, along the wedge, it was assumed that a quadratic function would be satisfactory:

$$\sigma(z)_{\bar{y}} = az + bz^2 \tag{1}$$

and that a, b, and z would be linear functions of the position along the wedge (along $\bar{y}$). That is,

$$a = \gamma_1 + \gamma_3\bar{y} \tag{2}$$

$$b = \gamma_2 + \gamma_4\bar{y} \tag{3}$$

$$z = c + b'\bar{y} \tag{4}$$

where γ_1, γ_2, γ_3, and γ_4 are constants for each specimen. The displacement at the center, c, and the slope of the wedge, b', can be determined from Equations (20) and (31) in Appendix III.

Combining Equations (1), (2), (3), and (4), the stress at any position along $\bar{y}$ would be related to strain by the equation

$$\sigma(z)_{\bar{y}} = (\gamma_1 + \gamma_3\bar{y})(c + b'\bar{y}) + (\gamma_2 + \gamma_4\bar{y})(c + b'\bar{y})^2. \tag{5}$$

The equation implies that for a given specimen, a family of stress elongation curves can be calculated as a function of position along the wedge once the modulus coefficients γ_1, γ_2, γ_3, and γ_4 have been determined. The given information necessary to solve for these coefficients is: (1) the contribution to torque about the $\bar{x}$ axis at any position along $\bar{y}$ is $\gamma \cdot \sigma \cdot dA$, and (2) the contribution to the total force is $\sigma \cdot dA$. Therefore, at equilibrium,

$$\iint \bar{y}\sigma dA = 0 \tag{6}$$

$$\iint \sigma dA = F \tag{7}$$

where F is the measured load on the specimen as determined by the load cell and A is the area of the specimen under stress.[23]

By expanding Equation (5) and substituting for σ in Equations (6) and (7), one gets a system of two equations in the four unknowns (γ_1, γ_2, γ_3, and γ_4), the solution of which can be estimated through a regression analysis. The calculations are shown in Appendix IV.

Table II lists the typical information obtained for a stress-strain test on a particular specimen. The variation in α means that the coordinate system has to continually be rotated during loading so that the $\bar{y}$ axis lies along the wedge. This indicates that the wedge is not opening uniformly because of the variation in modulus along the $\bar{x}$ direction. There appears to be no consistent pattern in the variation of α, except that it usually approaches a constant value with increasing load, indicating that the specimen generally conforms to a stable orientation prior to failure.

An example of the way the data in Table II can be interpreted is[24]:

1. The increasingly negative value for b' (wedge slope) indicates that the deformation was becoming more nonuniform with loading.

[23]Because of the small wedge angle, any contribution to the force or torque arising from the distance between the specimen and the pivot point (universal) would be negligible.

[24]Note this is with respect to a negative value for b' [Equation (4)].

TABLE II

REDUCTION OF z-DIRECTION STRESS-STRAIN DATA FOR SPECIMEN IIA 1 ILLUSTRATING NONUNIFORMITY OF SPECIMEN BEHAVIOR

Average Stress, kg./cm.^{2}	Apparent Strain, %	Center Displacement, cm. $\times 10^4$	Angle of Rotation, radians	Wedge[a] Slope, $\times 10^4$
0.61	0.015	0.053		-0.008
1.22	0.031	0.110	0.68	-0.026
2.45	0.062	0.216	1.00	-0.053
3.67	0.094	0.330	1.05	-0.105
4.89	0.132	0.462	0.92	-0.168
6.11	0.185	0.647	0.91	-0.258
7.34	0.239	0.836	0.95	-0.444
8.23	0.329	1.150	0.95	-0.753

Modulus coefficients:

$$\gamma_1 = 4.39 \times 10^3 \text{ kg./cm.}^2 \pm 68 = + 1.5\%$$

$$\gamma_3 = 1.23 \times 10^3 \text{ kg./cm.}^5 \pm 1.37 \times 10^2 = + 11.0\%$$

$$\gamma_2 = -4.16 \times 10^5 \text{ kg./cm.}^2 \pm 3.76 \times 10^4 = + 9.0\%$$

$$\gamma_4 = -2.55 \times 10^4 \text{ kg./cm.}^3 \pm 6.20 \times 10^4 = + 243.0\%$$

[a] Negative values mean the open portion of the wedge was in the $-\bar{y}$ direction. Positive values mean open portion was in the positive $\bar{y}$ direction (Fig. 16).

2. The positive value for γ_3 indicates that the modulus was decreasing toward the open end of the wedge.
3. The negative value for γ_2 indicates that the modulus of the specimen was decreasing with increasing displacement.
4. The negative value for γ_4 indicates that the modulus was decreasing as a combination of effects, involving both distance toward the open end of the wedge and increasing strain.

Table III lists the coefficients describing strain and modulus variations for a number of specimens used in this work. It should be noted that in this table all values for the coefficients have been converted in sign so that they describe the modulus variation with the wedge slope, $\underline{b}'$, having a positive value in the direction of the $+\bar{\underline{y}}$ axis. The important observations to note in this table are:

1. γ_3, which describes the change in modulus along the $\bar{\underline{y}}$ axis, was always negative, which indicated that the modulus was always decreasing toward the open end of the wedge.
2. γ_2, which describes the change in modulus with displacement, was always negative, indicating that as the specimen was strained the modulus decreased.
3. γ_4, which describes the change in modulus as a combination of both distance along $\bar{\underline{y}}$ and displacement in the $\underline{z}$-direction, indicated that the modulus decreased with strain more slowly toward the open end of the wedge.

An indication of the magnitude of nonuniform mechanical behavior within a single specimen was obtained by computing stress-elongation curves at various points along the $\bar{\underline{y}}$ axis. The computed values for the modulus

TABLE III

REDUCTION OF DATA ILLUSTRATING NONUNIFORMITY IN STRAIN AND MODULUS ACCORDING TO THE MODEL EQUATION

	Specimen	Wedge Slope, $\times 10^4$	γ_1, kg./cm.^{2} $\times 10^{-3}$		γ_3, kg./cm.^{3} $\times 10^{-2}$		γ_2, kg./cm.^{2} $\times 10^{-5}$		γ_4, kg./cm.^{3} $\times 10^{-5}$	
			Value	Δ[a]	Value	Δ	Value	Δ	Value	Δ
Stress-strain	IA 1	0.526	3.78	0.070	-9.44	1.59	-5.29	0.290	2.40	0.58
	IA 2	0.794	5.07	0.139	-2.91	2.77	-7.65	0.913	5.59	1.45
	IA 3	0.098	4.14	0.138	-8.44	3.41	-6.90	0.685	3.19	1.66
	IA 4	0.138	3.55	0.030	-1.50	0.74	-4.09	0.089	3.15	0.22
	IA 5	0.569	4.77	0.079	-21.10	1.73	-8.59	0.421	6.53	0.78
	IIA 1	0.753	4.39	0.068	-12.30	1.37	-4.16	0.376	0.26	0.62
	IIA 2	0.447	5.96	0.131	-26.00	3.10	-10.56	0.623	8.15	1.26
	IIA 3	0.346	4.86	0.106	-4.84	2.43	-6.21	0.479	0.42	0.99
	IIA 4	0.762	5.61	0.057	-30.30	1.19	-8.32	0.314	6.34	0.52
	IIA 5	0.525	4.40	0.065	-9.83	1.43	-5.05	0.291	1.40	0.55
	IIB 1	0.603	5.06	0.138	-15.70	2.97	-7.69	0.729	3.78	1.31
	IIB 2	0.168	5.17	0.090	-7.86	2.20	-7.40	0.286	1.77	0.68
	IIB 3	0.456	4.62	0.047	-10.70	1.05	-6.22	0.232	2.18	0.45
	IIB 4	0.211	4.36	0.157	-7.04	3.12	-5.24	0.632	2.07	1.12
	IIB 5	0.184	4.53	0.045	-2.37	1.11	-5.60	0.167	0.38	0.39
	IIB 6	0.325	4.99	0.031	-6.73	0.72	-7.27	0.136	1.70	0.29
	IIB 7	0.438	4.75	0.042	-10.70	0.97	-6.68	0.188	2.62[b]	0.38
	IIB 8	0.146	5.22	0.067	-2.85	1.64	-7.72	0.263	-1.10[b]	0.63
	IIB 9	0.026	5.49	0.035	-1.82	0.87	-8.47	0.145	-0.72[b]	0.36
	IIB10	0.314	5.57	0.074	-9.97	1.70	-8.78	0.392	2.52	0.81
	IC 1	0.61	3.16	0.107	-12.70	2.39	-2.92	0.40	2.70	0.75
	IC 3	0.52	4.22	0.147	-18.40	2.91	-1.90	1.10	1.93	1.74
	IC 4	0.12	3.31	0.070	-2.34	1.74	-3.39	0.25	0.30	0.60

[a] Δ is the standard deviation assuming uniform weighting of Equations (39) and (40) in Appendix IV.

[b] There was a change in wedge slope just prior to failure.

TABLE III (Continued)

REDUCTION OF DATA ILLUSTRATING NONUNIFORMITY IN STRAIN AND MODULUS ACCORDING TO THE MODEL EQUATION

	Specimen	Wedge Slope, $\times 10^4$	γ_1, kg./cm.^{2} $\times 10^{-3}$		γ_3, kg./cm.^{3} $\times 10^{-2}$		γ_2, kg./cm.^{2} $\times 10^{-5}$		γ_4, kg./cm.^{3} $\times 10^{-5}$	
			Value	Δ[a]	Value	Δ	Value	Δ	Value	Δ
Stress-strain	IC 8	0.12	3.63	0.125	-11.90	3.16	-5.16	0.37	3.10	0.92
	IC 9	0.74	3.06	0.116	-16.50	2.46	-3.63	0.47	2.91	0.80
	ID 1	0.42	3.15	0.075	-5.19	1.70	-3.66	0.31	0.77	0.63
	ID 3	0.61	4.52		-23.00		-7.79		6.66	
	ID 6	0.62	3.61	0.737	-11.00	15.00	-2.04	4.74	7.66	7.88
	ID 7	0.23	3.29	0.051	-2.37	1.23	-3.71	0.19	0.29	0.44
	IE 2	1.61	2.13	0.071	-9.47	1.55	-1.86	0.23	1.25	0.40
	IE 3	2.27	1.66	0.053	-10.60	1.16	-1.41	0.12	1.38	0.22
	IE 5	0.46	2.51	0.052	-3.94	1.24	-2.28	0.19	0.50	0.42
	IE 9	1.46	2.61	0.135	-11.40	2.96	-2.96	0.48	2.10	0.83
	IF 2	1.14	3.92	0.259	-18.10	5.71	-7.17	1.24	5.56	2.23
	IF 6	1.67	2.16	0.071	-9.18	1.56	-2.03	0.24	1.36	0.42
	IF 7	1.93	2.38	0.197	-12.50	4.08	-2.23	0.75	1.64	1.23
	IF 9	0.51	2.32	0.053	-2.86	1.28	-2.27	0.15	0.51	0.34
Post creep	IB 7	1.11	2.85	0.236	-14.90	5.15	-3.36	0.75	2.84	1.83
	IB 8	1.26	3.56	0.125	-29.10	2.57	-4.13	0.52	4.34	0.82
	IB 9	0.56	3.86	0.157	-17.60	3.46	-4.56	0.91	3.30	1.65
	IB10	0.51	5.39	0.138	-26.70	3.17	-10.80	0.80	9.04	1.51
Rubber dental dam	RDD 1	0.27	2.28	0.027	-5.96	0.65	-0.62	0.13	0.75	0.27
	RDD 2	0.12	2.48	0.050	-5.01	1.24	-1.42	0.17	0.93	0.40
	RDD 3	0.13	1.78	0.026	-0.74	0.64	-0.85	0.09	1.04	0.22
	RDD 4	0.53	2.43	0.017	-11.70	0.39	-0.43	0.09	0.88	0.16

[a] Δ is the standard deviation assuming uniform weighting of Equations (39) and (40) in Appendix IV.

coefficients were substituted into Equation (5) and the equation solved for σ at various positions along $\bar{y}$. Two specimens, representing maximum and minimum degrees of nonuniform mechanical behavior, are graphically represented in Fig. 17 and 18, respectively. The letters A, B, and C, with respect to Fig. 17, specify where along the wedge the curves were computed. The variation of mechanical behavior for some of the other test specimens are shown in Appendix V.

The concept of strain variation, resulting from differences in modulus across the specimen surface, seems reasonable in view of the variability in structure. It has been demonstrated that in the in-plane direction for a 26-pound kraft sack paper, the local variation in permanent deformation could be as much as 25 times higher in one area than in another (35). By measuring the displacement between particles fixed to the surface of the paper, it was observed that the local variation from millimeter to millimeter at a permanent extension of 1.3% varied from 0.2 to 4.7%.

The data reduction describes the deformation behavior only with respect to the assumptions made and does not identify the causes. However, it does provide a technique whereby one can estimate the magnitude of variation in mechanical properties that would result in wedge-type deformation, if it was the causative factor.

LOAD-ELONGATION DATA

Load-elongation data were obtained at several basis weights and two different densities in order to characterize the viscoelastic behavior and to identify the importance of these structural parameters in affecting the z-direction deformation.

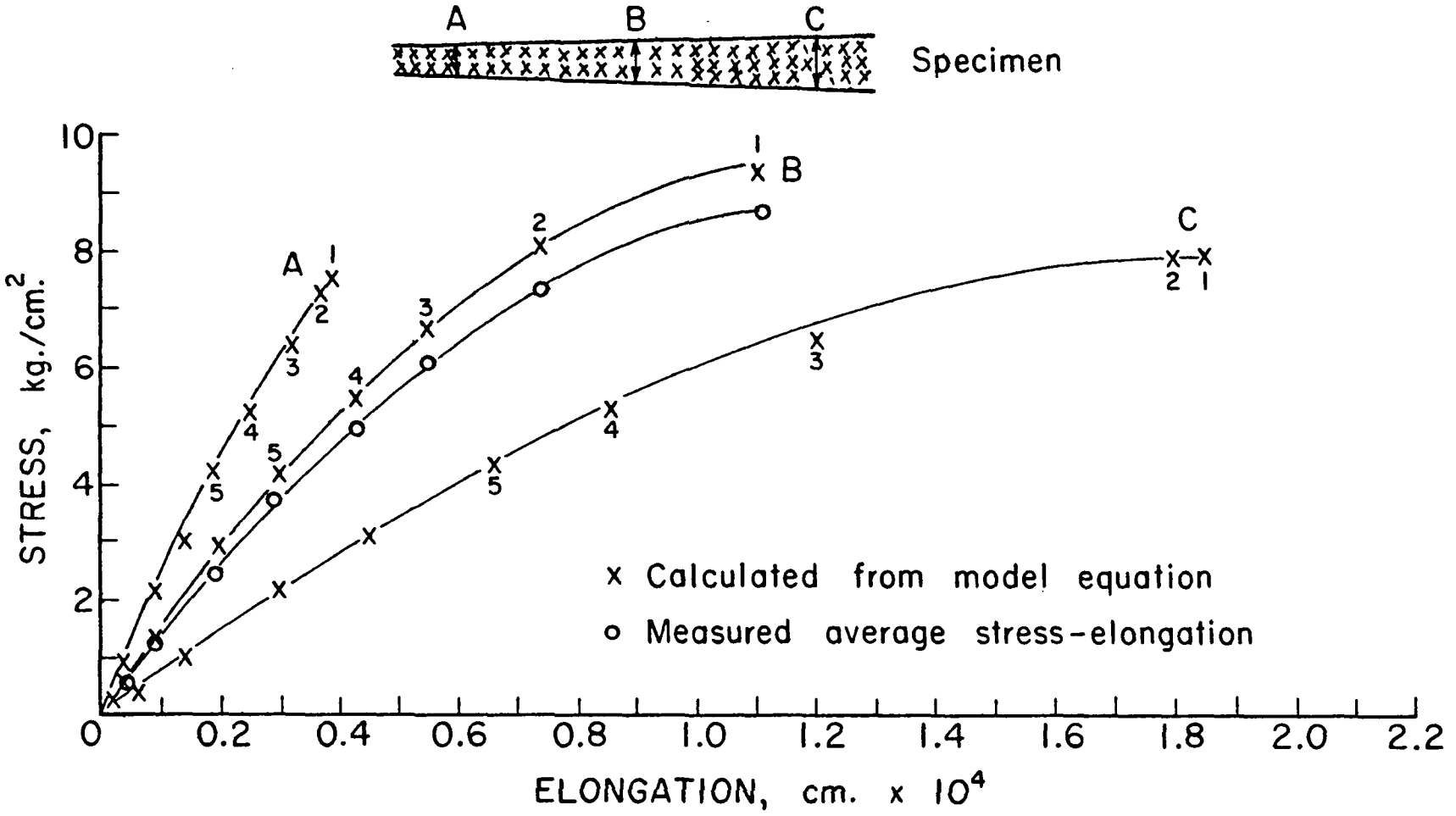

Figure 17. Stress-Elongation Variation Along the Wedge for Specimen IIA4. Arabic Numbers Group Points According to Wedge Slope

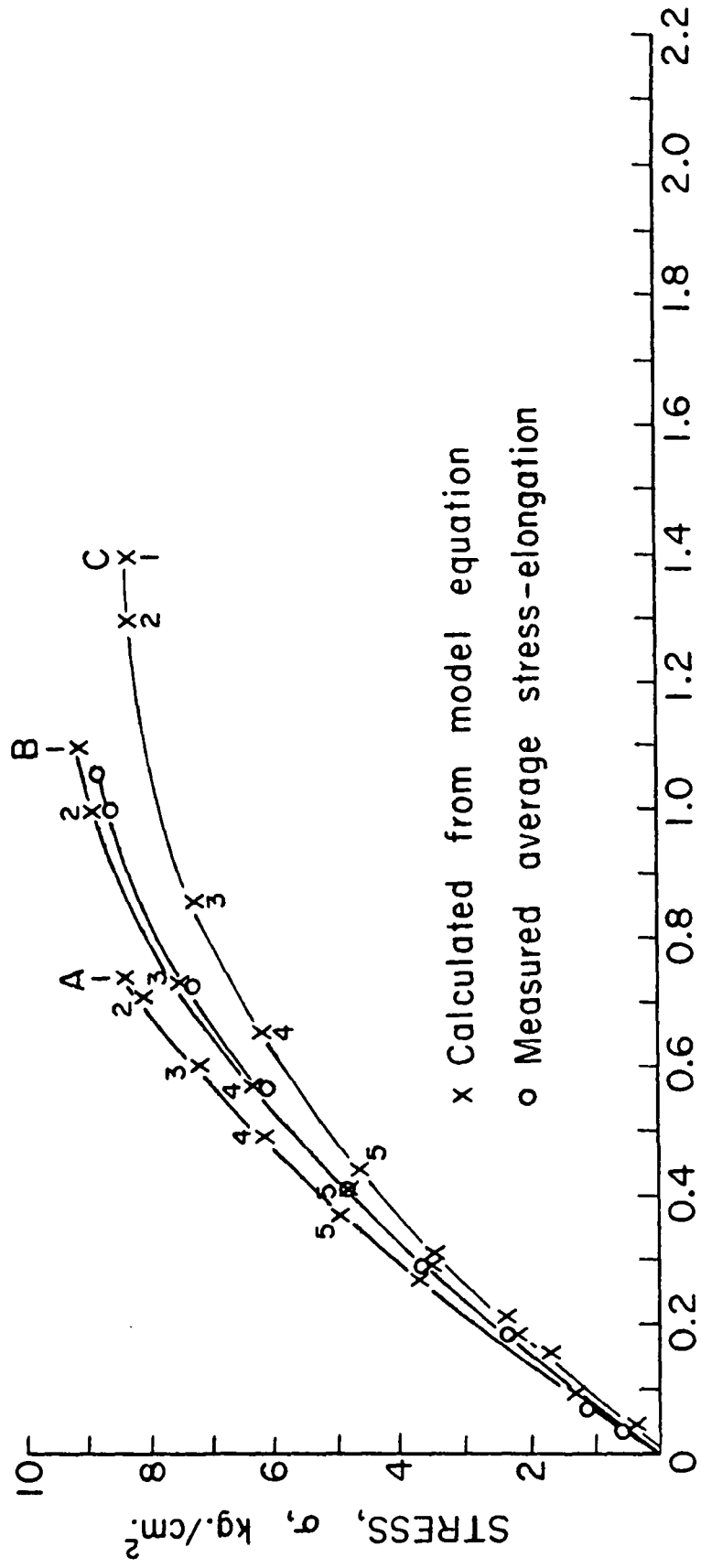

Figure 18. Stress-Elongation Variation Along the Wedge for Specimen IIA3.
Arabic Numbers Group Points According to Wedge Slope

REPRODUCIBILITY OF AVERAGE STRESS-STRAIN CURVES

The normal practice for studying load-elongation behavior was to determine average stress-average strain (for the three LVDT's) curves for each 1-inch diameter specimen. A typical curve, as plotted from the experimental data, is shown in Fig. 19.[25] A group of these curves, illustrating the reproducibility between and within specimens, is shown in Fig. 20. The average curves were quite reproducible for similar specimens, which aided in analyzing the mechanical behavior in the z-direction.

Table IV lists the physical and mechanical properties of test specimens determined from average stress-strain curves of the type shown in Fig. 19. All mechanical properties related to deformation were computed at 95% of the failure stress because the rate of deformation became so rapid after this point that it was not possible to measure strain accurately while switching from one transducer (LVDT) to another.

BASIS WEIGHT

The effect of basis weight on the z-direction stress-strain behavior is shown in Fig. 21-24. The general decrease in failure stress with increasing basis weight (Table IV) was also observed by Wink and Van Eperen (33). They concluded that the Pierce weak-link theory (36) would account for a portion of the basis weight effect, but they attributed the major cause to stress concentration as described by Van den Akker (3). This theory suggests that at higher basis weights there would be greater flexing of fiber segments resulting in

[25] This curve was obtained by fitting a third-degree polynominal equation to the data points shown in the figure. The polynomial has been forced to go through zero. The rate of stressing in all load-elongation tests was 0.3 kg./cm.^{2}/sec., unless otherwise stated.

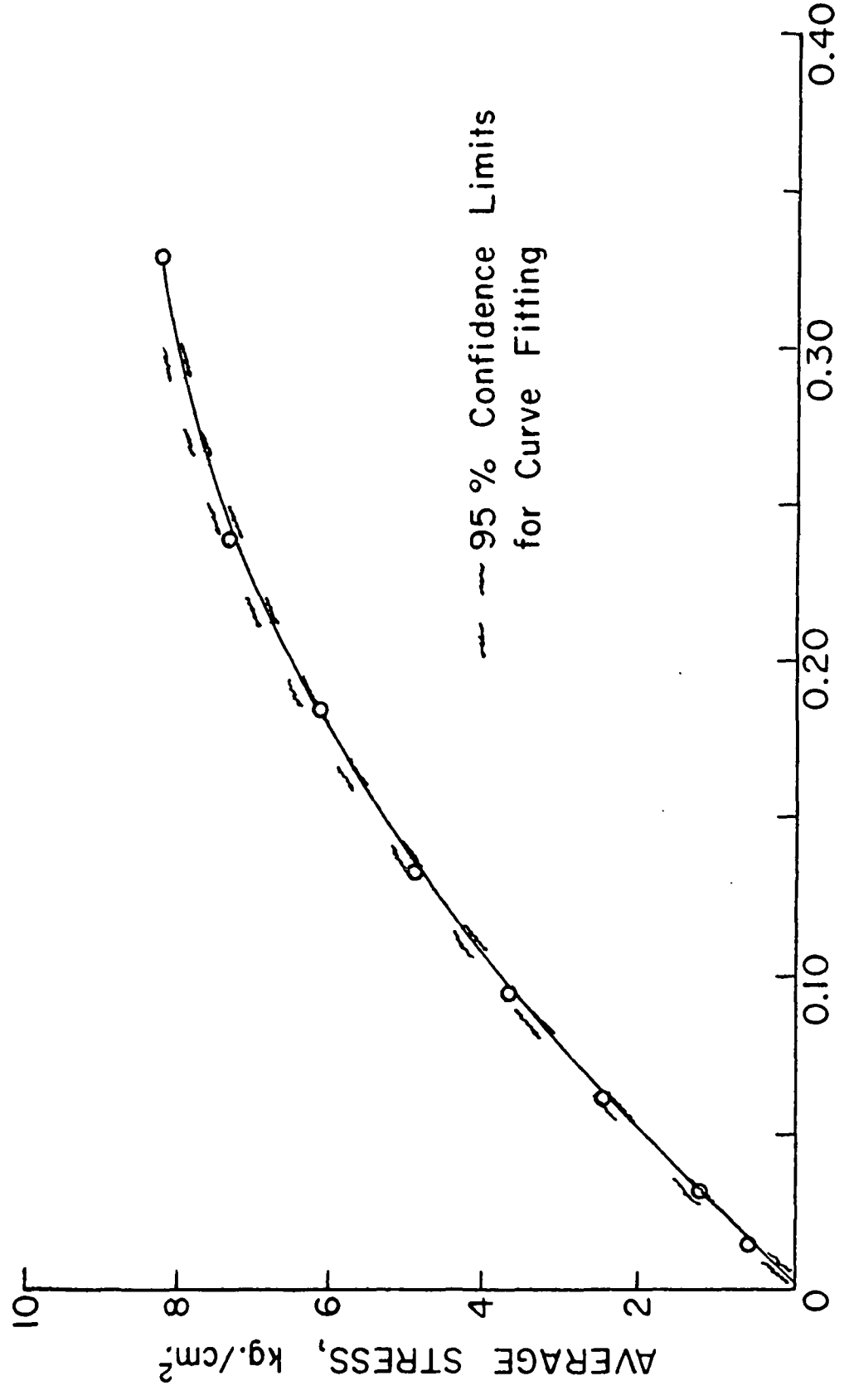

Figure 19. Typical Experimentally Determined Average Stress-Average Apparent Strain Curve for Specimen IIA1

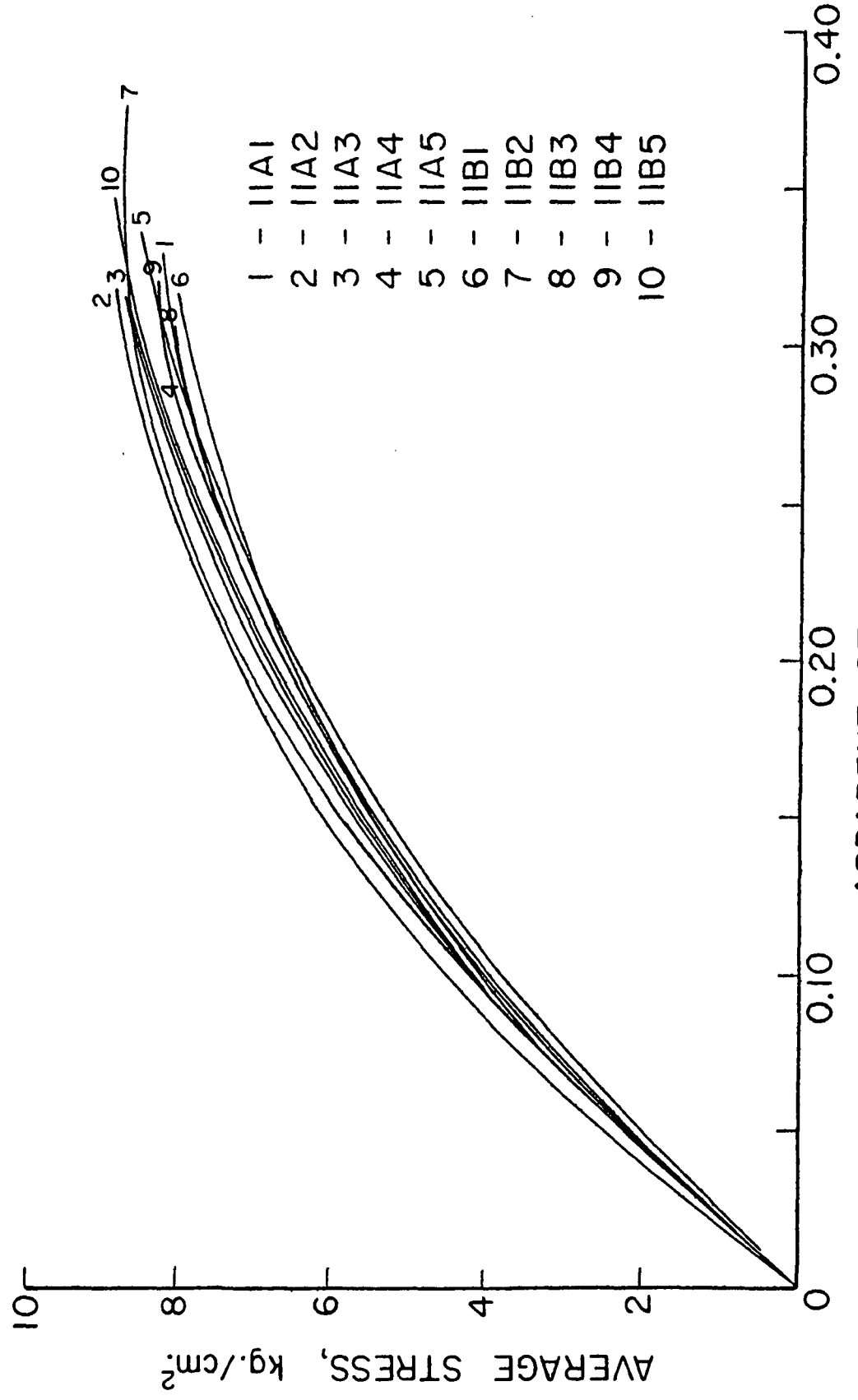

Figure 20. z-Direction Stress-Strain Variability Between and Within Similar Handsheets

TABLE IV

PHYSICAL PROPERTIES OF SPECIMENS AT EACH SHEET-MAKING CONDITION

Specimen	Thickness[a], cm.	Basis Weight, g./m.^{2}	Apparent Density, g./cc.	95% Failure Stress[b], kg./cm.^{2}	Apparent Failure Strain at 95% of Failure Stress[c], %	Apparent Failure Energy at 95% of Failure Stress[d], kg.-cm./g.	Apparent Initial Modulus[e], kg./mm.^{2}	
							M.R.	P.R.
Basis weight								
IC 1	0.0300	251	0.837	6.60	0.426	0.0202	31.6	30.2
IC 3	0.0287	242	0.842	6.73	0.238	0.0104	42.2	40.5
IC 4	0.0279	242	0.866	7.46	0.353	0.0174	33.1	35.1
IC 8	0.0305	264	0.865	6.60	0.404	0.0201	36.3	39.6
IC 9	0.0282	240	0.853	6.24	0.406	0.0176	30.6	32.2
ID 1	0.0368	311	0.845	6.24	0.325	0.0140	31.5	33.2
ID 3	0.0373	319	0.854	7.09	0.336	0.0172	45.2	44.7
ID 6	0.0378	318	0.841	6.11	0.258	0.0110	36.1	44.0
ID 7	0.0368	315	0.856	6.85	0.340	0.0157	32.9	33.6
IE 2	0.0536	445	0.831	5.87	0.521	0.0218	21.3	22.4
IE 3	0.0531	449	0.845	5.26	0.709	0.0271	16.6	14.7

[a] Thickness was measured with a Federal gage and because of the technique used and adhesive penetration, it represents only an apparent span. The true value could vary considerably from the apparent value.

[b] Kg. = kg. of force = 9.8 newtons; stress rate = 17.8 kg./cm.^{2}/min.

[c] Strain measured at 95% of failure stress. At higher levels of stress, the strain rate is too high to be accurately measured with existing experimental techniques.

[d] Determined from area under best-fit curve to load-elongation data points.

[e] M.R. means the initial modulus (γ_1) as determined from the mathematical analysis of data discussed earlier in this report. P.R. means modulus was determined from the initial slope of a best-fit curve determined from a polynomial regression analysis.

TABLE IV (Continued)

PHYSICAL PROPERTIES OF SPECIMENS AT EACH SHEET-MAKING CONDITION

Specimen	Thickness[a], cm.	Basis Weight, g./m.^{2}	Apparent Density, g./cc.	95% Failure Stress[b], kg./cm.^{2}	Apparent Failure Strain at 95% of Failure Stress[c], %	Apparent Failure Energy at 95% of Failure Stress[d], kg.-cm./g.	Apparent Initial Modulus[e], kg./mm.^{2}	
							M.R.	P.R.
IE 5	0.0523	430	0.821	5.99	0.366	0.0151	25.1	21.6
IE 9	0.0551	463	0.840	5.87	0.465	0.0200	26.1	28.3
IF 2	0.0622	523	0.841	5.63	0.339	0.0149	39.2	43.9
IF 6	0.0625	510	0.816	5.63	0.493	0.0204	21.6	21.8
IF 7	0.0615	500	0.813	5.38	0.447	0.0179	23.8	24.3
IF 9	0.0617	516	0.836	5.87	0.449	0.01891	23.2	25.0
Stress-strain								
IA 1	0.0384	330	0.862	6.80	0.361	0.0181	37.8	36.6
IA 2	0.0373	322	0.863	6.97	0.273	0.0132	50.7	46.6
IA 3	0.0384	332	0.866	6.11	0.246	0.0100	41.4	42.8
IA 4	0.0358	310	0.866	7.68	0.410	0.0225	35.5	35.2
IA 5	0.0381	330	0.865	6.97	0.303	0.0151	47.7	46.8

[a] Thickness was measured with a Federal gage and because of the technique used and adhesive penetration, it represents only an apparent span. The true value could vary considerably from the apparent value.

[b] Kg. = kg. of force = 9.8 newtons; stress rate = 17.8 kg./cm.^{2}/min.

[c] Strain measured at 95% of failure stess. At higher levels of stress, the strain rate is too high to be accurately measured with existing experimental techniques.

[d] Determined from area under best-fit curve to load-elongation data points.

[e] M.R. means the initial modulus (γ_1) as determined from the mathematical analysis of data discussed earlier in this report. P.R. means modulus was determined from the initial slope of a best-fit curve determined from a polynomial regression analysis.

TABLE IV (Continued)

PHYSICAL PROPERTIES OF SPECIMENS AT EACH SHEET-MAKING CONDITION

Specimen	Thickness[a], cm.	Basis Weight, g./m.^{2}	Apparent Density, g./cc.	95% Failure Stress[b], kg./cm.^{2}	Apparent Failure Strain at 95% of Failure Stress[c], %	Apparent Failure Energy at 95% of Failure Stress[d], kg.-cm./g.	Apparent Initial Modulus[e], kg./mm.^{2}	
							M.R.	P.R.
IIA 1	0.0351	328	0.935	8.23	0.329	0.0175	43.9	43.7
IIA 2	0.0361	338	0.937	9.06	0.322	0.0195	59.6	56.6
IIA 3	0.0345	327	0.947	8.82	0.310	0.0171	48.6	48.6
IIA 4	0.0356	331	0.931	8.66	0.312	0.0176	56.1	47.4
IIA 5	0.0348	327	0.941	8.66	0.336	0.0182	44.0	43.8
IIB 1	0.0366	332	0.909	8.13	0.316	0.0176	50.6	51.7
IIB 2	0.0348	321	0.923	8.77	0.387	0.0250	51.7	49.1
IIB 3	0.0361	334	0.925	8.13	0.311	0.0164	46.2	45.9
IIB 4	0.0361	333	0.925	8.32	0.316	0.0166	43.7	42.6
IIB 5	0.0340	315	0.925	8.96	0.352	0.0203	45.30	45.8
IIB 6	0.0363	327	0.901	8.44	0.321	0.0187	49.9	48.5
IIB 7	0.0353	323	0.915	8.38	0.340	0.0194	47.5	46.8
IIB 8	0.0363	332	0.913	8.72	0.322	0.0192	52.2	54.5
IIB 9	0.0361	328	0.909	8.83	0.295	0.0176	54.9	56.8

[a] Thickness was measured with a Federal gage and because of the technique used and adhesive penetration, it represents only an apparent span. The true value could vary considerably from the apparent value.

[b] Kg. = kg. of force = 9.8 newtons; stress rate = 17.8 kg./cm.^{2}/min.

[c] Strain measured at 95% of failure stress. At higher levels of stress, the strain rate is too high to be accurately measured with existing experimental techniques.

[d] Determined from area under best-fit curve to load-elongation data points.

[e] M.R. means the initial modulus (γ_1) as determined from the mathematical analysis of data discussed earlier in this report. P.R. means modulus was determined from the initial slope of a best-fit curve determined from a polynomial regression analysis.

TABLE IV (Continued)

PHYSICAL PROPERTIES OF SPECIMENS AT EACH SHEET-MAKING CONDITION

Specimen	Thickness[a], cm.	Basis Weight, g./m.^{2}	Apparent Density, g./cc.	95% Failure Stress[b], kg./cm.^{2}	Apparent Failure Strain at 95% of Failure Stress[c], %	Apparent Failure Energy at 95% of Failure Stress[d], kg.-cm./g.	Apparent Initial Modulus[e], kg./mm.^{2}	
							M.R.	P.R.
IIB10	0.0348	318	0.913	8.60	0.276	0.0156	55.7	56.9
Rubber dental dam[f]								
RDD 1	0.0269	289	1.07				22.8	23.6
RDD 2	0.0274	293	1.07				24.8	26.5
RDD 3	0.0272	292	1.07				17.7	15.9
RDD 4	0.0274	292	1.06				24.3	21.0
Post-creep stress strain								
IB 7	0.0376	327	0.869	6.46	0.517	0.0245	28.5	27.5
IB 8	0.0378	331	0.874	6.79	0.410	0.0180	35.6	29.8
IB 9	0.0381	328	0.862	7.07	0.282	0.0124	38.6	41.9

[a] Thickness was measured with a Federal gage and because of the technique used and adhesive penetration, it represents only an apparent span. The true value could vary considerably from the apparent value.

[b] Kg. = kg. of force = 9.8 newtons; stress rate = 17.8 kg./cm.^{2}/min.

[c] Strain measured at 95% of failure stress. At higher levels of stress, the strain rate is too high to be accurately measured with existing experimental techniques.

[d] Determined from area under best-fit curve to load-elongation data points.

[e] M.R. means the initial modulus (γ_1) as determined from the mathematical analysis of data discussed earlier in this report. P.R. means modulus was determined from the initial slope of a best-fit curve determined from a polynomial regression analysis.

[f] Were not loaded to failure. When failure occurs, it is at the rubber-adhesive interface.

TABLE IV (Continued)

PHYSICAL PROPERTIES OF SPECIMENS AT EACH SHEET-MAKING CONDITION

Specimen	Thickness[a], cm.	Basis Weight, g./m.^{2}	Apparent Density, g./cc.	95% Failure Stress[b], kg./cm.^{2}	Apparent Failure Strain at 95% of Failure Stress[c], %	Apparent Failure Energy at 95% of Failure Stress[d], kg.-cm./g.	Apparent Initial Modulus[e], kg./mm.^{2}	
							M.R.	P.R.
IB10	0.0381	338	0.886	7.20	0.279	0.0139	53.9	53.2
Creep and creep recovery								
IB 4	0.0389	333	0.857					
IB 5	0.0376	330	0.878					
IB 6	0.0376	324	0.863					
Load-unload cycling								
IA 6	0.0373	320	0.857					
IA 9	0.0384	336	0.877					
IIA 7	0.0338	310	0.918					
IIA 9	0.0358	330	0.921					

[a] Thickness was measured with a Federal gage and because of the technique used and adhesive penetration, it represents only an apparent span. The true value could vary considerably from the apparent value.

[b] Kg. = kg. of force = 9.8 newtons; stress rate = 17.8 kg./cm.^{2}/min.

[c] Strain measured at 95% of failure stress. At higher levels of stress, the strain rate is too high to be accurately measured with existing experimental techniques.

[d] Determined from area under best-fit curve to load-elongation data points.

[e] M.R. means the initial modulus (γ_1) as determined from the mathematical analysis of data discussed earlier in this report. P.R. means modulus was determined from the initial slope of a best-fit curve determined from a polynomial regression analysis.

TABLE IV (Continued)

PHYSICAL PROPERTIES OF SPECIMENS AT EACH SHEET-MAKING CONDITION

	Specimen	Thickness[a], cm.	Basis Weight, g./m.^{2}	Apparent Density, g./cc.
Viscoelastic characterization	IA11	0.0366	319	0.871
	IA13	0.0374	320	0.856
	IA14	0.0366	314	0.858
	IIA11	0.0350	330	0.944
	IIA12	0.0348	324	0.932
	IIA13	0.0340	318	0.937
Light scattering	IG 1	0.0361	308	0.853
	IG 2	0.0358	304	0.850
	IG 3	0.0376	321	0.854
	IG 4	0.0366	302	0.827
	IG 5	0.0376	325	0.865
	IG 6	0.0383	327	0.853
	IG 7	0.0381	328	0.861
	IG 8	0.0376	325	0.865
	IG 9	0.0371	315	0.850
	IIC 1	0.0342	321	0.939
	IIC 2	0.0350	314	0.897
	IIC 3	0.0348	316	0.908
	IIC 4	0.0350	319	0.912
	IIC 5	0.0340	310	0.912
	IIC 6	0.0343	310	0.904
	IIC 7	0.0350	321	0.917
	IIC 8	0.0353	321	0.908
	IIC 9	0.0361	325	0.899

[a]Thickness was measured with a Federal gage and because of the technique used and adhesive penetration, it represents only an apparent span. The true value could vary considerably from the apparent value.

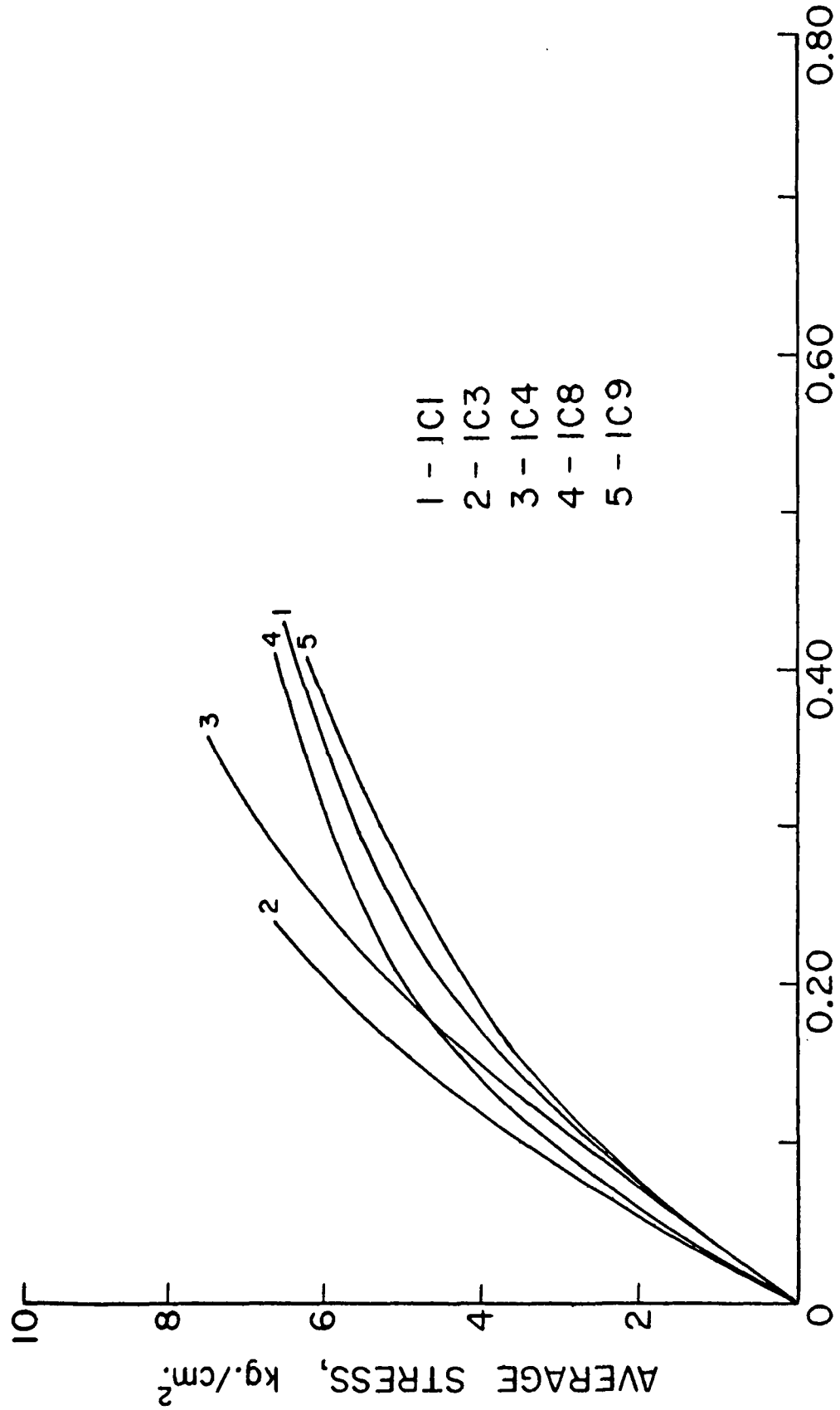

Figure 21. Stress-Strain Behavior at an Average Basis Weight of 250 g./m.^{2} for Five Specimens from the Same Handsheet

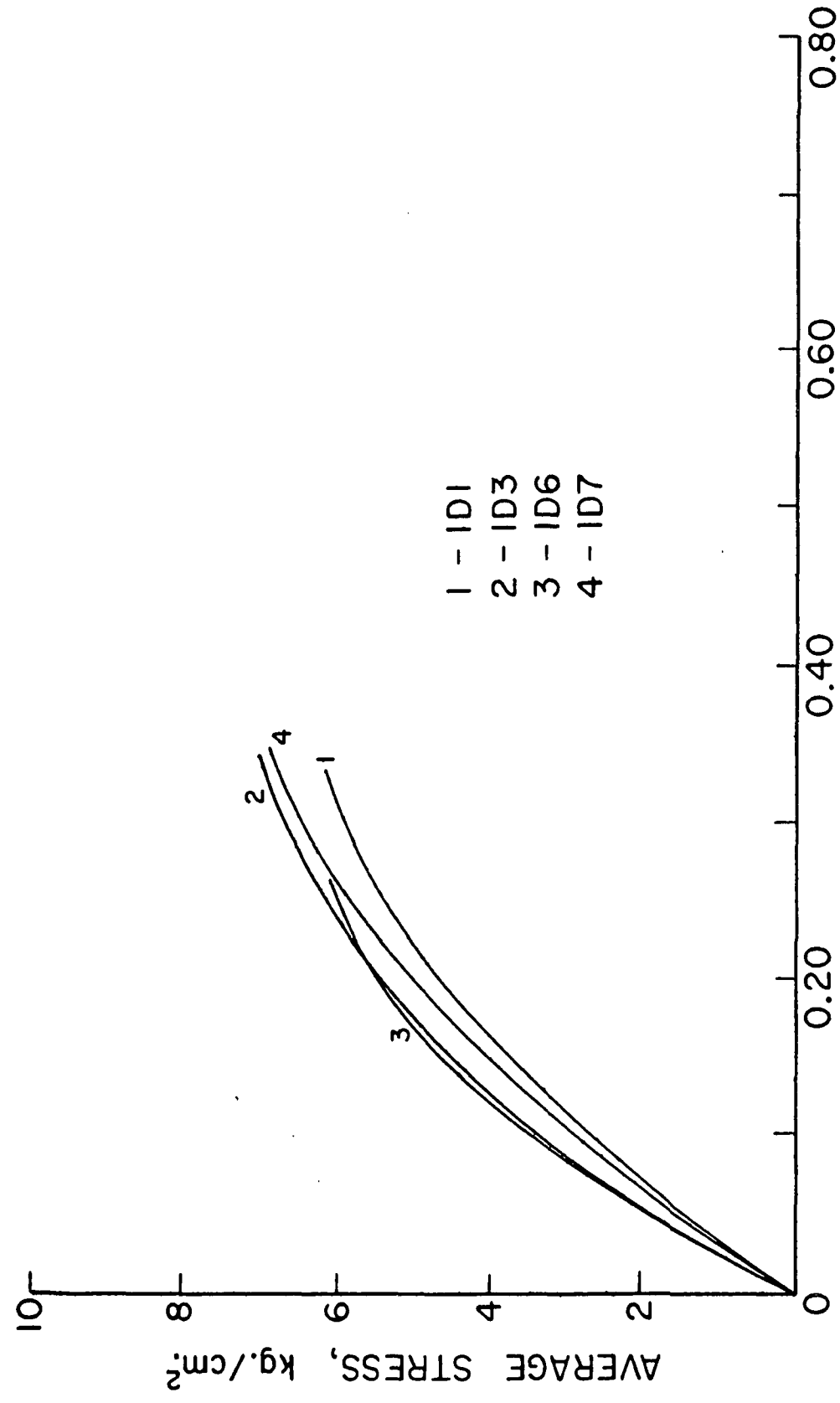

Figure 22. Stress-Strain Behavior at an Average Basis Weight of 316 g./m.^{2} for Four Specimens from the Same Handsheet

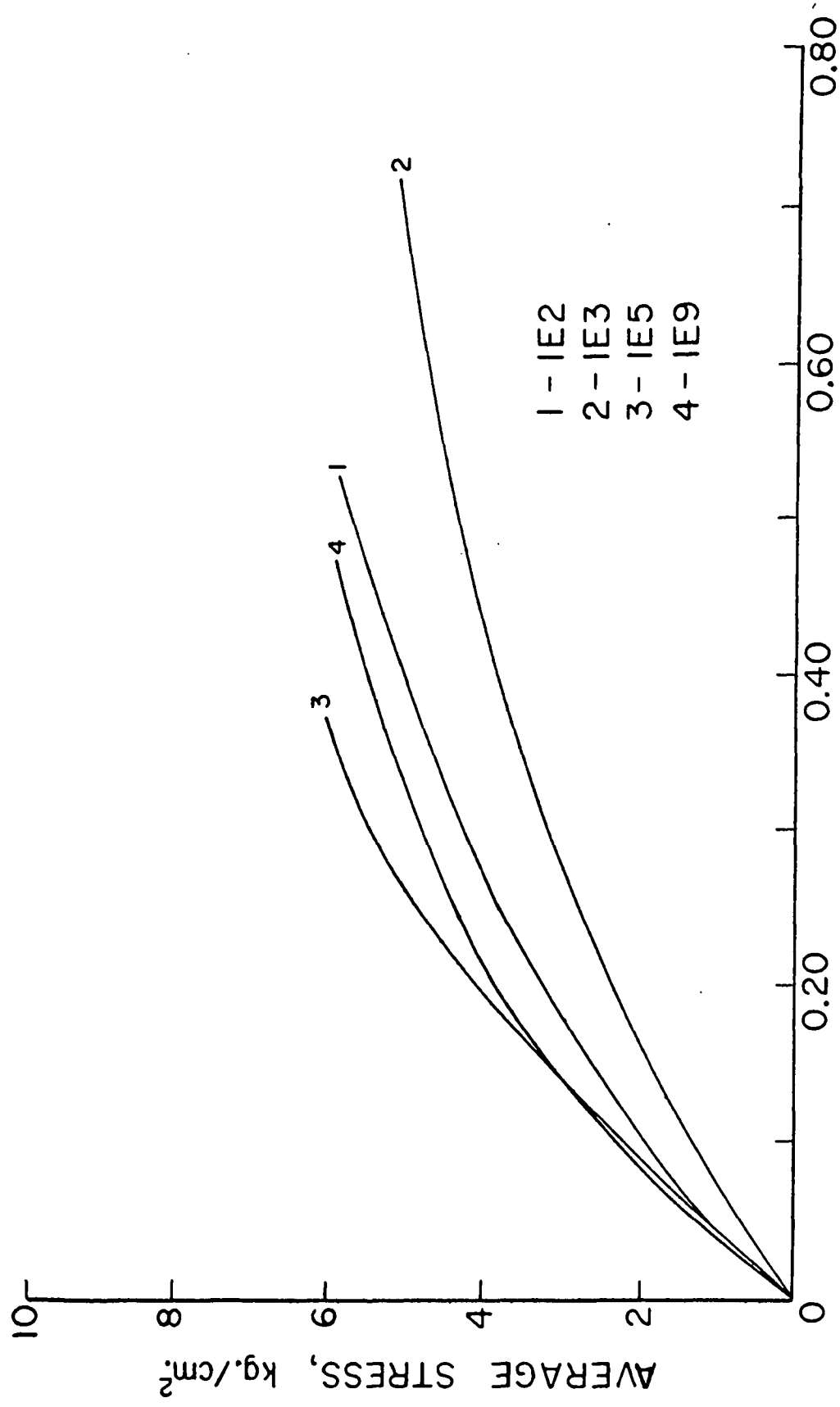

Figure 23. Stress-Strain Behavior at an Average Basis Weight of 447 g./m.^{2} for Four Specimens from the Same Handsheet

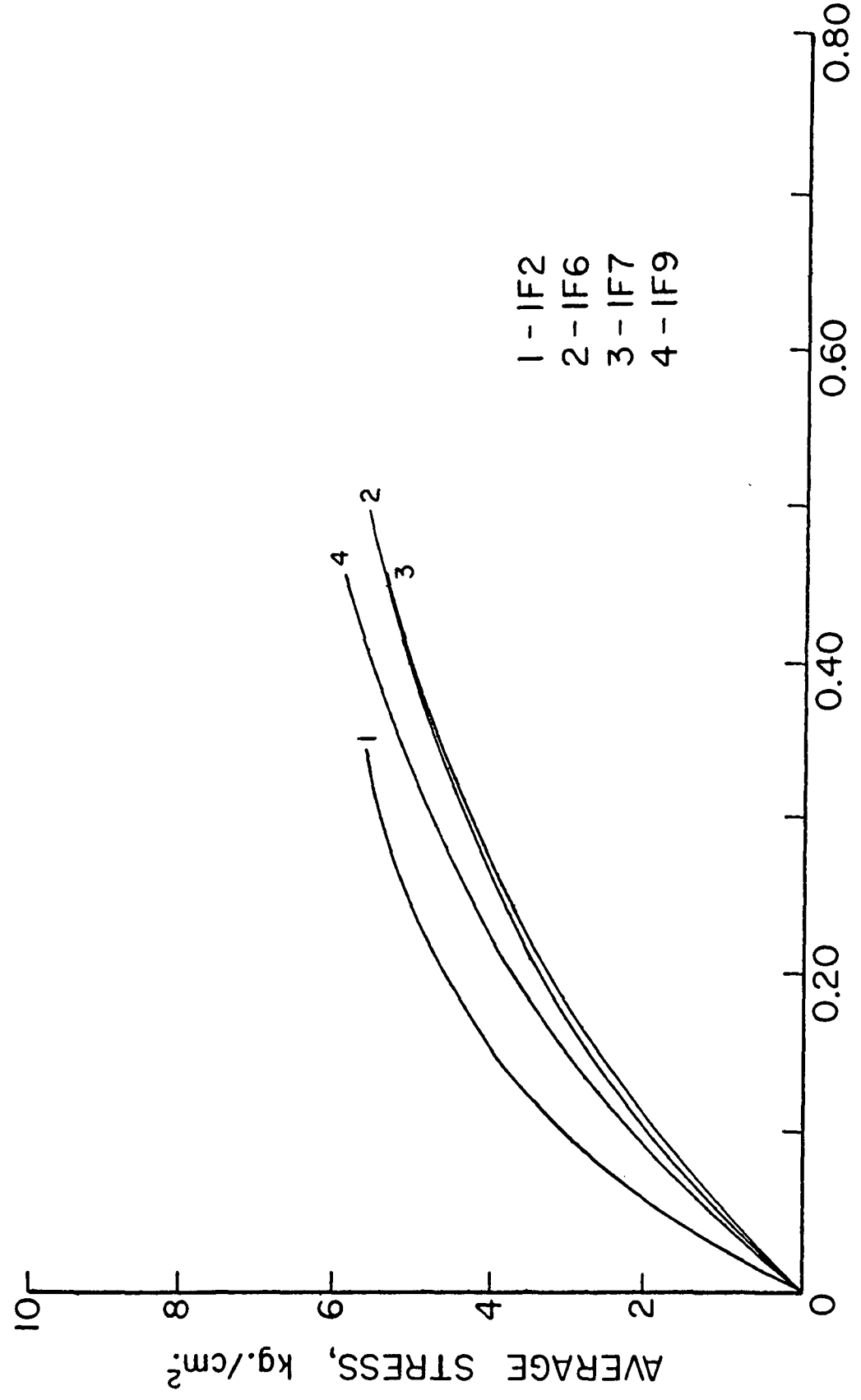

Figure 24. Stress-Strain Behavior at an Average Basis Weight of 512 g./m.² for Four Specimens from the Same Handsheet

increased stress concentrations around the periphery of fiber-to-fiber bonds. This would cause bonds to fail at observed loads much less than that corresponding to the true bond failure stress. It was further pointed out that even in the idealized sheet, only two fibers thick, in which segments were prevented from bending by the rigid adhesive, there would still be stress concentrations from the flexing of the fiber wall, which would lessen the true bond failure stress. As the thickness of the test specimen is increased, the constraint of the adhesive on the surface fibers should diminish in importance, and the flexing of the fiber segments and the stress concentration should increase. The effect should be at a maximum at the central plane of the sheet and, hence, failure should occur at or near that plane. This was found to be the case for the hard, rigid Epon 907 adhesive, but not when the adhesive was relatively soft and of low modulus, as in the case of double-faced Scotch tape or its equivalent (33).

The basis weight effect observed by Wink and Van Eperen diminished above 200 g./m.^{2} In the present work, all the basis weights shown in Fig. 21-24 were above 200 g./m.^{2}[26] However, because of adhesive penetration effects, the effective span, and therefore basis weight, could be less than 200 g./m.^{2} for some specimens. In addition, the proportional change in effective span with increasing basis weight is greater than the proportional change in measured caliper. For example, if the adhesive penetration was assumed to be about 2.5 mils on each side, then a specimen with a 10-mil caliper would have an effective span of only 5 mils, whereas a specimen with a 20-mil caliper would have an effective span of 15 mils, the ratio being 3 to 1 compared to a ratio of only 2 to 1 based on caliper measurements. Although it is difficult to determine quantitatively

[26]The pulps were similar, but Wink and Van Eperen used the fraction retained on a 150-mesh screen, whereas in the present work the combined fractions retained on the 25- and 35-mesh screens were used, and therefore one would expect a greater amount of adhesive penetration.

the amount of adhesive penetration, one can assume that this effect is a likely cause for part of the increase in apparent strain with increasing basis weight.

It is also possible that decreasing basis weight might cause an increase in failure stress because of the increase in tensile stresses directed radially outward from the center of the specimen (37).[27] This is caused by the increased effect of adhesive restraint with decreasing specimen thickness preventing contraction, or necking, of the specimen. When a fibrous structure such as paper is bonded between two hard materials and a tensile stress is applied across the surface, the specimen must also contact laterally if it is to undergo elongation. However, the restraint of the adjoining adhesive resists the lateral contraction, which effectively subjects the paper to tensile stresses directed radially outward. The actual value of the axial stress necessary to cause yielding depends on the geometry of the specimen with respect to its t/D (thickness/diameter) ratio. As the t/D ratio decreases, the specimen is not capable of contraction in the same way as a standard tensile specimen, while still conforming to interface constraints. Hence, as the radial stresses increase, due to the decreasing t/D ratio with decreasing basis weight, the value of axial stress necessary to cause yielding increases.

Since the higher basis weight specimens were also formed at a higher consistency, it was possible that the effects of basis weight could have been caused by changes in the degree of flocculation resulting in poorer formation within the handsheet. However, tests run at different drainage times, which should increase

[27]The discussion in this reference pertains to metals.

the amount of flocculation and result in poorer formation[28], had a negligible effect on the mechanical behavior.

DENSITY

The effect of apparent density shown in Fig. 25 is in line with the expected behavior. A decrease in apparent density would increase the bending and flexing of fibers because of the decreased bonded area and bond strength. This would weaken the specimen and increase the strain over that of a more dense specimen at an equivalent load.

Wink and Van Eperen (33) obtained some interesting failure stress data on a few specimens that had been dried under high compacting stresses. The z-direction failure stress doubled with a change in compacting stress from 3.5 to 490 kg./cm.^{2} They found that the z-direction tensile strength per unit bonded area remained fairly constant over a broad range of compacting stresses, but it increased sharply at the higher stress levels. These authors suggested that at the higher compacting stresses lumen bonding might be expected to reduce the flexing of the fiber wall and, consequently, the stress concentration.

The experimental data for both basis weight and apparent density seem logical with respect to earlier conclusions related to compression response (p. 17), where it was suggested that fiber bending and flexibility[29] were the two most important structural parameters related to deformation in both compression and tension.

---

[28] It is very difficult to separate these two effects. Flocculation alone might be expected to increase the z-tensile strength due to greater z-orientation of the fibers (38, 39).

[29] In this case, fiber wall flexibility would be related to the transverse deformation of the fibers.

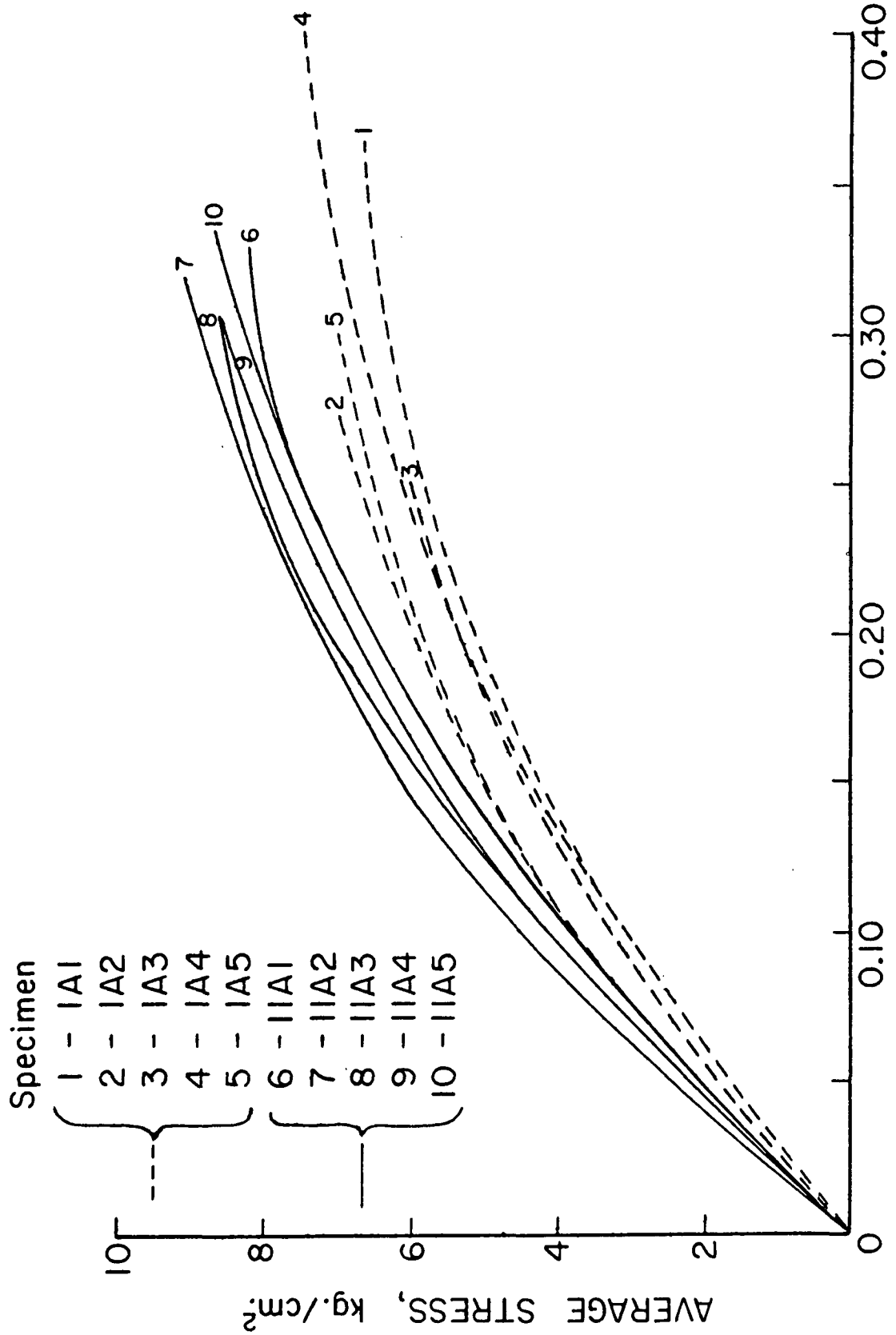

Figure 25. Relationship Between Specimen Density Changed by Drying Pressure and z-Direction Stress-Strain Behavior. Apparent Density: 1A-Series, 0.87 g./cc.; 2A-Series, 0.94 g./cc.

With both increasing basis weight and decreasing apparent density, the reproducibility in mechanical behavior also was lower. Both effects are expected to increase the probability of weak zones within the structure. The greater likelihood of weak zones would increase the initiation and propagation of failure throughout the structure.

BASIS WEIGHT AND DENSITY VARIATION AS PROBABLE CAUSES OF NONUNIFORM MECHANICAL BEHAVIOR

At least part of the nonuniform mechanical behavior within a single specimen, as determined from the mathematical analysis (p. 51) should be due to the variation in basis weight and apparent density within specimens. The density and basis weight distribution were determined by punching out 0.65-cm. diameter specimens from a 311-g./m.^{2} handsheet dried under a compacting stress of 7.5 kg./cm.^{2} The caliper of each specimen was determined, prior to punching, with a Federal gage[30]. The average apparent density was 0.846 g./cc. and the density of each specimen varied from a low of 0.807 g./cc. to a high of 0.894 g./cc., which represents a difference of about 0.09 g./cc. The difference in the average apparent densities of handsheets dried at two different pressures was about 0.07 g./cc.[31] This means that the nonuniform stress-strain behavior within a single specimen could be expected, based on density distribution alone, to be as large as that shown for the two handsheets at two different densities (Fig. 25). If it is considered that the density variation within a single specimen may even be greater if determined on a smaller scale, then it is conceivable that the variation in stress-strain behavior within a single specimen could be as large as that computed from the earlier model equation (Fig. 17 and 18).

[30]Anvil diameter = 3/16 inch; anvil pressure = 50 p.s.i.

[31]Density was determined on 2.54-cm. diameter specimens with the Federal gage. The caliper was measured in five places.

It is unlikely that the variation in basis weight within a single specimen would significantly affect the variation in mechanical behavior, since the basis weight variation was not nearly as great as that exhibited in Fig. 21-24. However, if the possibility of point variations in basis weight across the specimen surface because of adhesive penetration is considered, there might be a significant effect.

VISCOELASTICITY

The viscoelastic behavior of paper in the z-direction is illustrated in Fig. 26. These curves were constructed from data on three specimens from the same handsheet. The elastic (instantaneous and delayed) and plastic responses were determined at each load level on separate specimens.[32] The specimens exhibited little apparent plastic deformation except near the failure stress, indicating a high degree of recovery over a considerable portion of the stress-strain curve.

Further indication of the high degree of recovery of deformation was obtained through progressive load-unload cycling of specimens. The typical behavior is illustrated in Fig. 27 and 28. It is difficult to attach any significance to the behavior of the initial slope of the curves with progressive cycling because it sometimes increases, decreases, or remains the same.

DISCUSSION OF LOAD-ELONGATION DATA

Although the general shape of the stress-strain curves shown in the previous figures is similar to those observed for in-plane tensile loading,

[32] Each component of deformation was determined 30 seconds after the desired level of stress was reached at a stress rate of 0.615 kg./cm.^{2} Ten minutes were allowed for recovery.

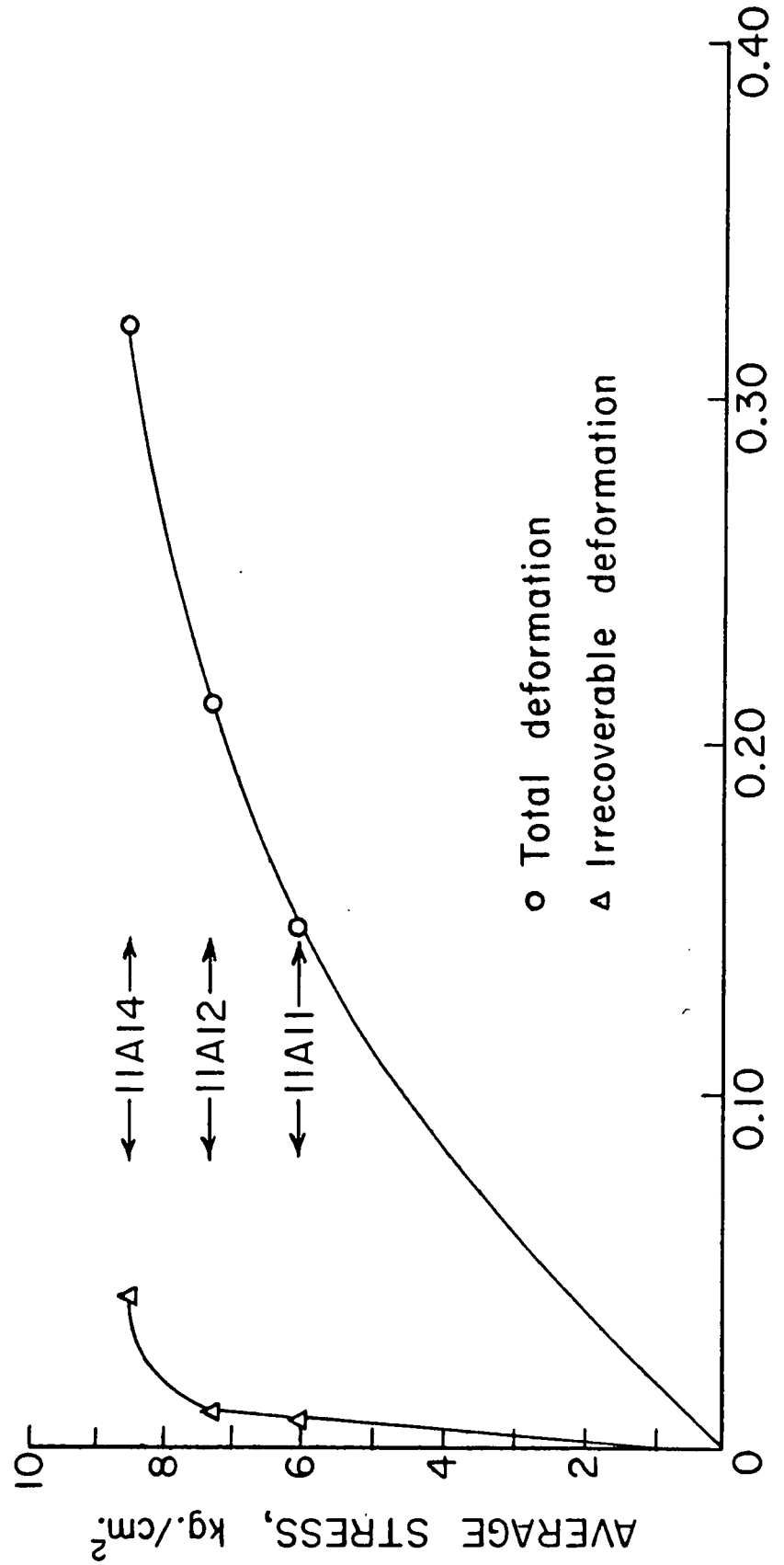

Figure 26. Viscoelastic Characterization for Handsheet IIA in the z-Direction. The Specimens Shown Between the Two Data Points at a Given Level of Stress Were Those Used to Obtain That Set of Data Points Within the Handsheet. Each Deformation was Determined 30 Seconds After the Desired Level of Stress was Reached at a Stress Rate of 0.615 kg./cm.^{2} Ten Minutes were Allowed for Recovery

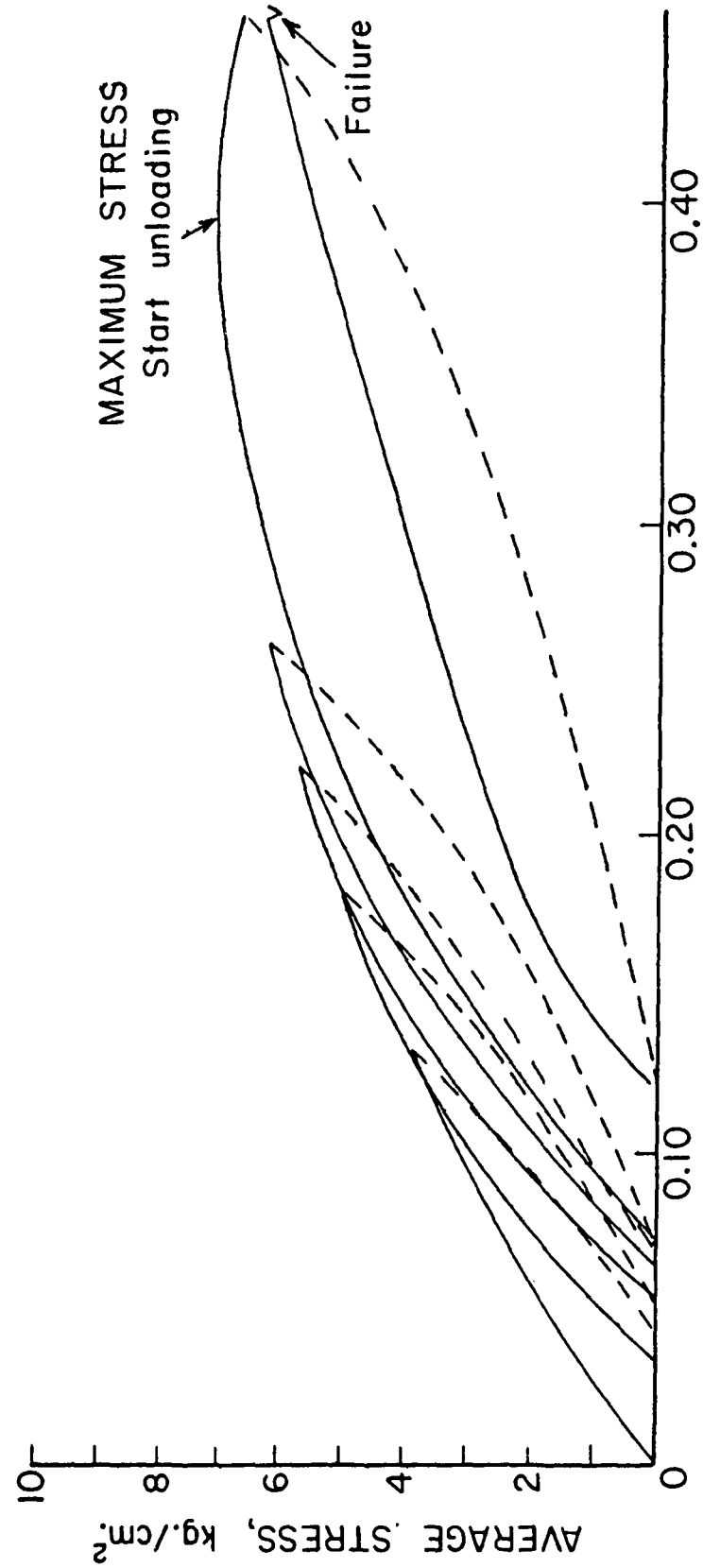

Figure 27. The Effect of Progressive Load-Unload Cycling on the z-Direction Stress-Strain Behavior of Specimen IA9. Rate of Stressing = 0.296 kg./cm.^{2}/sec. Strain is Total Deformation Divided by the Initial Unstretched Specimen Thickness

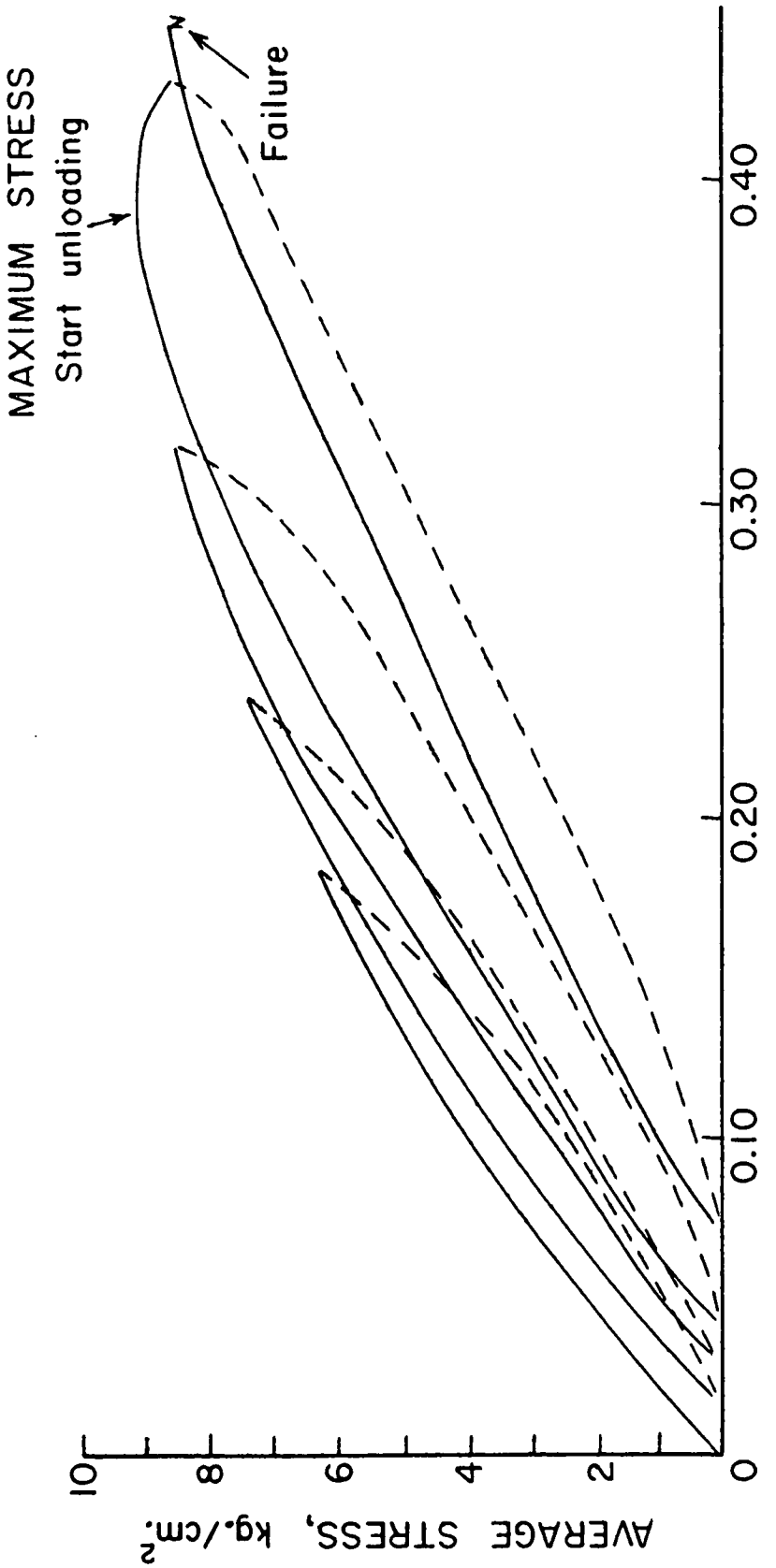

Figure 28. The Effect of Progressive Load-Unload Cycling on the z-Direction Stress-Strain Behavior of Specimen IIA7. Rate of Stressing = 0.96 kg./cm.^{2}/sec. Strain is Total Deformation Divided by the Initial Unstretched Specimen Thickness

there are major differences in the mechanical properties. Both the initial modulus and the apparent failure strain are about an order of magnitude lower than that generally observed for the in-plane direction. The failure stress in the z-direction is about one hundred times less than in the in-plane direction.

The lower failure stress is reasonable if one considers the manner in which the force is applied to the structure. The bending and flexing of the fiber walls causes bonds to fail by a peeling action, which requires less force than the shearing-type bond failure that would be expected to occur in an in-plane tensile test.[33] Because of the relative ease of interfiber bond failure in the case of z-direction loading, the individual fibers are subjected to relatively low levels of stress, which results in the low strain observed. This general phenomenon is shown in Fig. 29, in which the peeling failure of fiber-to-fiber bonds is illustrated to occur with z-direction stresses.

The transverse modulus[34] of individual fibers is estimated to be about ten times lower than the axial modulus (40), and therefore the fibers should deform much more readily in the transverse direction than axially. The low z-direction bond failure stress limits the tensile transverse strain of the fibers prior to failure.

In the z-direction stress-strain curve, the initial modulus is quite low. The slope of the load-elongation curve decreases with strain from the origin, and no linear immediate elastic region is noted. The low initial modulus is

[33] This can be readily demonstrated by placing a piece of tape on a surface and trying to remove it by pulling perpendicular to the surface (peeling) and tangentially to the surface (shearing).

[34] Although it is not strictly correct to use the term "modulus" in this case, for want of a better word it is used to describe the ratio of the stress to strain when the force is applied perpendicular to the fiber axis.

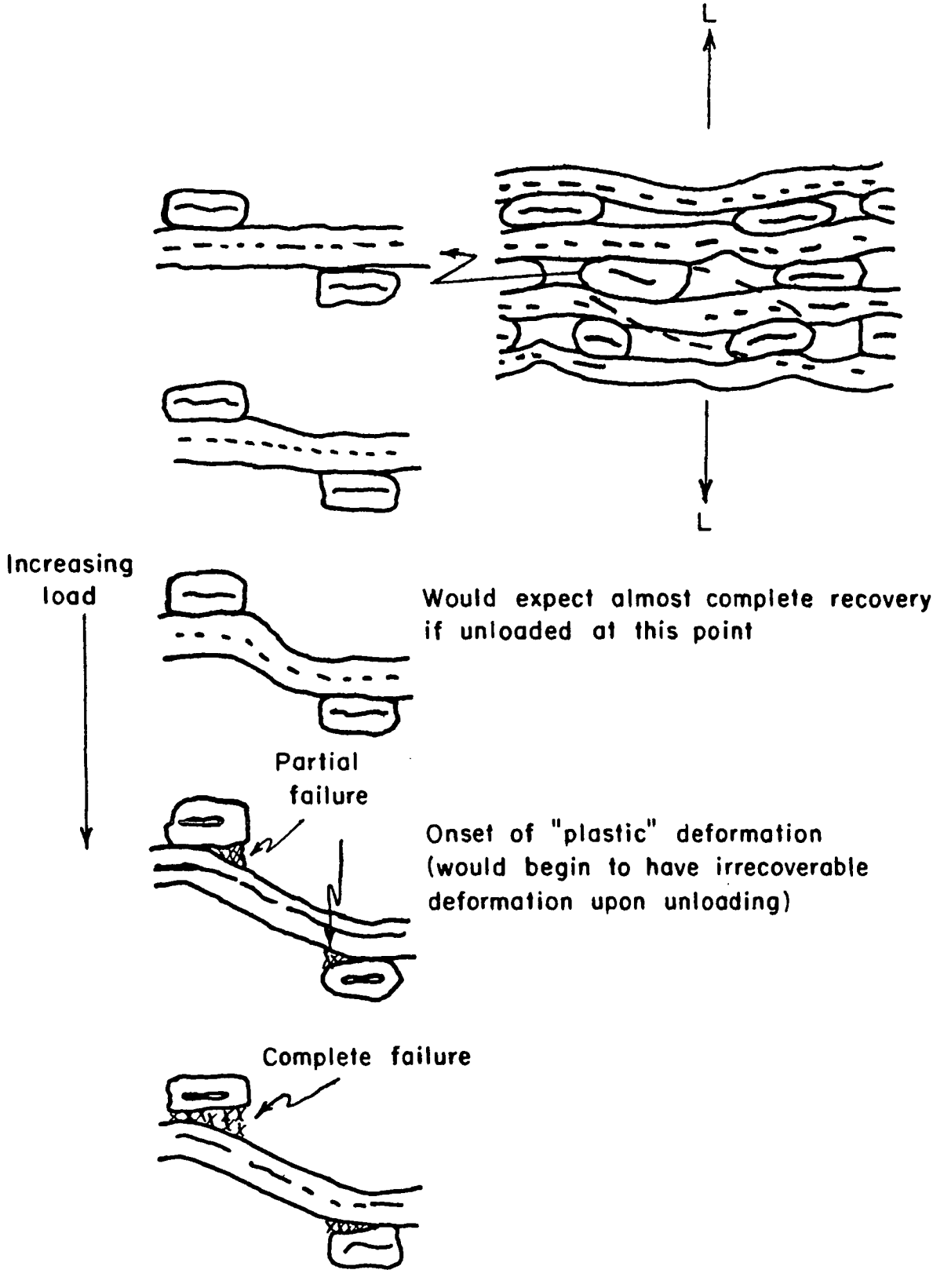

Figure 29. Speculative Deformation Mechanism for a Simple Fiber Model

consistent with the estimated difference between transverse and axial modulus (approximately 1:10) of individual fibers.

Another important aspect of z-direction load-elongation behavior is the high percentage of recoverability. This was evident in Fig. 26-28 where recovery was relatively high until failure. Even near failure, the strain was principally elastic.

EXAMINATION OF FAILURE ZONE

Evidence of both fiber-to-fiber bond failure and complete fiber failure was observed in the failure zone (Fig. 30 and 31). Interfiber bond failure appears to vary from little disturbance at the surfaces, with only fibrils and a few bundles of fibrils protruding from the debonded areas, to debonded areas where there are also larger fragments torn away (Fig. 30). Complete fiber failure (Fig. 31) either occurred during the chipping and refining processes or was a result of the individual fibers being subjected to high axial stresses during the final stages of failure. The evidence does not prove that fibers break during z-tensile loading.

Both the structures shown in Fig. 30 and 31, illustrating debonded areas, and those shown in Appendix I, illustrating the surface structure, indicate that the interfiber bonds vary from point contact to intimate contact of all sizes of fibrils from the walls of both fibers.

CREEP AND CREEP RECOVERY

Time, in addition to stress and strain, is an important parameter in studying the mechanical properties of paper. Creep curves allow one to examine the deformation as a function of time at various constant-load levels. The

Magnification = 800X

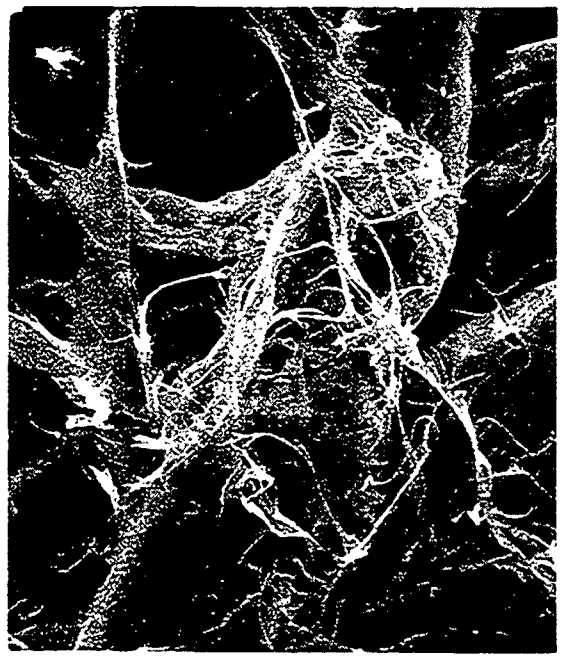

Magnification = 800X

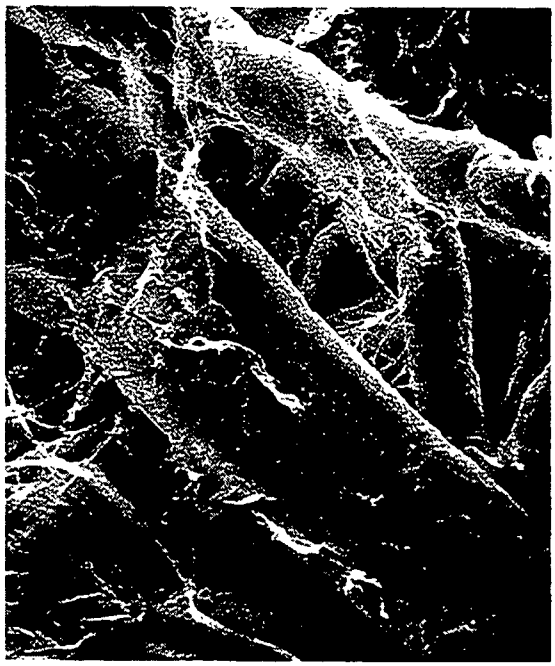

Magnification = 800X

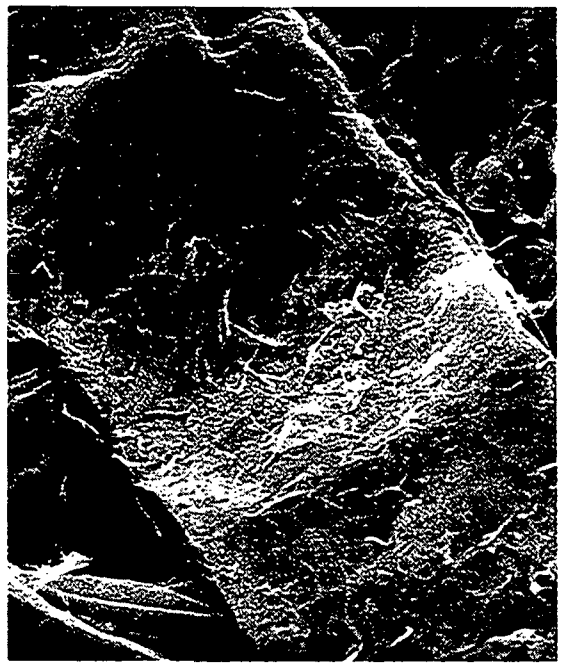

Magnification = 1000X

Figure 30. Electron Micrographs of the Debonded Areas in Failure Zone Showing Protruding Fibrils and Fragments Torn Away from Fiber Wall. Specimens Were Pressure Dried at 7.0 kg./cm.^{2}

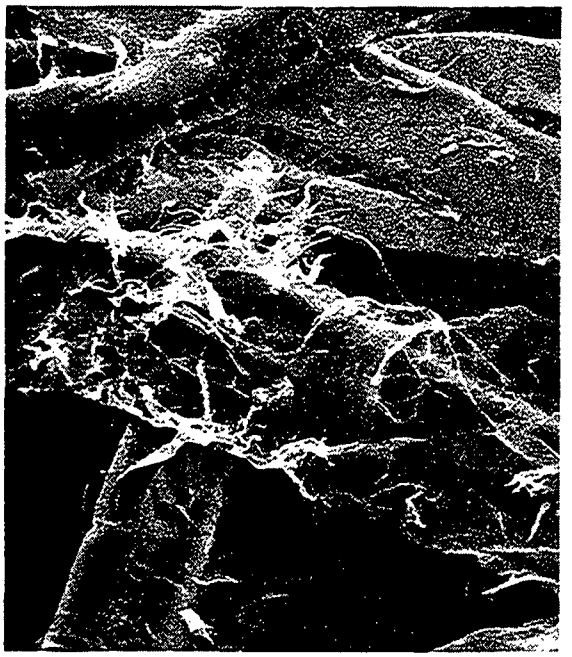

Magnification = 450X

Magnification = 450X

Magnification = 450X

Magnification = 800X

Figure 31. Electron Micrographs Showing Broken Fibers in Failure Zone (see Text). Specimens were Pressure Dried at 7.0 kg./cm.^{2}

objective of this portion of the work was only to examine the relationship between creep and creep recovery for a limited number of specimens. The procedure for obtaining the creep data was to rapidly apply the load through the chain loading mechanism (Fig. 5) in the same way as for a load-elongation test.[35] The specimens were loaded and unloaded at a rate of 0.615 kg./cm.^{2}/sec. (approximately 10 seconds to reach maximum load). Deformation was measured from the existing condition as a function of time from the instant of load application in creep tests, or load removal in creep recovery tests. The first readings in both cases were obtained at thirty seconds of elapsed time.

The strains in both creep and creep recovery tests were calculated relative to the initial caliper (the assumed initial span). The changes in initial span, even with repeated cycling were negligible. Although creep recovery represents a contraction in length, it is plotted as a positive deformation. All tests were run at 50% R.H. and 73°F.

Typical creep and creep recovery behavior is shown in Fig. 32-34 for specimens taken from Handsheet IB. The creep stress (5.5 kg./cm.^{2}) was approximately 73% of the failure stress as determined in a load-elongation test on similar specimens at a rate of stressing of 0.3 kg./cm.^{2}/sec. At a creep stress of 6.10 kg./cm.^{2}, which was approximately 81% of the normal failure stress, all of the specimens failed within 4,000 seconds (Fig. 35). The variation in creep behavior was considerable, indicating differences in initial structure between the specimens.

All specimens had a greater extension at failure in a creep test than at failure during a load-elongation test. (Compare Fig. 35, p. 94, to Fig. 25, p. 79.) Because of the longer time interval during the last stages of failure in a

[35]Prior to running a creep test of long duration, care must be taken to insure that any drift effects are stabilized.

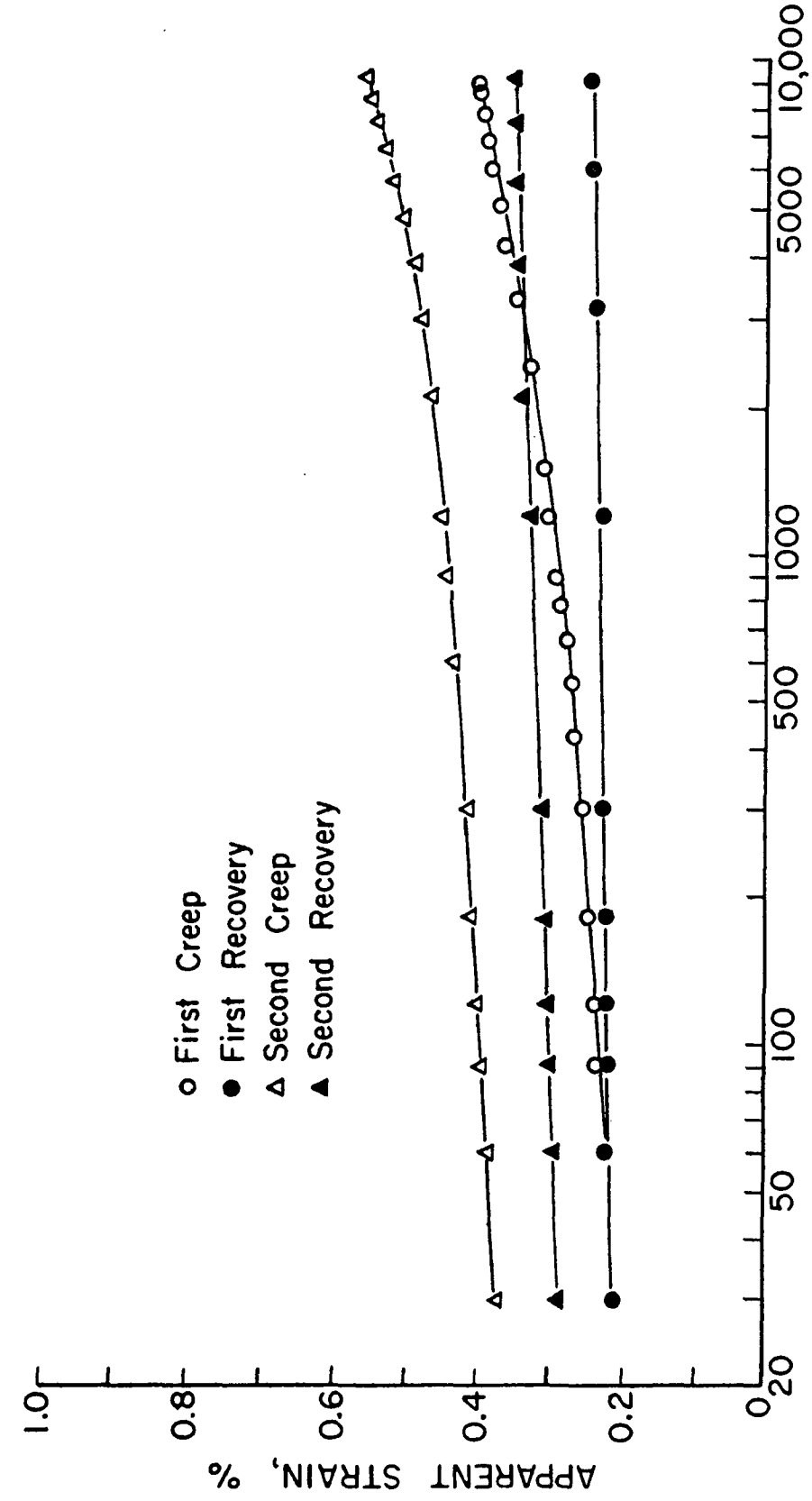

Figure 32. z-Direction Creep and Creep Recovery Curves for Specimen IB7.
Creep Stress = 5.5 kg./cm.^{2}

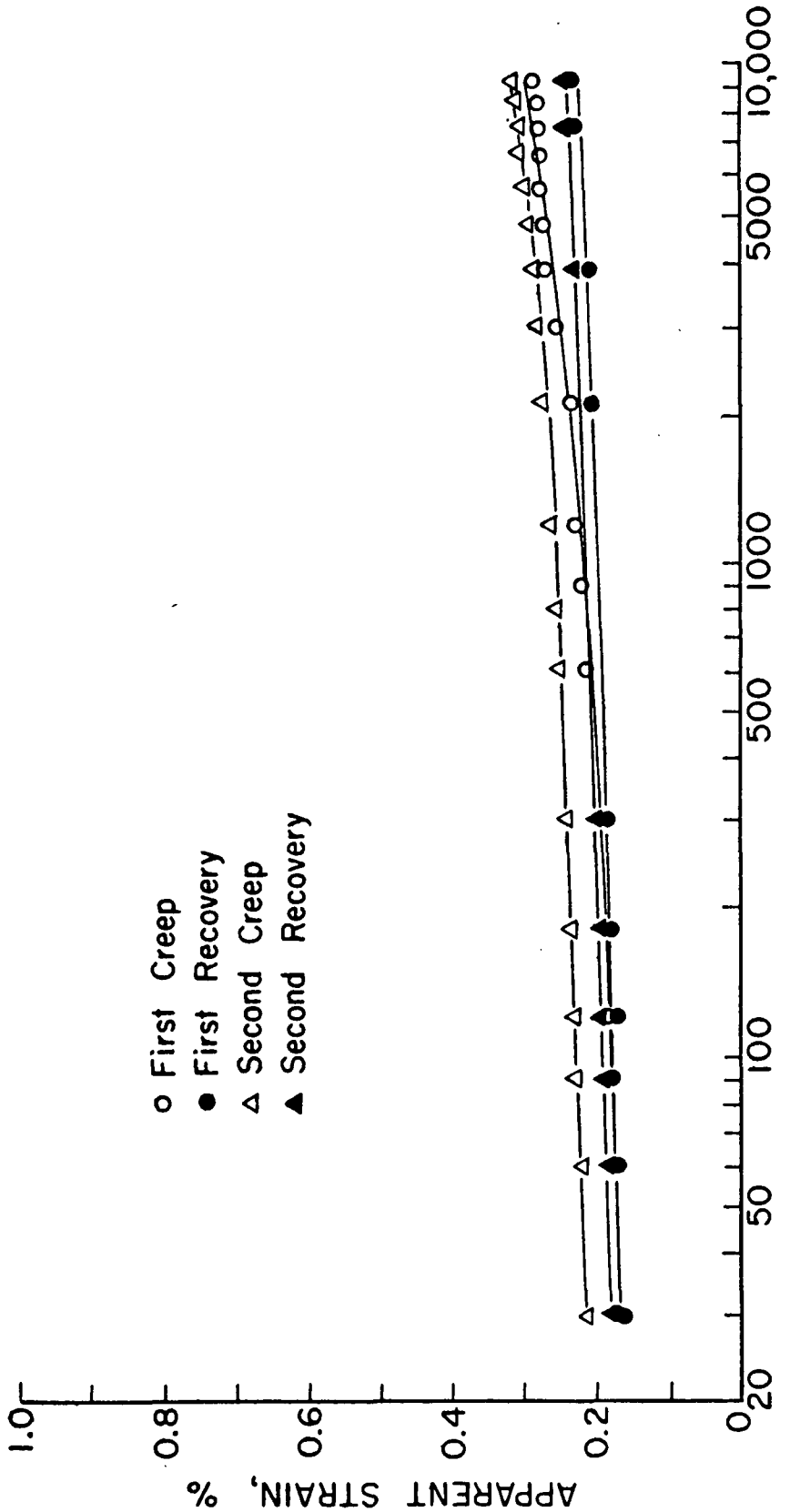

Figure 33. z-Direction Creep and Creep Recovery Curves for Specimen IB8.
Creep Stress = 5.5 kg./cm.^{2}

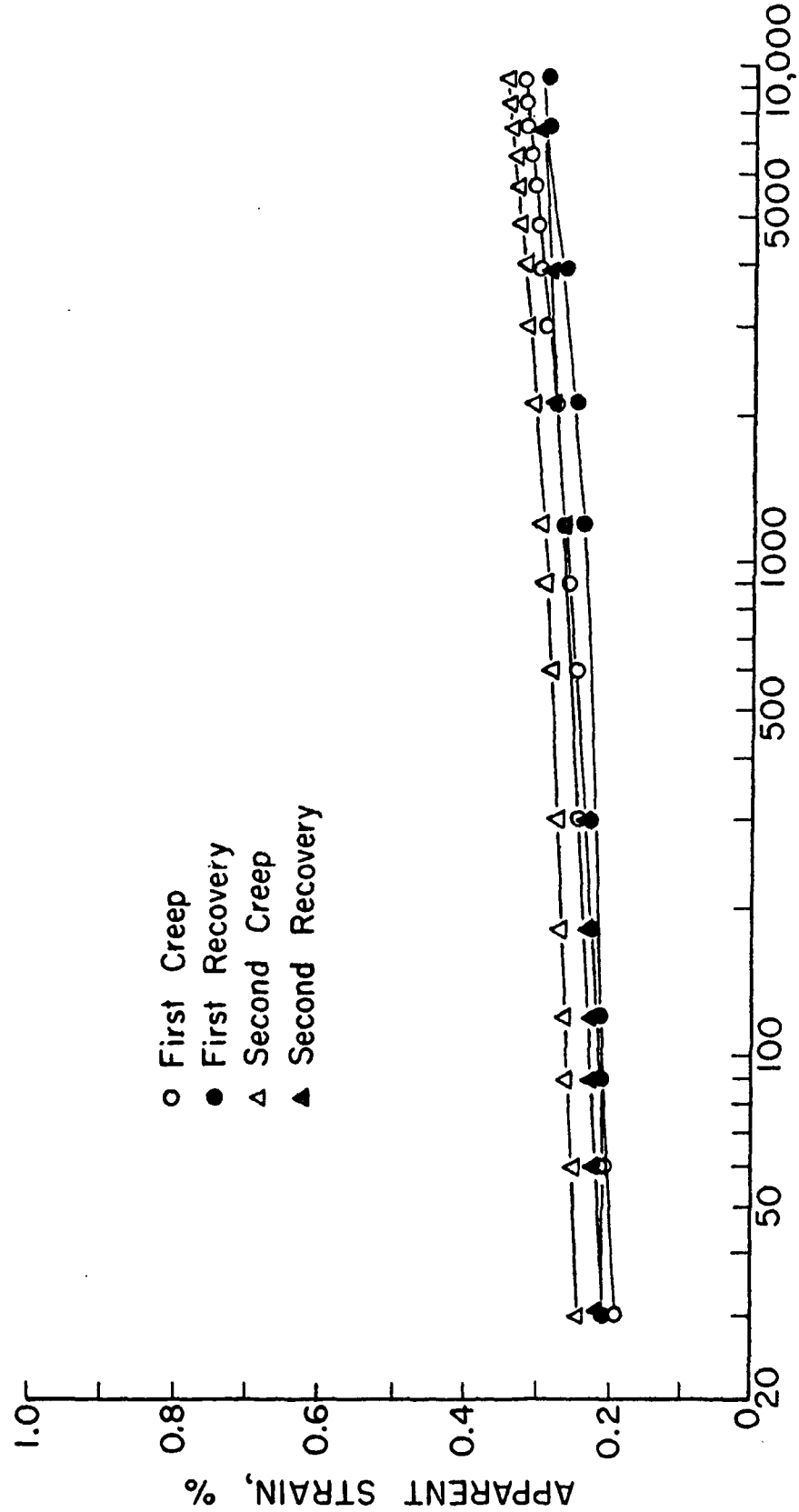

Figure 34. z-Direction Creep and Creep Recovery Curves for Specimen IB9.
Creep Stress = 5.5 kg./cm.^{2}

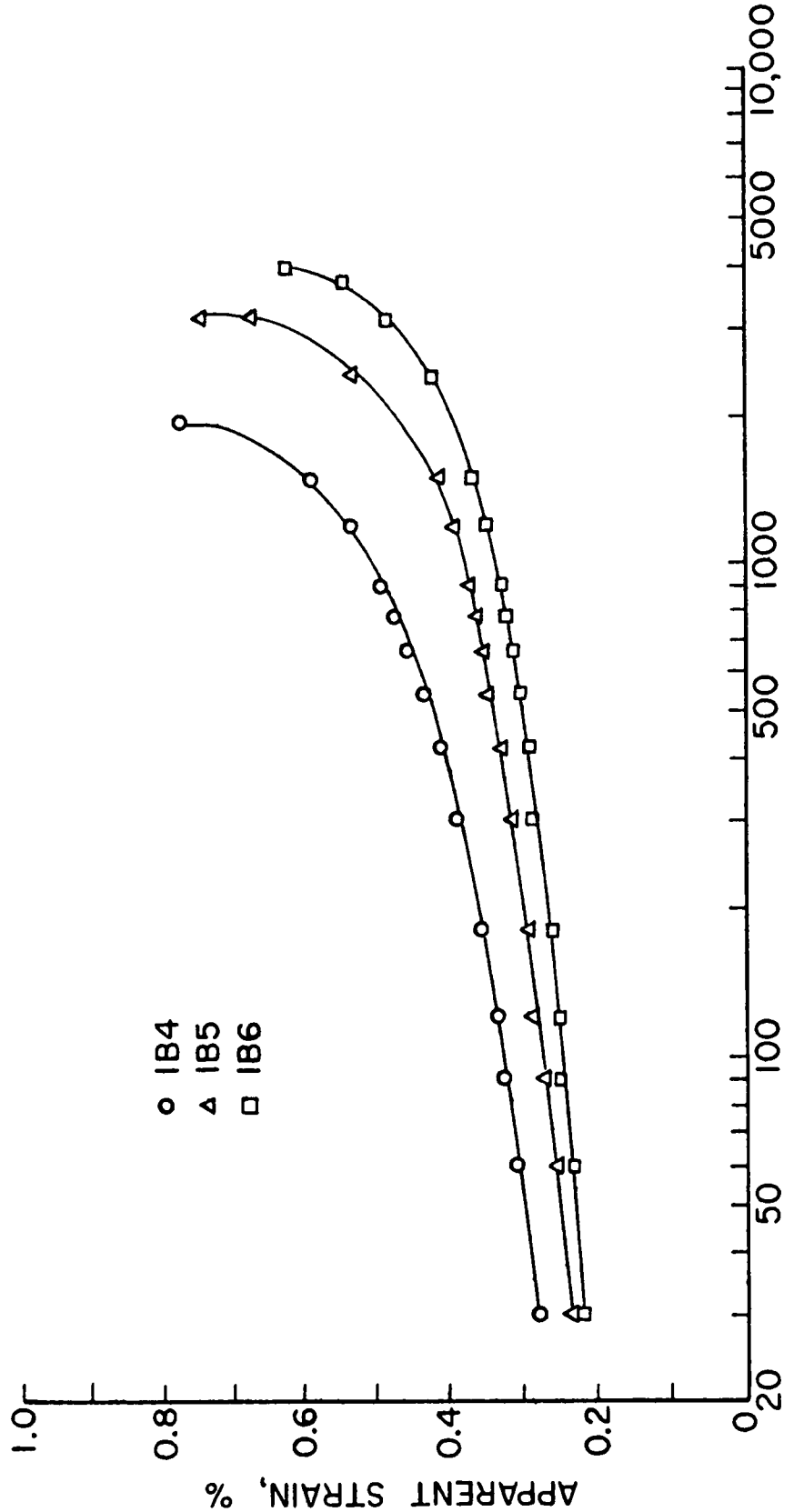

Figure 35. z-Direction First-Creep Behavior.
All Specimens Failed During Creep Test.
Creep Stress = 6.10 kg./cm.^{2}

creep test as compared to a load-elongation test, the deformation can be more accurately measured closer to the point of catastrophic failure. This would tend to give higher results for the creep failure strain, and might account for a portion of the increased strain during a creep test. It is probable, however, that part of the increased strain was a result of increased intrafiber deformation prior to bond failure during creep tests.

A summary of the creep and creep recovery tests is presented in Table V. The apparent elastic modulus was determined by dividing the creep stress by the extrapolated deformation of the specimen at 10 seconds, or the approximate time at which the creep stress was reached. This deformation was considered to be the elastic portion of the total deformation for the purpose of estimating an apparent elastic modulus.

There are several unusual effects occurring in z-direction creep that are not typical of the normal creep behavior of paper in the in-plane direction. A comparison of the deformation in the first- and second-creep tests shows that the creep deformation in the second creep test was greater than the deformation at any equivalent time in the first creep test for both Specimens IB 7 and IB 8. Brezinski (8) found the opposite to be true for tensile creep in the in-plane direction. There was a decrease in the apparent elastic modulus in the second creep test, when calculated at an extrapolated time of 10 seconds, which indicates that there was no strain hardening effect during creep. This is not consistent with the earlier load-elongation data, which indicated that the apparent initial elastic modulus could increase, decrease, or remain constant with repeated load-elongation cycling. It may be that the elastic modulus of the specimens, if determined at very short times, would show an increase in modulus

TABLE V

SUMMARY OF CREEP AND CREEP RECOVERY BEHAVIOR FOR HANDSHEET IB

Specimen	IB 4	IB 5	IB 6	IB 7	IB 8	IB 9
Apparent density, g./cc.	0.857	0.878	0.863	0.869	0.874	0.862
Creep stress, kg./cm.^{2}	6.10	6.10	6.10	5.5	5.5	5.5
Duration of 1st-creep test, sec. $\times 10^{-3}$	1.95	3.30	3.98	9.0	9.3	9.3
Duration of 2nd-creep test, sec. $\times 10^{-3}$	--	--	--	9.3	9.3	9.3
Total 1st-creep deformation, %	0.768	0.745	0.624	0.403	0.283	0.323
Total 2nd-creep deformation at time equal to 1st test duration, %	--	--	--	0.563	0.307	0.348
Difference between 1st and 2nd-creep deformations at time equal to 1st test duration, %	--	--	--	0.160	0.024	0.008
Nonrecoverable deformation for 1st-creep test, %	--	--	--	0.152	0.055	0.031
Nonrecoverable deformation for 2nd-creep test, %	--	--	--	0.213	0.062	0.047
Deformation at 10 sec. for 1st creep, %	0.235	0.195	0.190	0.185	0.160	0.170
Deformation at 10 sec. for 2nd creep, %	--	--	--	0.325	0.200	0.220
Apparent elastic modulus at 10 sec. for 1st creep, kg./mm.^{2}	25.9	31.3	32.1	29.7	34.4	34.4
Apparent elastic modulus at 10 sec. for 2nd creep, kg./mm.^{2}	--	--	--	16.9	27.5	25.0
Recovery at 10 sec. for 1st creep, %	--	--	--	0.205	0.155	0.180
Recovery at 10 sec. for 2nd creep, %	--	--	--	0.265	0.165	0.200
Wedge slope at 1200 sec. for 1st creep	0.964	1.06	1.14	0.258	0.312	0.259
Wedge slope at 1200 sec. for 2nd creep	--	--	--	0.681	0.441	0.273

with repeated creep cycling. However, such data could not be obtained experimentally, and extrapolation to shorter times was not reliable.

The decrease in apparent elastic modulus may be caused by time-dependent bond breaking, such as a gradual peeling failure. The fact that the specimens are weakened during a creep test is illustrated in Fig. 36, which shows the post-creep stress-strain behavior of the test specimens that had previously been subjected to creep cycling. The increase in strain of the weaker specimen might be an indication of bond peeling failure. One might speculate that such failure during a creep test would enable the fibers to bend more during a subsequent load-elongation test. This bending would contribute to greater deformation.

Another unusual observation shown in Table V was the increase in elastic recovery following the second creep test. The wedge effect also was observed to increase in the second creep test.

Creep rate versus time curves are shown in Fig. 37-40. In general, for most substances, creep rates decrease with time. If interfiber bond breaking controlled the creep rate, it might be expected to increase if the bond breakage decreased the load-bearing area within the structure, and all other effects remained the same. It was observed for the specimens that didn't fail that the creep rate decreased with time in all cases. However, when the specimens failed during creep (Fig. 40), the creep rate was observed to first decrease and then increase over a considerable time period prior to failure. It is suspected that interfiber bond breaking processes are responsible for the increasing creep rate phenomenon.

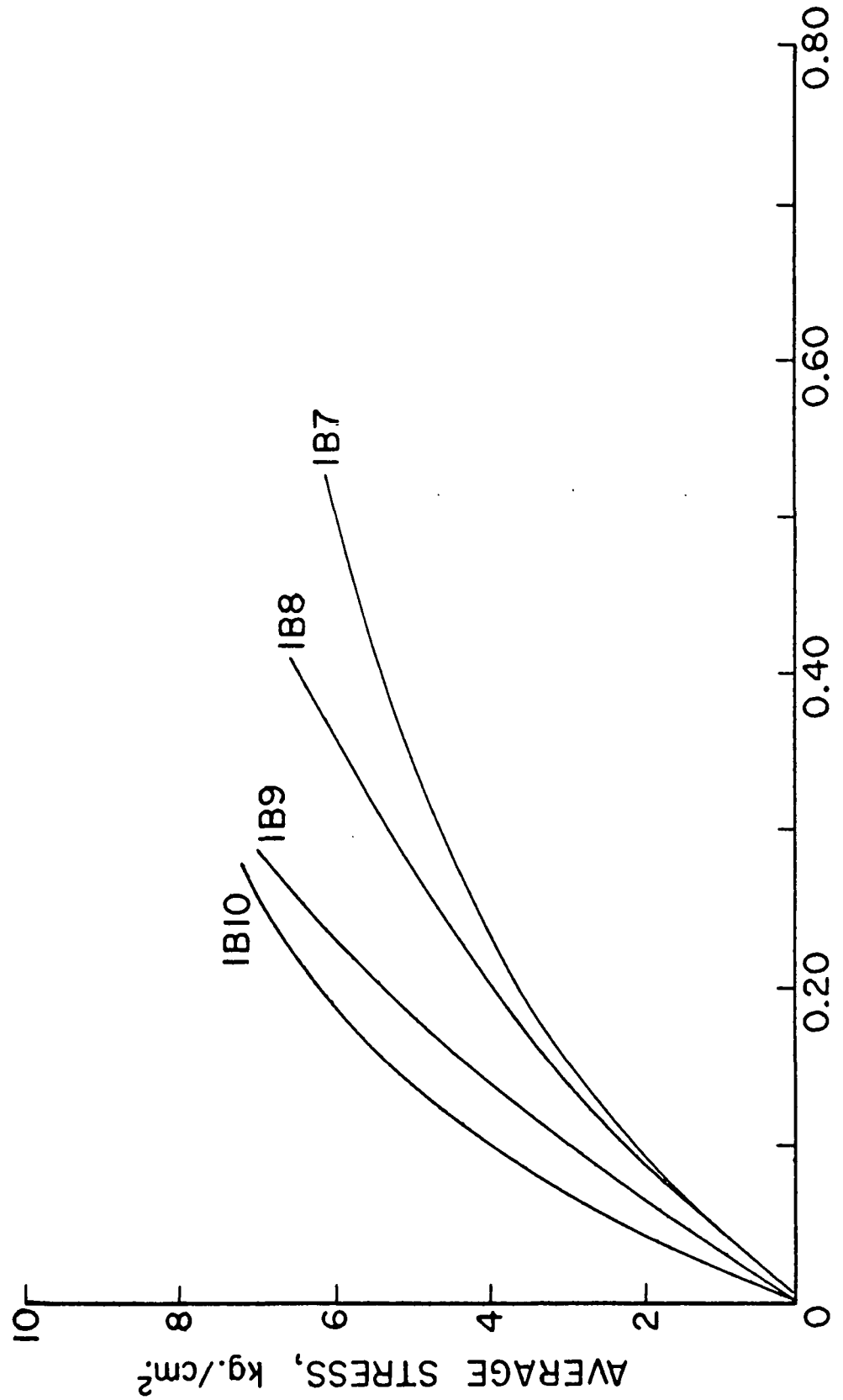

Figure 36. Post-Creep Stress-Strain Curves Indicating a General Weakening of the Specimen. Creep Tests for Specimens IB7, IB8, and IB9 were Shown in Figures 32, 33, and 34, Respectively. Specimen IB10 has Undergone no Creep

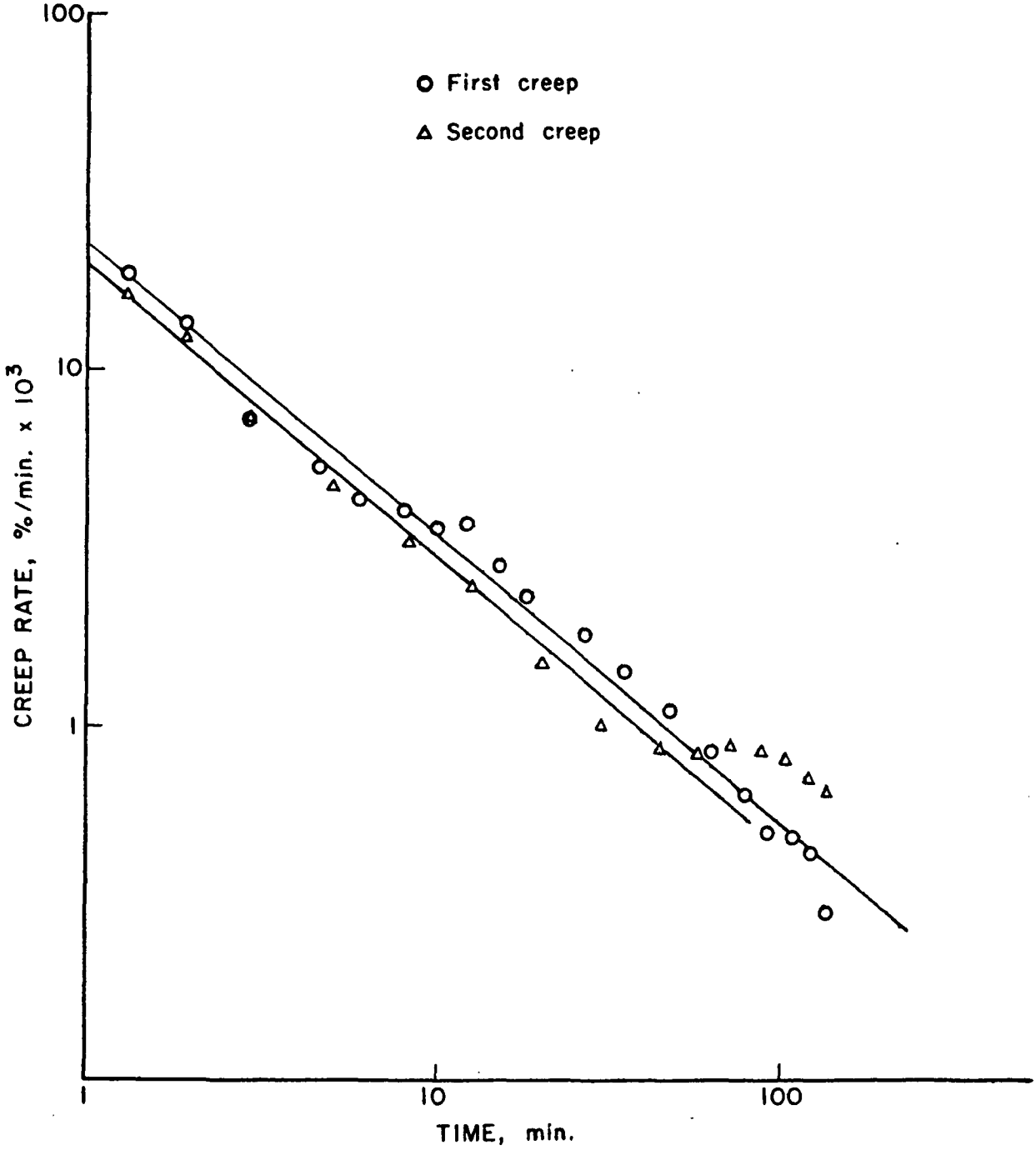

Figure 37. Creep Rate as a Function of Time for Specimen IB7. Creep Stress = 5.5 kg./cm.^{2}

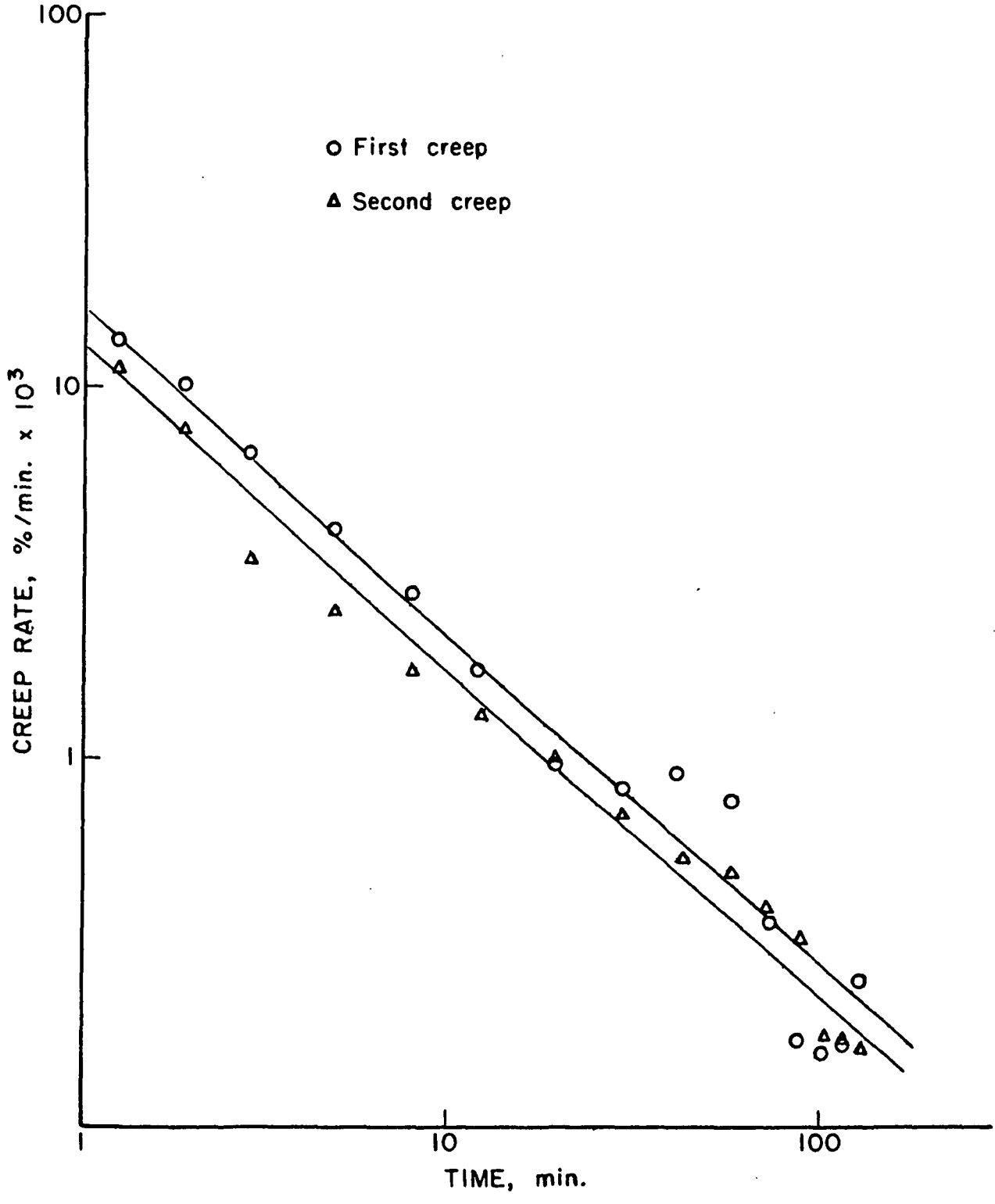

Figure 38. Creep Rate as a Function of Time for Specimen IB8.
Creep Stress = 5.5 kg./cm.^{2}

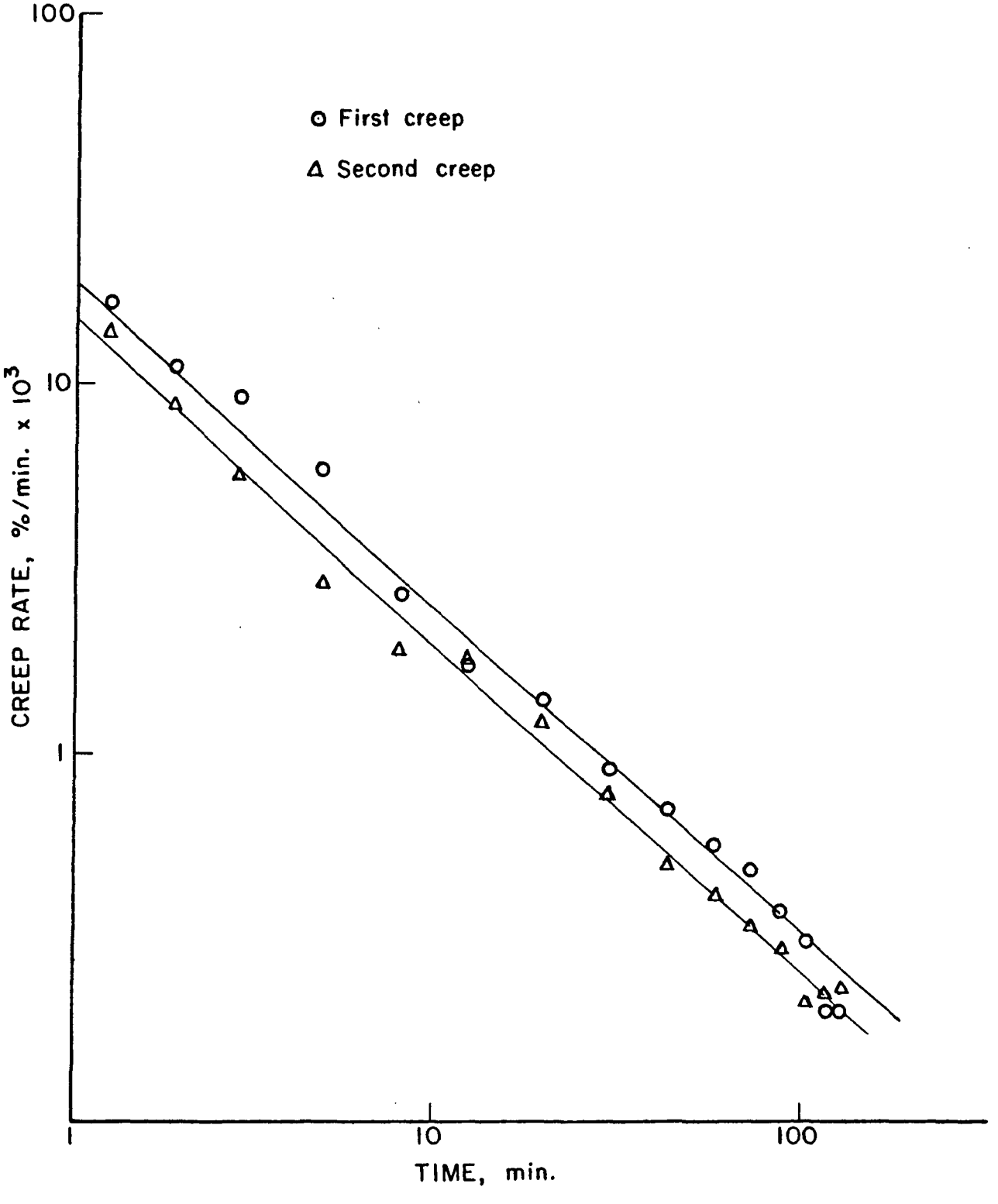

Figure 39. Creep Rate as a Function of Time for Specimen IB9.
Creep Stress = 5.5 kg./cm.^{2}

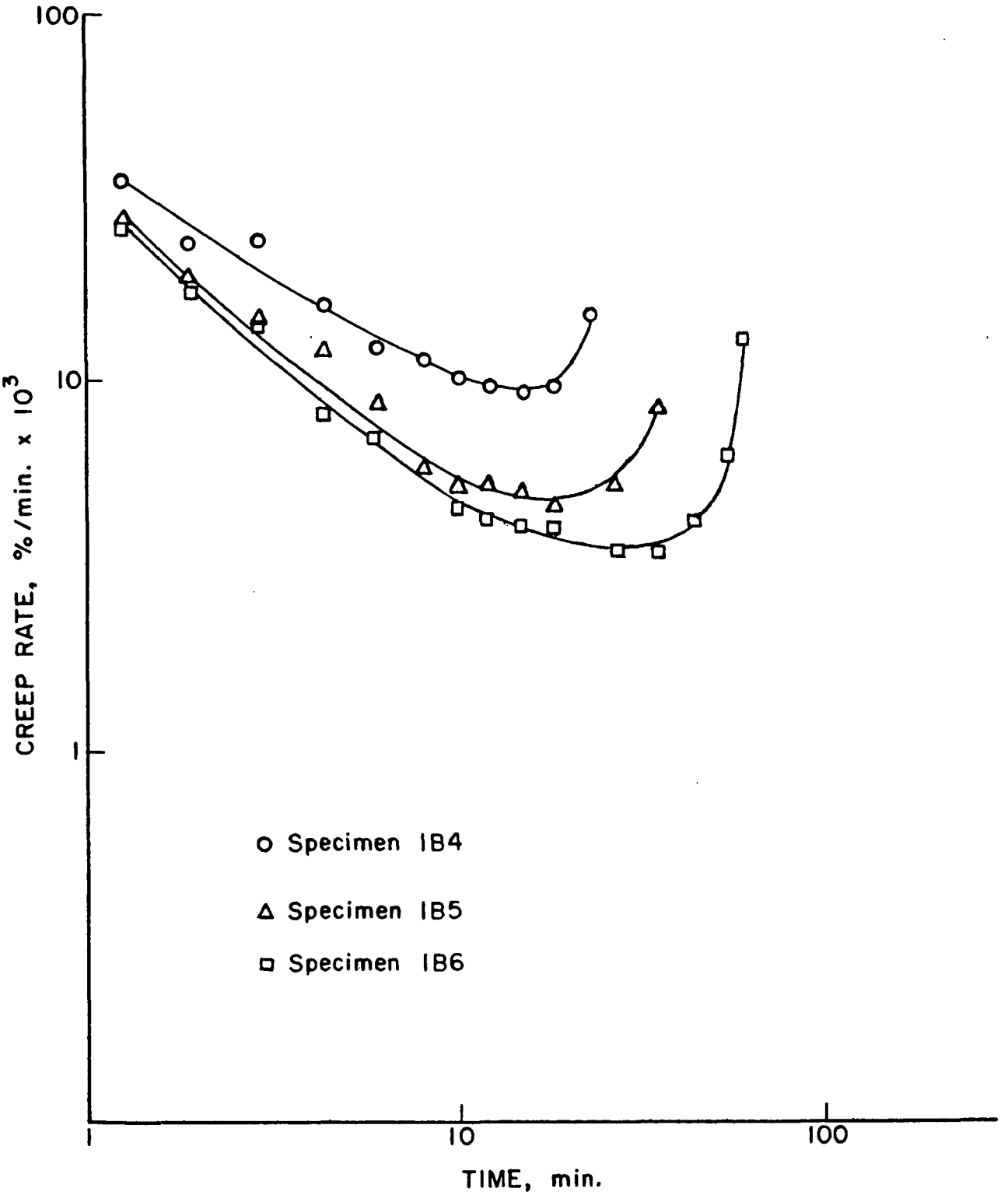

Figure 40. Creep Rate as a Function of Time for Specimens IB4, IB5, and IB6. Creep Stress = 6.10 kg./cm.^{2}

LIGHT SCATTERING

If it is assumed that the changes in the scattering coefficient are a good index of the relative change in bonded area, then measuring changes in the light-scattering properties of a specimen at different levels of stress should be a suitable technique for measuring the degree of interfiber bond breakage occurring during deformation.

The light-scattering technique for the determination of unbonded area is subject to a number of limitations. Briefly, the general problems arising in interpreting light-scattering data as a measure of bonding are:

1. Some areas may be optically bonded but not molecularly bonded. Therefore, increased light scattering could develop even if bonds were not broken.
2. The light-scattering method is incapable of detecting new surface areas, unless they are separated by more than one half the wavelength of the light used.
3. The light-scattering power of the individual fibers may change irreversibly.

Difficulties particular to the z-direction are:

1. The Kubelka-Munk theory applies to a homogeneous system in which interfiber bond breakage would be expected to occur uniformly throughout the specimen. This may not be the case in the z-direction.
2. The optical measurement techniques were not standard in that they involved specimens adhesive bonded between Lucite disks.

Preliminary experimental work indicated that at best only qualitative interpretations in light scattering with loading would be possible with the available techniques. However, it was still thought that by measuring changes in the scattering coefficient as a result of loading the following information could be obtained: (1) No change in scattering coefficient over the entire stress-strain curve would indicate that the z-direction tensile behavior is determined by intrafiber mechanisms, (2) changes in scattering coefficient over the entire stress-strain curve would suggest that interfiber bond-breaking processes could play an important role.

In measuring the stress-induced changes in light scattering, a specimen was brought to the desired stress level at a rate of stressing of 0.615 kg./cm.^{2}/sec. The load was held constant for 30 seconds, after which time the specimen was unloaded at the same rate. The technique for obtaining the light-scattering data, with its special modifications, was described in the experimental section.

The light-scattering properties for the specimens of different basis weight and density used throughout this experimental program are listed in Table VI. The handsheets subjected to the higher drying pressure are more bonded than those of the lower drying pressure, as indicated by the significantly lower values for the specific scattering coefficient.

The effect of the mounting procedure (adhesive bonding specimens to Lucite disks and then mounting on steel cylinders) on the light-scattering properties is illustrated in Table VII. The mounting of the specimens caused significant changes in the light-scattering values. These changes stem from a variety of sources, such as adhesive penetration, bubbles in the adhesive, aging of the

TABLE VI

LIGHT-SCATTERING PROPERTIES OF SPECIMENS USED IN EXPERIMENTAL PROGRAM

Specimen	Thickness, cm.	Basis Weight, g./cm.^{2}	Density, g./cc.	Scattering Power, SW	Absorption Power, KW	Specific Scattering Coefficient, $\underline{S}$, cm.^{2}/g.	Specific Absorption Coefficient, $\underline{K}$, cm.^{2}/g.
				Basis Weight			
IC 1	0.0300	251	0.837	4.934	0.0752	196.6	2.998
IC 3	0.0287	242	0.842	4.785	0.0727	197.7	3.005
IC 4	0.0279	242	0.866	4.638	0.0737	191.7	3.049
IC 8	0.0305	264	0.865	5.045	0.0753	191.1	2.854
IC 9	0.0282	240	0.853	4.639	0.0738	193.3	3.075
ID 1	0.0368	311	0.845	6.015	0.1069	193.4	3.439
ID 3	0.0373	319	0.854	6.231	0.1033	195.3	3.240
ID 6	0.0378	318	0.841	6.090	0.1017	191.5	3.201
ID 7	0.0368	315	0.856	6.143	0.1019	195.0	3.234
IE 2	0.0536	445	0.831	8.915	0.1274	200.3	2.864
IE 3	0.0531	449	0.845	8.611	0.1266	191.8	2.821
IE 5	0.0523	430	0.821	8.746	0.1301	203.4	3.025
IE 9	0.0551	463	0.840	9.246	0.1330	199.7	2.872
IF 2	0.0622	523	0.841	10.292	0.1562	196.8	2.986
IF 6	0.0625	510	0.816	10.494	0.1604	205.8	3.146
IF 7	0.0615	500	0.813	10.376	0.1530	207.9	3.066
IF 9	0.0617	516	0.836	10.599	0.1626	205.4	3.152
				Pressure Drying, 3.5 kg./cm.^{2}			
IG 1	0.0361	308	0.853	5.851	0.1040	190.0	3.377
IG 2	0.0358	304	0.850	5.882	0.1054	193.5	3.466
IG 3	0.0376	321	0.854	6.286	0.1034	195.8	3.222
IG 4	0.0366	302	0.827	5.873	0.0988	194.5	3.272
IG 5	0.0376	325	0.865	6.181	0.0993	190.2	3.056
IG 6	0.0383	327	0.853	6.251	0.1021	191.1	3.121
IG 7	0.0381	328	0.861	6.251	0.1021	190.6	3.111
IG 8	0.0376	325	0.865	6.266	0.1047	192.8	3.222
IG 9	0.0371	315	0.850	6.019	0.1030	191.1	3.269

TABLE VI (Continued)

LIGHT-SCATTERING PROPERTIES OF SPECIMENS USED IN EXPERIMENTAL PROGRAM

Specimen	Thickness, cm.	Basis Weight, g./cm.^{2}	Density, g./cc.	Scattering Power, SW	Absorption Power, KW	Specific Scattering Coefficient, S, cm.^{2}/g.	Specific Absorption Coefficient, K, cm.^{2}/g.
			Pressure Drying, 7.0 kg./cm.^{2}				
IIC 1	0.0342	321	0.939	5.268	0.0928	164.1	2.891
IIC 2	0.0350	314	0.897	5.223	0.0965	166.3	3.075
IIC 3	0.0348	316	0.908	5.228	0.0928	165.4	2.935
IIC 4	0.0350	319	0.912	5.279	0.0954	165.5	2.989
IIC 5	0.0340	310	0.912	5.115	0.0889	165.0	2.866
IIC 6	0.0343	310	0.904	5.253	0.0940	169.5	3.034
IIC 7	0.0350	321	0.917	5.357	0.0993	166.9	3.093
IIC 8	0.0353	321	0.908	5.426	0.1007	169.0	3.137
IIC 9	0.0361	325	0.899	5.619	0.0997	172.9	3.068

TABLE VII

EFFECT OF PREPARATION AND HANDLING ON THE LIGHT-SCATTERING PROPERTIES

Specimen	Condition	Scattering Power, SW	Absorption Power, KW	Specific Scattering Coefficient, S, $cm.^2/g.$	Specific Absorption Coefficient, K, $cm.^2/g.$
IH 1	S[a]	6.294	0.0956	189.6	2.878
	F[b]	6.554	0.1331	197.4	4.010
	M[c]	6.799	0.1563	204.8	4.710
IH 2	S	6.194	0.0877	193.6	2.741
	F	6.379	0.1284	199.3	4.011
	M	6.255	0.1453	195.5	4.542
IH 3	S	6.447	0.0932	199.0	2.876
	F	6.481	0.1216	200.0	3.752
	M	6.867	0.1429	211.9	4.410
IH 4	S	6.522	0.0959	194.1	2.854
	F	6.698	0.1321	199.4	3.931
	M	6.910	0.1536	205.7	4.573
IH 5	S	6.122	0.0889	195.0	2.831
	F	6.185	0.1140	197.0	3.631
	M	6.096	0.1361	194.1	4.336
IH 6	S	6.386	0.0970	198.3	3.012
	F	6.220	0.1154	193.2	3.585
	M	6.432	0.1371	199.8	4.259
IH 7	S	6.354	0.0918	194.9	2.814
	F	6.216	0.1196	190.7	3.667
	M	6.043	0.1360	185.4	4.171

[a] Standard specimen before preparation.

[b] Specimen fixed between Lucite disks with Ecobond 45 (clear).

[c] Specimen and Lucite disks were mounted between steel loading cylinders with two-sided tape, and then removed from between the cylinders by wedging with a razor blade.

adhesive, etc. This must be taken into consideration with respect to the magnitudes of the coefficients used to characterize the light-scattering properties.

A major source of error affecting the analysis of the results appears to be damage to the specimens during the breaking of the two-sided tape joint which holds the Lucite cylinder to the steel cylinder for loading purposes (Fig. 13). This can result in changes in the specific light-scattering coefficient as high as 12 $cm.^2/g$.

Two important observations could be made (Table VIII). First, some specimens could be brought to a relatively high load without any evidence of interfiber structural damage, and second, stress-induced changes in light-scattering properties tend to support a delamination type of failure.

With respect to the first observation, Specimens IIC 2, IIC 4, IIC 6, and IIC 7 exhibited no indication of interfiber structural damage as indicated by light scattering. This was in spite of the fact that Specimens IIC 6 and IIC 7 were brought to a higher level of stress than IIC 5 and IIC 8, which did exhibit evidence of interfiber structural damage.[36] This indicates that at least some specimens can reach a relatively high level of loading (approximately 85% of failure load) without any evidence of interfiber structural damage as indicated by a change in the scattering coefficient. Whether it was loading or the handling procedures that caused the structural damage in the other specimens is not known.

[36]This difference could have been because Specimens IIC 6 and IIC 7 were at the given stress level for only 15 seconds, rather than the normal 30 seconds, because of failure of the two-sided tape joint.

TABLE VIII

EFFECT OF z-DIRECTION LOADING ON THE LIGHT-SCATTERING PROPERTIES

Specimen	Stress, kg./cm.^{2}	Condition	Scattering Power, SW	Absorption Power, KW	Specific Scattering Coefficient, S, cm.^{2}/g.	Specific Absorption Coefficient, K, cm.^{2}/g.	Change in Specific Scattering Coefficient, ΔS, cm.^{2}/g.[a]
IIC 1	0	S[b]	5.268	0.0928	164.1	2.891	
		F[c]	5.507	0.1193	171.6	3.717	
		L[d]	5.455	0.1274	170.0	3.968	-1.6
IIC 2	3.66	S	5.223	0.0965	166.3	3.075	
		F	5.312	0.1135	169.2	3.616	
		L	5.327	0.1123	169.7	3.575	0.5
IIC 3	0	S	5.228	0.0928	165.4	2.935	
		F	5.401	0.1098	170.9	3.473	
		L	5.408	0.1164	171.1	3.680	0.2
IIC 4	4.88	S	5.279	0.0954	165.5	2.989	
		F	5.357	0.1244	167.9	3.899	
		L	5.258	0.1255	164.8	3.934	-3.1
IIC 5	6.10	S	5.115	0.0889	165.0	2.866	
		F	5.234	0.1094	168.8	3.530	
		L	5.677	0.1170	183.1	3.774	14.3

[a] Difference between L and F.

[b] Standard specimen before preparation.

[c] Specimen fixed between Lucite disks with Ecobond 45 (clear).

[d] Same specimen after having been mounted between steel loading cylinders, loaded, and removed from between steel cylinders.

TABLE VIII (Continued)

EFFECT OF z-DIRECTION LOADING ON THE LIGHT-SCATTERING PROPERTIES

Specimen	Stress, kg./cm.^{2}	Condition	Scattering Power, SW	Absorption Power, KW	Specific Scattering Coefficient, S, cm.^{2}/g.	Specific Absorption Coefficient, K, cm.^{2}/g.	Change in Specific Scattering Coefficient, ΔS, cm.^{2}/g.[a]
IIC 6	7.32	S[b]	5.253	0.0940	169.5	3.034	
		F[c]	5.332	0.1083	172.0	3.494	
		L[d]	5.281	0.1161	170.4	3.746	-1.6
IIC 7	7.32	S	5.357	0.0993	166.9	3.093	
		F	5.500	0.1126	171.3	3.508	
		L	5.392	0.1177	168.0	3.667	-3.1
IIC 8	6.10	S	5.426	0.1007	169.0	3.137	
		F	5.589	0.1128	174.1	3.513	
		L	6.022	0.1177	187.6	3.668	13.5
IIC 9	7.92	S	5.619	0.0997	172.9	3.068	
		F	5.807	0.1146	178.7	3.525	
		L	6.746	0.1208	207.6	3.716	28.9[e]

[a] Difference between L and F.

[b] Standard specimen before preparation.

[c] Specimen fixed between Lucite disks with Ecobond 45 (clear).

[d] Same specimen after having been mounted between steel loading cylinders, loaded, and removed from between steel cylinders.

[e] Specimen had completely failed.

The second interesting observation was that the failure stress of Specimens IIC 5 and IIC 8, after testing, was only about one fourth the normal failure stress of the specimens dried under a pressure of 3.5 kg./cm.^{2}, even though these latter specimens had a lower bonded area: That is, Specimens IIC 5 and IIC 8 had undergone extensive structural damage to the point of having little z-direction strength, yet these same specimens still had a higher bonded area than specimens with approximately four times the z-tensile strength.[37] This suggests that damage may be along weak layers (delamination type), resulting in relatively small changes in scattering coefficient, but a large decrease in strength. This was further supported by visual examination of specimens that had failed under z-direction loading, which indicated a delamination type of failure.

In summary, the light-scattering work provided the following information:

1. Structural damage caused by handling could be high enough to completely overshadow any damage that might be caused by stressing.
2. Specimens could be stressed up to 85% of their normal failure stress over a short period without exhibiting any structural damage as indicated by light scattering.
3. Changes in the light-scattering coefficient of about 14 cm.^{2}/g., for the higher density specimens, indicated extensive interfiber structural damage as evidenced by a reduction in failure stress to about one fifth the normal value. Even though these higher density specimens were now only about one fourth as strong as the lower density specimens, light scattering still showed that they

[37] Compare a scattering coefficient of 184 cm.^{2}/g. for a loaded specimen dried at a pressure of 7.0 kg./cm.^{2} (this is the sum of the normal scattering coefficient of 170 cm.^{2}/g. plus the change due to loading of 14 cm.^{2}/g.) to 195 cm.^{2}/g. for an unloaded specimen dried at a pressure of 3.5 kg./cm.^{2} The latter has a z-direction failure stress about four times the former.

had a higher relative bonded area. This indicates that the specimens may be failing by a type of local delamination process.

PROPAGATION OF FAILURE

Because of the eventual "wedge effect" occurring within z-tensile specimens as failure is approached, it was speculated that plastic deformation begins in a weak area of the specimen and then propagates throughout the structure in some time-dependent way. This would mean that a greater amount of plastic deformation should be occurring toward the open portion. Support of this concept is given in Table IX where it can be seen that the apparent plastic deformation is related to the wedge effect. The wedge slope, b', is observed to show a permanent increase after each loading cycle. This increase also correlates with the increase in irrecoverable work. A similar effect for creep-creep recovery curves is shown in Table X, where the wedge effect was observed to increase after each creep and creep recovery cycle.

WORK TO RUPTURE

The energy, or work, in straining a specimen is the area under the load-elongation curve. Since both the load per unit area of specimen and the elongation are small in the z-direction, it follows that the amount of work required to rupture the specimen will also be low.

The work to rupture a specimen was examined under conditions of both constant rate of loading and creep, and the results are shown in Table XI. It should be noted that these values are not exact because of the difficulty of accurately measuring the strain at failure and because of the need to estimate the work required to reach the desired creep load. The important observation, however, is that the work-to-rupture values are approximately one hundred times

TABLE IX

EFFECT OF PROGRESSIVE LOAD-UNLOAD CYCLING ON THE PERMANENCE OF THE WEDGE EFFECT AND AMOUNT OF IRRECOVERABLE WORK

Specimen	Load Cycle	Average Stress, kg./cm.^{2}	Apparent Strain, %	Wedge Slope[a] × 10^4	Irreversible Work[b], kg.-cm./g.
IA 6	2			-0.037	
	3	5.38	0.224	-0.046	0.00239
	4	6.60	0.385	-0.273	0.01090
IA 9	2			0.254	
	3	5.63	0.219	0.339	0.00159
	4	6.24	0.263	0.306	0.00212
	5	7.09	0.403	0.550	0.00900
IIA 7	1	6.24	0.182	-0.029	0.00189
	2	7.46	0.237	-0.065	
	3	8.56	0.316	-0.099	0.00518
	4	9.17	0.406	-0.130	0.00886
IIA 9	1	6.24	0.177	-0.009	0.00166
	2	7.46	0.231	+0.023	0.00235
	3	8.56	0.278	0.023	0.00418
	4	9.29	0.370	0.033	0.00774

[a]Determined at zero load immediately following load cycle. Negative values mean the open portion of the wedge was in the $-\underline{y}$-direction. Positive values mean open portion was in the $+\underline{y}$-direction (Fig. 16).

[b]The difference between the area under the load curve and the area under the unload curve divided by the weight of the specimen under stress.

lower than in the in-plane direction, and that time apparently affects the work going into the specimen, because of its effect on the failure strain.

One of the more interesting aspects of these low values for work in the $\underline{z}$-direction is the implication this has on the calculation of a bonding strength value using Nordman's technique (11) (see p. 14). This theory is based on the concept that the irrecoverable energy involved in tensile straining of paper is the work required to rupture the fiber-to-fiber bonds, and the change in the optically apparent exposed surface, as measured by the change in scattering

TABLE X

EFFECT OF CREEP AND CREEP RECOVERY CYCLING ON THE PERMANENCE OF THE WEDGE EFFECT

Specimen	Recovery Cycle	Creep Stress, kg./cm.^{2}	Strain[a], %	Wedge Slope[b] × 10^4
IB 7	1	5.50	0.403	-0.355
	2	5.50	0.563	-0.623
IB 8	1	5.50	0.283	-0.201
	2	5.50	0.307	-0.269
IB 9[c]	1	5.50	0.323	-0.135
	2	5.50	0.348	+0.089

[a] Maximum strain during creep test.

[b] Determined immediately after recovery. The sign indicates the direction of the open end of the wedge (Fig. 16) with respect to the $\bar{y}$ axis.

[c] There was a change in the wedge slope during the creep test.

TABLE XI

COMPARISON OF WORK TO RUPTURE DETERMINED FROM CONSTANT RATE OF LOADING AND CREEP TEST

Specimen	Work to Rupture[a] at Constant Rate of Loading, kg.-cm./g.	Specimen	Work to Rupture at Creep Stress of 6.10 kg./cm.^{2},[b] kg.-cm./g.
IA 1	0.0181	IB 4	0.0458
IA 2	0.0132	IB 5	0.0458
IA 3	0.0100	IB 6	0.0372
IA 4	0.0225		
IA 5	0.0151	Average	0.0429
Average	0.0158		

[a] Work to 95% of failure stress.

[b] Includes an estimate of the work required to reach the creep stress ($\cong$ 0.007 kg.-cm./g.).

coefficient, is a measure of the area of fiber-to-fiber bond failure. Therefore, by plotting the irrecoverable work in a load-elongation cycle against accompanying increases in scattering coefficient, a bonding strength value can be determined from the slope of the best-fit straight line. The following equation describes the relationship:

$$\text{Bonding-strength value} = \Delta W/\Delta S \qquad (8)$$

where ΔW = irreversible work per unit weight, and

ΔS = change in specific scattering coefficient.

If it is assumed that a linear correlation exists between the change in scattering coefficient and the irreversible work per unit weight in the z-direction, then from Table IX it is estimated that the maximum irreversible work is about 0.008 kg.-cm./g. (7750 ergs/g.) for the II-series specimens. From Table VIII, it was shown that a change in scattering coefficient of about 14 $cm.^2/g.$ resulted in almost total failure of the specimen. Therefore, it is possible to estimate a bonding-strength value from Equation (8) in the z-direction to be about 560 $ergs/cm.^2$

Compared to values for in-plane tension ranging from 10^5 to 8×10^5 $ergs/cm.^2$ (16), it is observed that the z-direction bonding-strength value is as much as 200 to 2,000 times lower than that calculated for the in-plane direction. The weakness of the fiber-to-fiber bonds under z-direction stress limits the dissipation of energy through intrafiber mechanisms. This concept of the energy dissipated during straining being related to interfiber bond failure is in line with Van den Akker's "force-limited energy" where the force is that required to rupture the bond (16).

SUMMARY AND CONCLUSIONS

The tensile mechanical behavior of paper perpendicular to its plane (the z-direction) was studied in load-elongation and creep. All studies were conducted on handsheet specimens prepared from a mildly beaten and classified western hemlock sulfite pulp with basis weights between 250 and 500 g./m.^{2} All were dried under pressure and all were adhesive bonded to 1-inch diameter metal cylinders. The data were acquired at the standard conditions of 50% R.H. and 73°F.

For the particular specimens used in this work, the following principal experimental results were obtained:

1. Tensile strain in the z-direction was typically nonuniform as indicated by the nonparallel separation of the cylinder surfaces when a tensile load was applied. The nonuniform deformation over the specimen area was noted as the slope of the inclination of the cylinder surfaces (the wedge slope) relative to assumed parallelism before the application of load. Despite wide variations in the extent of wedge deformation, the average force versus average displacement curves were reasonably reproducible and satisfactory for the study of mechanical behavior.
2. Specimens of higher basis weight exhibited lower average failure stresses and higher apparent failure strains in load-elongation tests. Between-specimen reproducibility was poorer as the basis weight increased.
3. An increase in the apparent density of the specimens, through pressures applied during drying, resulted in an increased stress at failure, but had no effect on the apparent strain at failure.

4. The shapes of the average load-average elongation curves were typically concave toward the elongation axis. An initial linear elastic response to load could not be established with accuracy. If it occurred, it was limited to the strain region below about 0.05%. In tests at loading rates of approximately 0.3 kg./cm.^{2}/sec., the strain at failure could not be determined accurately, but fell within a range of 0.25 to 0.7%. Failure stresses were within a range of about 5-9 kg./cm.^{2}
5. In load-unload cycles to progressively higher loads, it was noted that the z-direction strain had a high percentage of recovery, even as the maximum stress level was approached. The recovery was always nonlinearly related to load, and the very large hysteresis effects were typical of time-dependent elasticity.
6. Load-elongation cycling had no consistent effect on the initial slope of the load-elongation curve.
7. Specimens would withstand loads of 73% of the failure load (as determined in load-elongation tests) for 10,000 seconds without rupture. For loads about 81% of the failure load, total failure occurred between 2,000 and 4,000 seconds.
8. Small time-dependent creep deformations were largely recoverable, but with greater creep deformations, the time-dependent recovery decreased as a percentage of the creep deformation. The apparent elastic recovery determined quickly after removal of the creep load was greater following a second creep test than following the first test (equal loads and times), suggesting a reduced elastic modulus as a result of time under load. The wedge slope always increased in a second creep test.

9. In tests at higher loads, the creep rate increased with time over an appreciable time period as the specimen approached the point of complete fracture. This was contrary to the reported behavior for in-plane creep.
10. In load-elongation tests, the specimens could be subjected to 85% of their normal breaking load without exhibiting a measurable change in the scattering coefficient.
11. A change in the scattering coefficient of 14 $cm.^2/g.$ for a specimen loaded to near failure was related to an extensive loss of strength, as evidenced by its subsequent failure at a stress of only one fifth the normal breaking stress. This rather small change in scattering coefficient relative to such a large change in strength suggested that debonding occurred within a limited zone in the specimen and was not distributed uniformly throughout the fibrous structure.
12. The nonrecoverable z-direction deformation could be correlated with the nonuniformity of strain.
13. The ratio of the irrecoverable work in a load-unload cycle to the change in scattering coefficient for that cycle was determined (in the worst case) to be about 500 $ergs/cm.^2$ (Nordman bonding-strength value). This was from 200 to 2,000 times less than the comparable values determined for paper in the in-plane direction.

The foregoing observations lead to the following description of the z-direction mechanical behavior of paper. Upon application of a z-direction tensile load, the specimen responds almost immediately in a nonlinear manner to the applied force. A regime in which the initial strain is proportional to stress is difficult to define experimentally, and if it exists, it must be confined to apparent strains of less than 0.05%. The slope of the load-elongation curve

at the zero stress-zero strain intercept is low, leading to estimated elastic moduli in the z-direction of only 20-60 kg./mm.^{2} These are typically one tenth of the apparent in-plane elastic moduli of paper. At very low stresses, usually between 1 and 2 kg./cm.^{2}, appreciable bending of the load-elongation curve begins toward the elongation axis. Removal of loads applied for short times results in practically complete recovery of the strain, but with a pronounced hysteresis effect. As the loads are increased further, recovery is still appreciable, but with even larger hysteresis effects. Only as the load approaches the point of ultimate failure of the specimen does the nonrecoverable deformation become important.

Repeated load-elongation cycling produces various changes in the initial slope of the load-elongation curve. In some instances, the initial slope increased in a second cycle, then remained the same for a number of cycles. In other instances, the initial slope decreased with repeated cycling. This variable behavior suggests that the consistent or true behavior is masked by the nonuniformity of strain over the specimen area. Following a second creep test, the rapid elastic strain increased in magnitude relative to that after the first creep test. It is expected that this increased elastic response represents a change due to interfiber bond rupture, localized within the specimen. Without such bond rupture, it is expected that the apparent elastic modulus would remain relatively constant with deformation in the z-direction.

Specimens could be loaded up to 85% of the breaking load without exhibiting any changes in optical properties. The fact that changes in the optical scattering coefficient occurred only as the failure stress was approached, in conjunction with their small magnitude despite very large reductions in specimen strength at that point, indicated that such changes were localized within the

specimen. Such a phenomenon would occur with delamination or crack propagation within a localized plane. The observation in creep tests to failure that the creep rate increased over an appreciable time period prior to final rupture is consistent with the concept of a propagating failure plane. The wedge-type strain nonuniformity, which is typical of z-direction tensile response, conforms further to the general concept of a structure exhibiting localized progressing failure. As the failure plane increases in size, the remainder of the specimen continues to support the load, but quite nonuniformly over the load-bearing area. The rate of failure plane propagation becomes very high in the load-elongation test near the point of maximum load, making it difficult to measure a maximum failure strain. In a creep test at high loads, the rate of failure propagation is slower and the final fracture period is extended in time and more easily observed. The maximum strain in creep failure is considerably greater than the maximum strain measurable in a load-elongation test, because of the improved capability of measuring strain and because of the potentially greater extensibility of fiber substance as a result of much greater time under load.

Intrafiber response as a sole mechanism of deformation in z-direction tension is viewed as limited to very low strain levels of perhaps 0.1 to 0.2%. At strains much beyond this point, the concentration of stress at the periphery of fiber-to-fiber bonds leads to progressive debonding of the structure, which soon is localized at narrow planes. Under these conditions, the major portion of the specimen structure is still relatively intact, thus providing relatively little change in the optical properties of the specimen. The early onset of fracture at a concentrated plane determines the strength of the specimen, and makes it virtually impossible to determine an average mechanical property for a hypothetically uniform fibrous structure.

The most plausible mechanism of failure of fiber-to-fiber bonds is by a bond-peeling mechanism in which stress concentrations occur both at a plane of failure within a specimen and at the periphery of the individual areas of bonding. Such a concentration of stress may be attributed to the geometry of the bonded areas and to the variations in structure from point to point in a specimen. The effect is undoubtedly enhanced because of nonuniform mechanical properties over the specimen area.

ACKNOWLEDGMENTS

I wish to thank my thesis advisory committee (Drs. J. P. Brezinski, R. W. Nelson, and R. M. Leekley) for their critical discussions and advice during this thesis. I would especially like to thank Dr. Brezinski for stressing the importance of thinking, and for his assistance with writing the final manuscript. A special note of thanks is also due Dr. Nelson for his help with the mathematical analysis of the data.

During the course of this thesis, there have been several people who I feel have done more than that which their jobs required. The names that stand out among these are Messrs. P. F. Van Rossum, M. C. Filz, Jr., and L. E. Dambruch for their assistance in design and construction of the experimental apparatus. I also feel that Mr. B. D. Andrews' reputation as the best man to see about acquiring auxiliary equipment remains intact.

The help of the following is also gratefully acknowledged: Mr. L. R. Dearth for his helpful discussions and assistance related to the optical properties of paper, Mr. K. W. Hardacker for his assistance in setting up the associated electronic equipment, Mr. W. A. Wink and Mr. R. H. Van Eperen for sharing their wealth of experience in paper evaluation, Mr. J. D. Hankey and Dr. R. A. Parham for preparing the light and electron micrographs, and Mr. F. R. Sweeney and Mr. D. E. Beyer for their fine photography.

There have been many others of the staff, student body, and faculty at I.P.C. who have contributed directly or indirectly to this thesis, and I thank you all. One of the "all-time great" papermakers, Dr. J. d'A. Clark, who inspired me to get into the pulp and paper area, once said: "A person was

really fortunate to be able to attend The Institute of Paper Chemistry." He was one hundred percent correct!

Thank you, Charlene, Kenny, and Kevin.

LITERATURE CITED

1. Dunning, C. E. An examination of the longleaf pine cell-wall morphology by electron microscopy of single fibers. Doctor's Dissertation. Appleton, Wis., The Institute of Paper Chemistry, 1968. 409 p.

2. Ebeling, K. I. Distribution of energy consumption during straining of paper. Doctor's Dissertation. Appleton, Wis., The Institute of Paper Chemistry, 1970. 737 p.

3. Van den Akker, J. A., Tappi 42, no. 12:940-7 (1959).

4. Asunmaa, S., and Steenberg, B., Svensk Papperstid. 61, no. 17B:686-95 (1958).

5. Buchanan, J. G., and Lindsay, R. A. A note on the structure of paper as revealed by the scanning electron microscope. In Bolam's Formation and structure of paper. Transactions of the Symposium held at Oxford, Sept., 1961. 1st ed. Vol. I. p. 101-8. London, Tech. Sect. Brit. Paper and Board Makers' Assoc., 1962.

6. Page, D. H., and Tydeman, P. A. A new theory of the shrinkage, structure, and properties of paper. Ref. (5), p. 397-413.

7. Swanson, J. W., Tappi 39, no. 5:257-70 (1956).

8. Brezinski, J. P. A study of the viscoelastic properties of paper by means of tensile creep tests. Doctor's Dissertation. Appleton, Wis., The Institute of Paper Chemistry, 1955. 242 p.

9. Algar, W. H. Effect of structure on the mechanical properties of paper. In Bolam's Consolidation of the paper web. Transactions of the Symposium held at Cambridge, Sept., 1965. 1st ed. Vol. II. p. 814-49. London, Tech. Sect. Brit. Paper and Board Makers' Assoc., 1966.

10. Rance, H. F., Tappi 39, no. 2:104-15 (1956).

11. Nordman, L., and Gustafsson, C., Paperi Puu 33, no. 2:36-41 (1951).

12. Nordman, L., Gustafsson, C., and Olofsson, G., Paperi Puu 34, no. 3:47-52 (1952).

13. Nordman, L., Gustafsson, C., and Olofsson, G., Paperi Puu 36, no. 8:315-20 (1954).

14. Nordman, L., Gustafsson, C., and Olofsson, G., Tappi 38, no. 12:724-7 (1955).

15. Nordman, L., Makkonen, T., and Balac, J. P., Papier 19, no. 7:362-7 (1965).

16. Van den Akker, J. A., Tappi 52, no. 12:2386-9 (1969).

17. Page, D. H., Paper Technol. 1, no. 4:407-11 (1960).

18. Page, D. H., and Tydeman, P. A., Paper Technol. 1, no. 5:519-30 (1960).

19. Sanborn, I. B. A study of irreversible, stress-induced changes in the macrostructure of paper. Doctor's Dissertation. Appleton, Wis., The Institute of Paper Chemistry, 1961. 105 p.

20. Van den Akker, J. A., Tappi 53, no. 13:385-400 (1970).

21. McIntosh, D. C., and Leopold, B. Bonding strength of individual fibers. Ref. (5), p. 265-70.

22. Mayhood, C. H., Jr., Kallmes, O. J., and Cauley, M. M., Tappi 45, no. 1:69-73 (1962).

23. Russel, J., Kallmes, O. J., and Mayhood, C. H., Tappi 47, no. 1:22-4 (1964).

24. Schniewind, A. P., Nemeth, L. J., and Brink, D. L., Tappi 47, no. 4:244-8 (1964).

25. Han, S. T., Pulp Paper Mag. Can. 70, no. 9:T134-6 (1969).

26. Spalding, C. W. Unpublished work, The Institute of Paper Chemistry, 1959.

27. Trice, W. H. Unpublished work, The Institute of Paper Chemistry, 1960.

28. Thode, E. F., and Ingmanson, W. L., Tappi 42, no. 1:74-83 (1959).

29. Ingmanson, W. L. Unpublished work, The Institute of Paper Chemistry, 1950.

30. Hermans, P. H. Physics and chemistry of cellulosic fibers. New York, Elsevier, 1949. 534 p.

31. Eames, A. C. The transverse tensile strength of clay-starch coatings as a function of adhesive distribution. Doctor's Dissertation. Appleton, Wis., The Institute of Paper Chemistry, 1959. 135 p.

32. Kaustinen, O., and Jappe, N. A. Unpublished work from Ref. (27), The Institute of Paper Chemistry, 1959.

33. Wink, W. A., and Van Eperen, R. H., Tappi 50, no. 8:393-400 (1967).

34. Institute Method 415, 1951.

35. Ranger, A. E., and Hopkins, L. F. A new theory of the tensile behavior of paper. Ref. (5), p. 300.

36. Pierce, F. T., J. Textile Inst. 17:T355-68 (1926).

37. Hayden, H. W., Moffatt, W. G., and Wulf, J. The structure and properties of materials. Vol. III. Mechanical behavior. New York, John Wiley and Sons, Inc., 1965. 247 p.

38. Aaltio, E. A., Svensk Papperstid. 63, no. 3:58-61 (1960).

39. Brezinski, J. P. The effect of sheet structure in multi-ply paperboard on the bonding between plies. Paper presented at the TAPPI Annual Meeting, Feb., 1962.

40. Kallmes, O. J., and Perez, M. Load-elongation properties of fibers. Ref. (9), Vol. I, p. 507-21.

41. Kubelka, D. J., Opt. Soc. Am. 38, no. 5:448-57 (1948).

42. Van den Akker, J. A., Tappi 32, no. 11:498-501 (1949).

43. Davies, O. L. Statistical methods in research and production. New York, Hafner, 1961. 396 p.

APPENDIX I

ELECTRON AND LIGHT MICROGRAPHS AND TEST SPECIMENS

Pressure Dried at 3.5 kg./cm.^{2}
Magnification = 200X

Pressure Dried at 7.0 kg./cm.^{2}
Magnification = 200X

Pressure Dried at 3.5 kg./cm.^{2}
Magnification = 400X

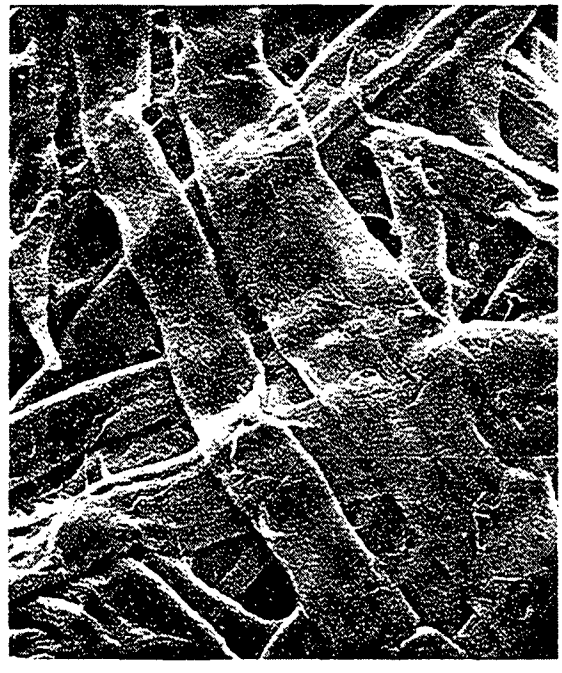

Pressure Dried at 7.0 kg./cm.^{2}
Magnification = 400X

Figure 41. Electron Micrographs of the Surface Structure of Test Specimens Illustrating the Collapsed Ribbonlike Nature of the Fibers

Magnification = 800X

Magnification = 1200X

Magnification = 1600X

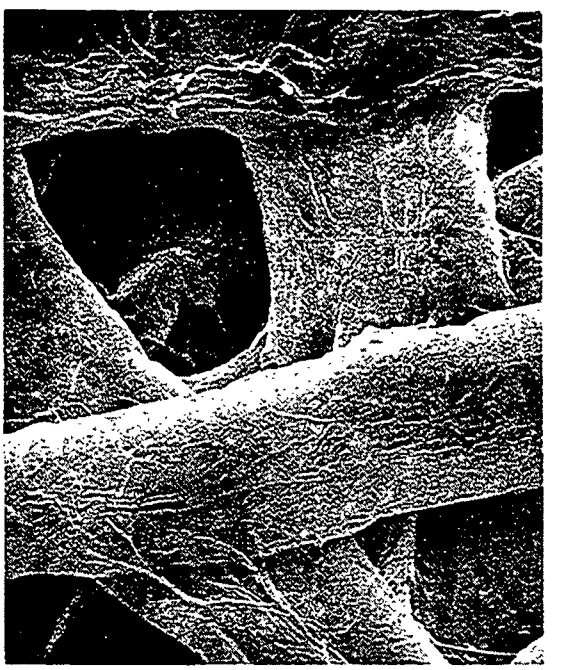

Magnification = 1600X

Figure 42. Electron Micrographs of the Surface Structure of Test Specimens Pressure Dried at 3.5 kg./cm.^{2}

Magnification = 800X

Magnification = 1000X

Magnification = 1400X

Magnification = 1600X

Figure 43. Electron Micrographs of the Surface Structure of Test Specimens Pressure Dried at 7.0 kg./cm.^{2}

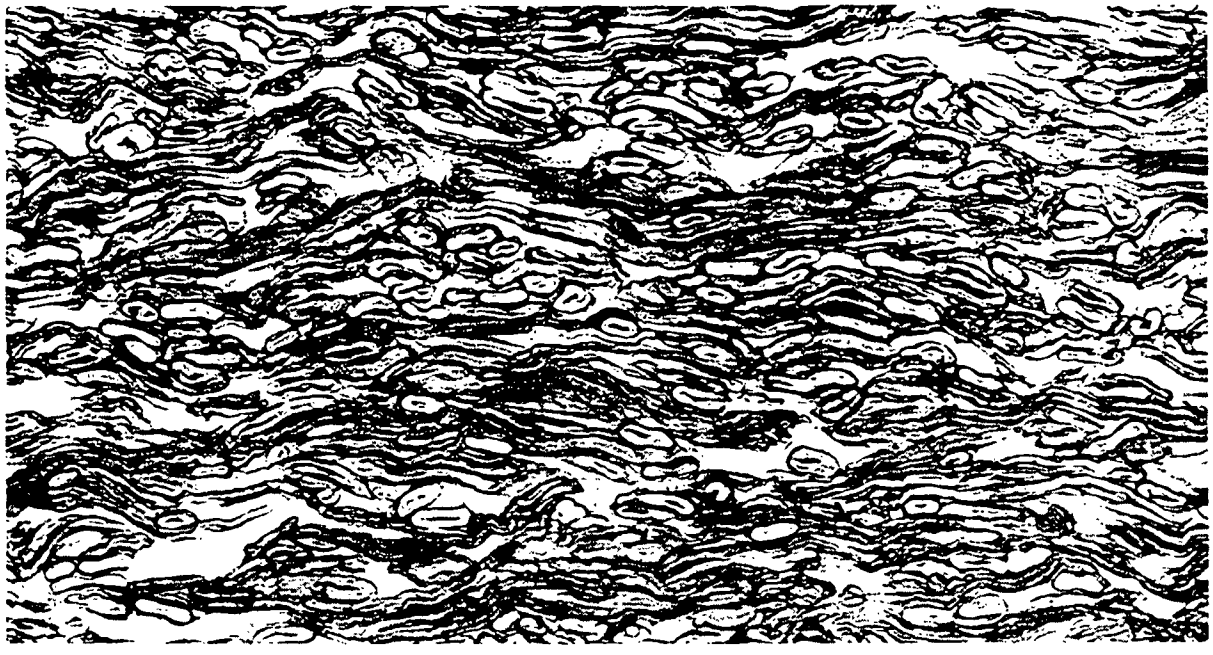

Pressure Dried at 7.0 kg./cm.^{2} Magnification = 185X

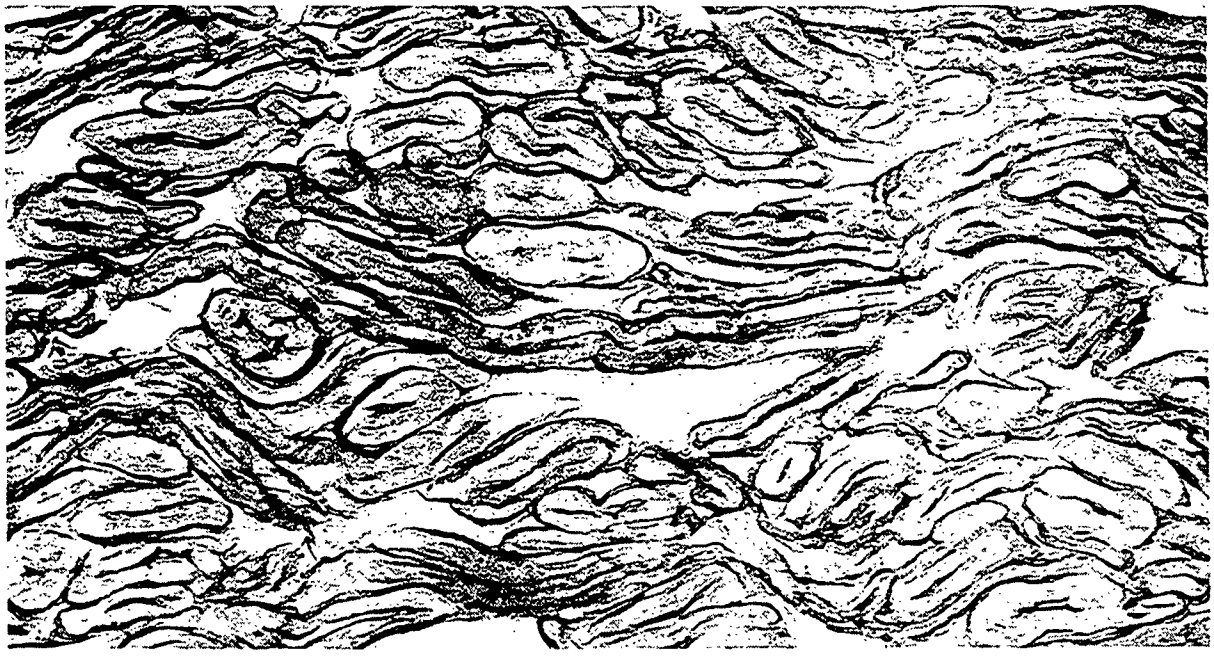

Pressure Dried at 7.0 kg./cm.^{2} Magnification = 475X

Figure 44. Light Micrographs of the Typical Cross-Sectional Structure of Test Specimens Mounted in "C" Stain

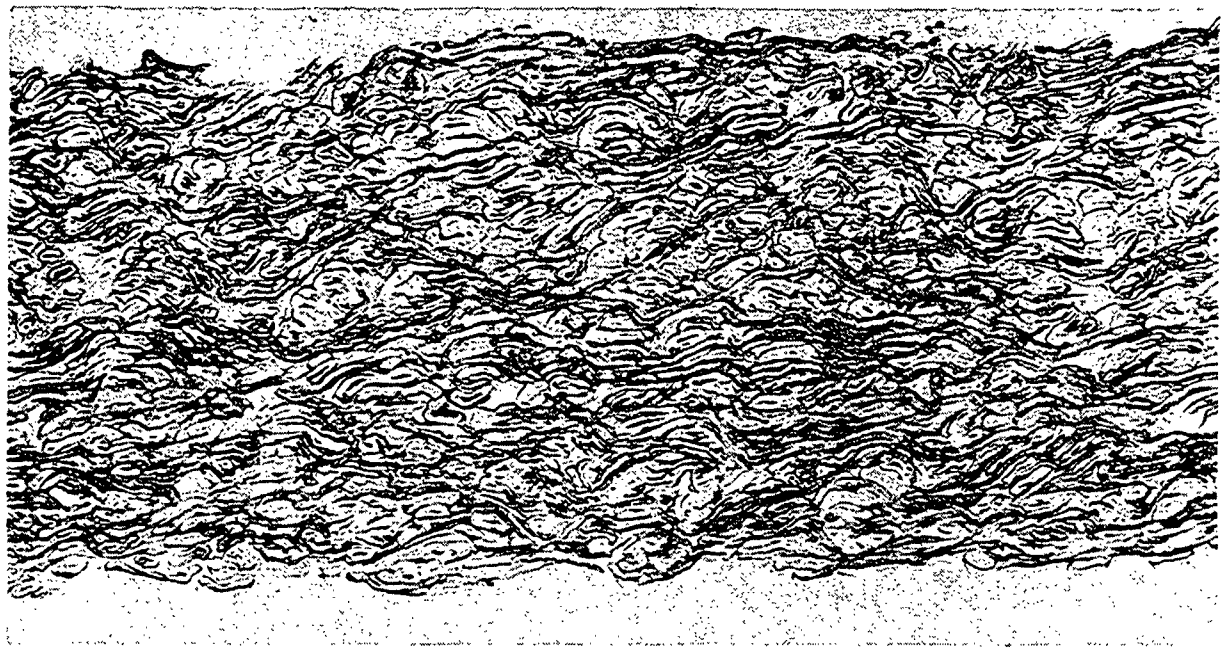

Pressure Dried at 3.5 kg./cm.^{2} Magnification = 185X

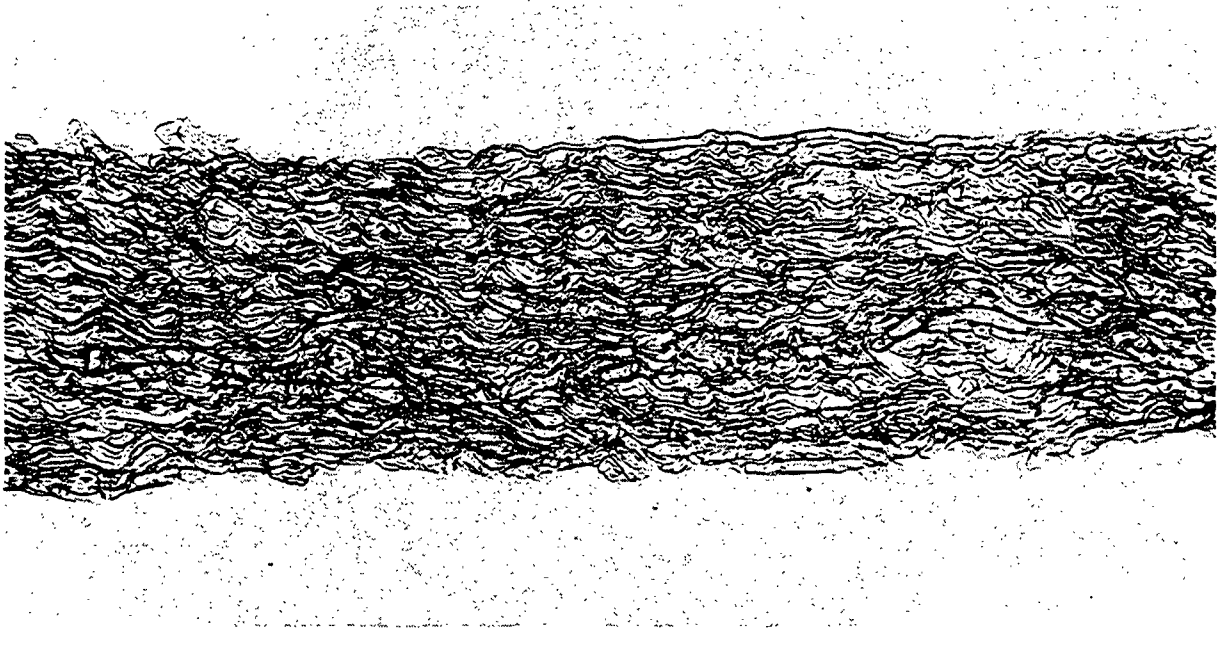

Pressure Dried at 7.0 kg./cm.^{2} Magnification = 125X

Figure 45. Light Micrographs of the Typical Cross-Sectional Structure of Test Specimens Mounted in Mineral Oil

APPENDIX II

STRESS-INDUCED CHANGES IN LIGHT-SCATTERING PROPERTIES

Special techniques were employed to measure the change in light-scattering properties of specimens before and after they had been subjected to loading. The data obtained were analyzed through the use of the Kubelka-Munk theory of light scattering (41), which can be stated mathematically as follows:

$$d(i_r/i_t) = [s(i_r/i_t)^2 - 2(s + k)(i_r/i_t) + s]dW \qquad (9)$$

where i_r and i_t are the intensities of the reflected and transmitted portions of the incident light, and s, k, and W are the specific scattering coefficient, specific absorption coefficient, and basis weight of a sheet, respectively. In the original Kubelka-Munk equation, differential thickness, dX, was used in place of differential basis weight, dW. However, Van den Akker (42) has shown that Equation (9) is valid. Kubelka (41) has solved Equation (9) and shown that the transmittance, T, reflectance (when backed by a black body), R_o, specific scattering coefficient, s, specific absorption coefficient, k, and basis weight, W, of a sheet are related as shown below.

$$(s + k)/s = A = (1 + R_o^2 - T^2)/2R_o \qquad (10)$$

$$sW = (1/B)[\text{arc sinh } (B/T) - \text{arc sinh } (B)] \qquad (11)$$

where $B = [A^2 - 1]^{\frac{1}{2}}$. This means that it is possible to measure only the transmittance, T, reflectance, R_o, and basis weight, W, of a specimen before and after a z-directional load-unload cycle to determine the effect of loading on the optically apparent exposed surface of that specimen.

APPENDIX III

REDUCTION OF DATA FROM A THREE- TO A TWO-DIMENSIONAL SYSTEM

In order to describe the variation in strain and modulus across the specimen surface, it was necessary to treat the three-dimensional system two-dimensionally.

Figure 46 shows the projection of the surface of the loading cylinder onto the xy-coordinate system. Each LVDT is represented by the three points: 1 = (x_1, y_1, z_1); 2 = (x_2, y_2, z_2); 3 = (x_3, y_3, z_3). The xy-coordinate system, as shown in Fig. 46, was established so that Point 1 is on the x axis, and therefore the chord connecting Points 2 and 3 is bisected by the x axis. For the simple case in which $z_2 = z_3$ and both are greater than z_1, the minimum displacement would occur at Point 1, and increase linearly in the direction of positive x. In this case, the coordinate system would not have to be rotated. However, this is an exceptional case, and the minimum and maximum points of strain almost always have to be computed from the measured displacements at Points 1, 2, and 3.

When the specimen is strained in the z-direction, there will be a corresponding displacement of the three points in the z-direction. These displacements are given by the equations:

$$z_1 = ax_1 + by_1 + c \tag{12}$$

$$z_2 = ax_2 + by_2 + c \tag{13}$$

$$z_3 = ax_3 + by_3 + c \tag{14}$$

where

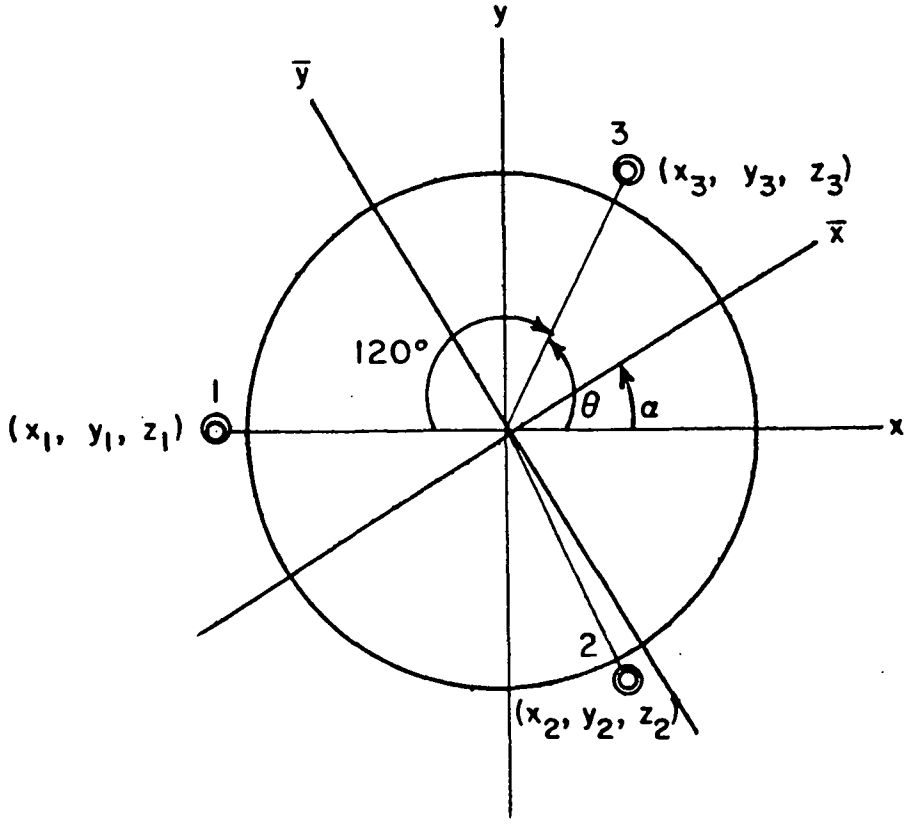

Legend

$\underline{xy}$ Coordinate System:

$\underline{x}_1 = -\underline{R}$ = radius defined by Points 1, 2, and 3

$\underline{x}_2 = \underline{x}_3 = \underline{R} \cos\theta$

$\underline{y}_1 = 0$

$\underline{y}_2 = -\underline{y}_3 = \underline{R} \sin\theta$

$\theta = \pi/3$

$\underline{\bar{x}\bar{y}}$ Coordinate System:

$\underline{\bar{x}} = \underline{x} \cos\alpha + \sin\alpha$

$\underline{\bar{y}} = -\underline{x} \sin\alpha + \underline{y} \cos\alpha$

Figure 46. Projection of Loading Cylinder Surface onto $\underline{xy}$ Coordinate System. $\underline{\bar{x}\bar{y}}$ Coordinate System Illustrates the Rotation of $\underline{xy}$ Coordinates Through α such that $\underline{\bar{y}}$ Now Lies on the Projection of a Line Running Through the Points of Minimum and Maximum Strain

$\underline{a}$ = slope of cylinder surface in $\underline{x}$-direction,

$\underline{b}$ = slope of cylinder in $\underline{y}$-direction, and

$\underline{c}$ = displacement of center of cylinder surface in $\underline{z}$-direction.

From Fig. 46, it is observed that by substituting the appropriate values for $\underline{x}_1$, $\underline{y}_1$, $\underline{x}_2$, $\underline{y}_2$, and θ, the above equations reduce to

$$z_1 = -aR + c \tag{15}$$

$$z_2 = ax_2 - by_3 + c \tag{16}$$

$$z_3 = ax_2 + by_3 + c. \tag{17}$$

It follows from these equations that

$$a = (z_2 + z_3 - 2z_1)/3R \tag{18}$$

$$b = (z_3 - z_2)/3R \tag{19}$$

$$c = (z_1 + z_2 + z_3)/3. \tag{20}$$

The above derivation has enabled one to describe the position of any point on the cylinder surface according to the general equation

$$z = ax + by + c. \tag{21}$$

The next step is to rotate the original coordinate system into a new coordinate system, $\underline{\bar{x}}\,\underline{\bar{y}}$, such that

$$z = a'\bar{x} + b'\bar{y} + c \tag{22}$$

where the new axis, $\underline{\bar{y}}$, is the projection of a line running through the minimum and maximum points of displacement, or in other words, the system is reduced to a two-dimensional plane running through the center of the wedge. When this is the case, $\underline{z}$ will depend on the vertical displacement and the position along $\underline{\bar{y}}$ only. Therefore, Equation (22) will reduce to

$$z = b'\bar{y} + c. \tag{23}$$

Hence, the original coordinate system must be rotated through some angle, α, such that the coefficient $\underline{a}'$ (slope of cylinder surface in $\underline{x}$-direction) will equal zero, which will then satisfy Equation (23).

In the new coordinate system $(\underline{\bar{x}},\underline{\bar{y}})$, $\underline{x}$ and $\underline{y}$ are defined by the equations:

$$x = \bar{x}\cos\alpha - \bar{y}\sin\alpha \tag{24}$$

$$y = \bar{x}\cos\alpha + \bar{y}\sin\alpha. \tag{25}$$

From Equation (21),

$$z = a(\bar{x}\cos\alpha - \bar{y}\sin\alpha) + b(\bar{x}\sin\alpha + \bar{y}\cos\alpha) + c, \tag{26}$$

or

$$z = (a\cos\alpha + b\sin\alpha)\bar{x} + (b\cos\alpha - a\sin\alpha)\bar{y} + c, \tag{27}$$

which is equivalent to Equation (22) where

$$a' = a\cos\alpha + b\sin\alpha \tag{28}$$

$$b' = b\cos\alpha - a\sin\alpha. \tag{29}$$

In order to satisfy Equation (23), that is $\underline{z}$ a function of $\underline{\bar{y}}$ and $\underline{c}$ only, the following conditions must exist:

$$a' = 0 = a\cos\alpha + b\sin\alpha \tag{30}$$

$$b' = b\cos\alpha - a\sin\alpha. \tag{31}$$

Therefore, Equation (23) is satisfied when

$$\alpha = \tan^{-1}(-a/b), \tag{32}$$

which is the angle through which the original coordinate system must be rotated so that the $\bar{y}$ axis is the projection of a line running from the point of minimum strain to the point of maximum strain. The slope of this new line is given by Equation (31).

APPENDIX IV

CALCULATION OF MODULUS COEFFICIENTS

Equation (5) stated:

$$\sigma = (\gamma_1 + \gamma_3\bar{y})(c + b'\bar{y}) + (\gamma^2 + \gamma_4\bar{y})(c + b'y)^2. \tag{33}$$

The given information needed to solve for the modulus coefficients (γ_1, γ_2, γ_3, and γ_4) is: (1) The contribution to torque about the $\underline{\bar{x}}$ axis at any position along $\underline{\bar{y}}$ is $\underline{\bar{y}} \cdot \sigma \cdot \underline{dA}$, and (2) the contribution to the total force is $\sigma \cdot \underline{dA}$. Therefore, at equilibrium,

$$\iint \bar{y}\sigma dA = 0 \tag{34}$$

$$\iint \sigma dA = F \tag{35}$$

where $\underline{F}$ is the measured load on the specimen as determined by the load cell.

The expanded form of Equation (33) is

$$\begin{aligned}\sigma = {} & \gamma_1 c + \gamma_2 c^2 + [\gamma_1 b' + \gamma_3 c + 2\gamma_2 cb' + \gamma_4 c^2]\bar{y} \\ & + [\gamma_3 b' + \gamma_2 b'^2 + 2\gamma_4 cb']\bar{y}^2 \\ & + \gamma_4 b' 2\bar{y}^3.\end{aligned} \tag{36}$$

Substituting Equation (36) into Equations (34) and (35), one gets

$$[\gamma_1 b' + \gamma_3 c + 2\gamma_2 cb' + \gamma_4 c^2]\iint \bar{y}^2 dA + \gamma_4 b'^2 \iint \bar{y}^4 dA = 0 \tag{37}$$

and

$$[\gamma_1 c + \gamma_2 c^2]A + [\gamma_3 b' + \gamma_2 b'^2 + 2\gamma_4 cb']\iint y^2 dA = F \tag{38}$$

where $\iint \underline{y}^2 \underline{dA} = (\pi/4) \cdot \underline{r}^4$; $\iint \underline{y}^4 \underline{dA} = (\pi/8)\underline{r}^6$; $\underline{r}$ and $\underline{A}$ = radius and area of cylinder surface, respectively.

Substituting these values into Equations (37) and (38) and rearranging gives

$$c\pi r^2\gamma_1 + [c^2\pi r^2 + b'^2(\pi/4)r^4]\gamma_2 + b'(\pi/4)r^4\pi_3 + cb'(\pi/2)r^4\gamma_4 = F \quad (39)$$

and

$$b'(\pi/4)r^4\gamma_1 + 2b'c(\pi/4)r^4\gamma_2 + c(\pi/4)r^4\gamma_3 + [c^2(\pi/4)r^4 + b'^2(\pi/8)r^6]\gamma_4 = 0. \quad (40)$$

The solution to this system of two equations in four unknowns (γ_1, γ_2, γ_3, and γ_4) can be determined through a regression analysis (43)[38]. Equations (39) and (40) can be written in the form

$$a_{11}t_{11} + a_{12}t_{12} + a_{13}t_{13} + a_{14}t_{14} = \bar{y}_{11} = F \quad (41)$$

and

$$a_{11}t_{21} + a_{12}t_{22} + a_{13}t_{23} + a_{14}t_{24} = \bar{y}_{22} = 0 \quad (42)$$

where $\underline{a}_{11} = \gamma_1$; $\underline{a}_{12} = \gamma_2$; $\underline{a}_{13} = \gamma_3$; $\underline{a}_{14} = \gamma_4$; and the $\underline{t}$'s are functions of the known values for $\underline{c}$, $\underline{b}'$, and $\underline{r}$ as shown in Equations (39) and (40).

The object is to determine values for the regression coefficients ($\underline{a}_{11}, \cdots, \underline{a}_{14}$) that will give rise to the least disagreement, overall, between the observed value and the expected value. As a measure of the overall disagreement, we take an equation of the form

$$Q = \Sigma(\bar{y}1k - q1k)^2 + \Sigma(\bar{y}2k - q2k)^2 \quad (43)$$

where $\bar{y}$ = observed value and $\underline{q}$ = expected value. That is, the sum of squares of the deviations of observed values of the dependent variables from those expected. In fitting by the method of least squares, we want to choose $\underline{a}_{11}, \cdots, \underline{a}_{14}$

[38]These equations are weighed uniformly in the regression analysis.

so as to minimize $\underline{Q}$. This may be done by taking the partial derivatives of $\underline{Q}$ with respect to $\underline{a}_{11},\cdots,\underline{a}_{14}$ and equating each to zero, giving a set of simultaneous equations for the desired values of $\underline{a}_{11},\cdots,\underline{a}_{14}$.

Carrying out this process for the present system of Equations (41) and (42), we have

$$Q = \Sigma[\bar{y}_{11} - (a_{11}t_{11} + a_{12}t_{12} + a_{13}t_{13} + a_{14}t_{14})]^2 + \Sigma[\bar{y}_{22} - (a_{11}t_{21} + a_{12}t_{22} + a_{13}t_{23} + a_{14}t_{24})]^2 \tag{44}$$

$$\partial Q/\partial a_{11} = 0 = \Sigma[\bar{y}1k - (a_{11}t_{11} + a_{12}t_{12} + a_{13}t_{13} + a_{14}t_{14}]t_{11} - \Sigma[\bar{y}2k - (a_{11}t_{21} + a_{12}t_{22} + a_{13}t_{23} + a_{14}t_{24}]t_{21}. \tag{45}$$

This gives

$$a_{11}\Sigma t_{11}^2 + a_{12}\Sigma t_{12}t_{11} + a_{13}\Sigma t_{13}t_{11} + a_{11}\Sigma t_{21}^2 + a_{12}\Sigma t_{22}t_{11} + a_{13}\Sigma t_{23}t_{11} = \Sigma\bar{y}_{11}t_{11} + \Sigma\bar{y}_{22}t_{21} \tag{46}$$

or

$$a_{11}[\Sigma t_{11}^2 + \Sigma t_{21}^2] + a_{12}[\Sigma t_{12}t_{11} + \Sigma t_{22}t_{21}] + a_{13}[\Sigma t_{13}t_{11} + \Sigma t_{23}t_{21}] + a_{14}[\Sigma t_{14}t_{11} + \Sigma t_{24}t_{21}] = \Sigma\bar{y}_{11}t_{11} + \Sigma\bar{y}_{22}t_{21}. \tag{47}$$

Repeating this procedure for the other three partial derivatives, one obtains

$$\partial Q/\partial a_{12} = 0,$$

or

$$a_{11}[\Sigma t_{11}t_{12} + \Sigma t_{21}t_{22}] + a_{12}[\Sigma t_{12}^2t_{22}^2] + a_{13}[\Sigma t_{13}t_{11} + \Sigma t_{23}t_{21}] + a_{14}[\Sigma t_{14}t_{11} + \Sigma t_{24}t_{21}] = \Sigma\bar{y}_{11}t_{11} + \Sigma\bar{y}_{22}t_{21}; \tag{48}$$

$$\partial Q/\partial a_{13} = 0,$$

or

$$a_{11}[\Sigma t_{11}t_{13} + \Sigma t_{21}t_{23}] + a_{12}[\Sigma t_{12}t_{13} + \Sigma t_{22}t_{23}] + a_{13}[\Sigma t_{13}^2 + \Sigma t_{23}^2] + a_{14}[\Sigma t_{14}t_{13} + \Sigma t_{24}t_{23}] = \Sigma \bar{y}_{11}t_{13} + \Sigma \bar{y}_{22}t_{23}; \quad (49)$$

$$\partial Q/\partial a_{14} = 0,$$

or

$$a_{11}[\Sigma t_{11}t_{14} + \Sigma t_{21}t_{24}] + a_{12}[\Sigma t_{12}t_{14} + \Sigma t_{22}t_{24}] + a_{13}[\Sigma t_{13}t_{14} + \Sigma t_{23}t_{24}] + a_{14}[\Sigma t_{14}^2 + \Sigma t_{24}^2] = \Sigma \bar{y}_{11}t_{14} + \Sigma \bar{y}_{22}t_{24}. \quad (50)$$

This procedure has converted Equations (41) and (42) into a system of four simultaneous equations for the regression coefficients $\underline{a}_{11},\cdots,\underline{a}_{14}$ [or γ_1, γ_2, γ_3, and γ_4 in Equations (39) and (40)]. These values which are the least-squares estimates, represent the dependence of $\bar{\underline{y}}_{11}$ and $\bar{\underline{y}}_{22}$ on $\underline{t}_{11},\cdots,\underline{t}_{14}$ and $\underline{t}_{21},\cdots,\underline{t}_{24}$, respectively. This system for the four simultaneous equations in four unknowns can now be solved by standard techniques, and the solutions for the modulus coefficients determined.

Computer programs have been written, and available ones modified to carry out these calculations.

APPENDIX V

VARIATION IN MECHANICAL BEHAVIOR

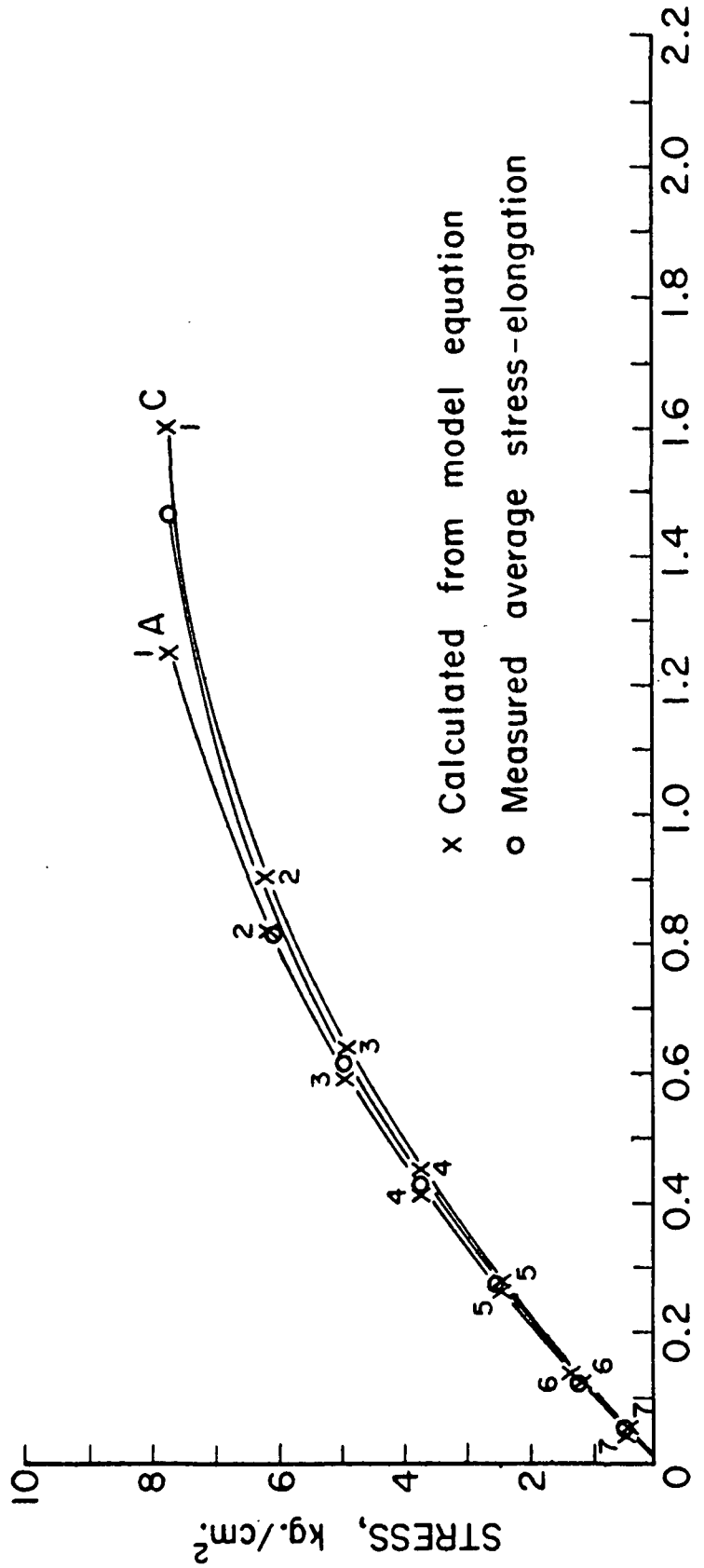

Figure 47. Stress-Elongation Variation Along the Wedge for Specimen IA4.
Arabic Numbers Group Points According to Wedge Slope

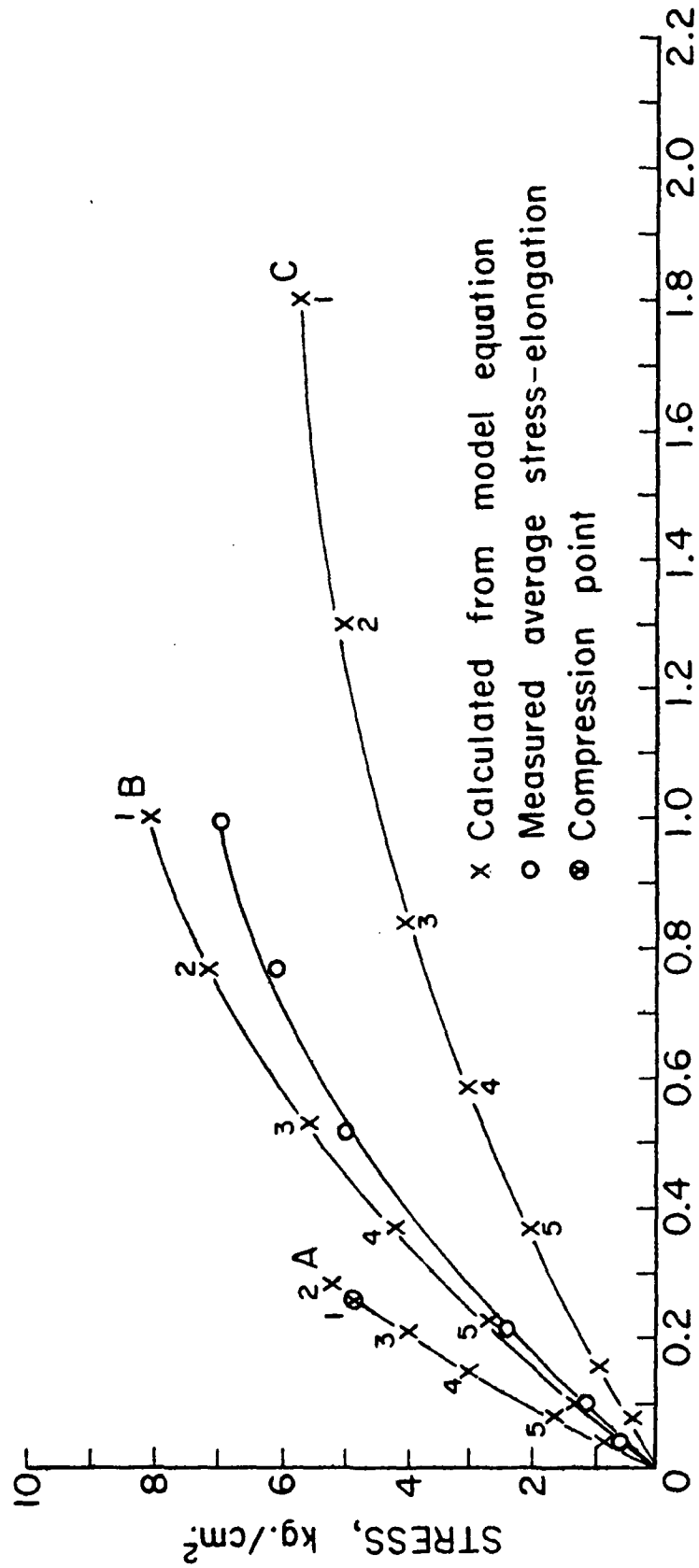

Figure 48. Stress-Elongation Variation Along the Wedge for Specimen IA2. Arabic Numbers Group Points According to Wedge Slope

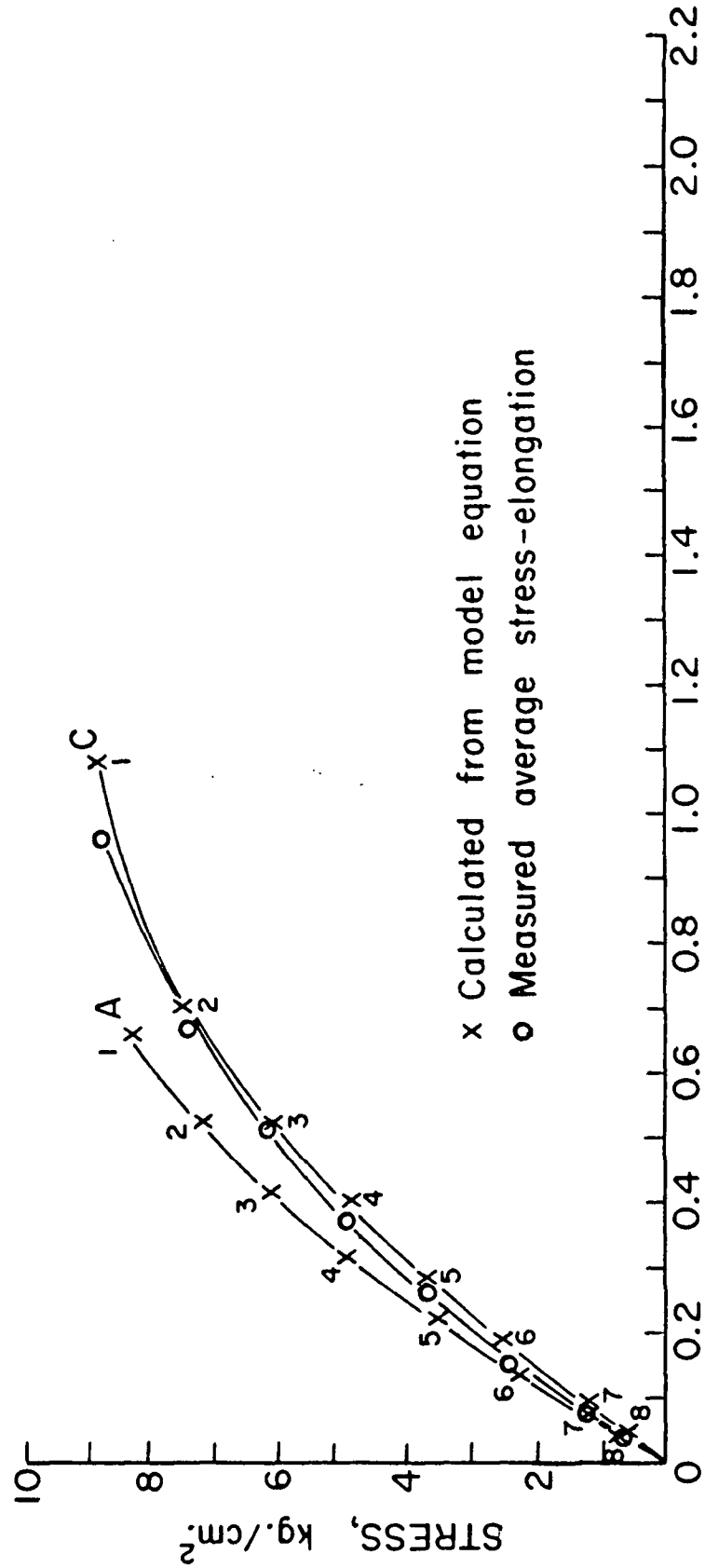

Figure 49. Stress-Elongation Variation Along the Wedge for Specimen IIB9.
Arabic Numbers Group Points According to Wedge Slope